

Development of an optimized methodology for tensile testing of carbon steels in hydrogen environment

Degree: **Materials Engineering**

Director: **Dra M^a Dolors Baró**

Author: **Pau Cuadros Fernández**

Co-Director: **Dr Lode Duprez**

June, 2009

Dolors Baró Mariné, Catedràtica de Física Aplicada del Departament de Física de la Universitat Autònoma de Barcelona.

FA CONSTAR:

Que ha fet el seguiment mitjançant tutories del treball de final de carrera concloent a la titulació d' Enginyeria de Materials titulat "Development of an optimized methodology for tensile testing of Carbon steels in hydrogen environment" de l'alumne Pau Cuadros Fernandez.

Al mateix temps considerem que és apte i autoritzem la seva presentació i posterior defensa.

I per què així consti, signem el present escrit.

M. D. Baró

Bellaterra, 18 de Juny de 2009

OCAS NV
John Kennedylaan 3
B-9060 Zelzate
Tel : + 32 9 345 12 11
Fax : + 32 9 345 12 04
www.ocas.be



Zelzate, June 16th 2009

CERTIFICATION FOR PROJECT PRESENTATION AND DEFENCE

Pau Cuadros has been working in OCAS on the project “Development of an optimized methodology for tensile testing of carbon steels in hydrogen environment”.
He was closely followed up and supervised, and meetings on a regular basis showed that he was progressing very well with this project.

I consider that Pau is suitable and well prepared and I hereby authorize his presentation and subsequent defence.

Lode Duprez
Program Manager Metal Processing R&D Portfolio



ACKNOWLEDGEMENTS

This work has been done with the collaboration of all the people of the Steel Researcher Center in Gent, OCAS, especially **Lode Duprez** from the Substrates and Metallic Coatings Development Departament who was in continuous dedication and **Frank Rootsaert** from the Physical Testing and Application Departament for the lessons on the Tensile Machine.

I have to be agreed with **M^a Dolors Baró** who gave me the opportunity to realize this work in OCAS.

The project is dedicated to my family, especially my parents, my brother and who were together with me during this internship.

Pau Cuadros Fernandez, 2009

MEMORY INDEX

1. INTRODUCTION.....	3
2. LITERATURE REVIEW.....	5
2.2. Hydrogen Embrittlement.....	5
2.3. Material Description.....	5
3. EXPERIMENTAL.....	8
3.1. Materials.....	8
3.2. Equipments & Techniques.....	15
4. H-CHARGING & SOLUBILITY.....	22
4.1. Sample geometry.....	22
4.2. Charging methods.....	23
4.3. Electrolyte solutions.....	27
4.4. Results and conclusion.....	28
5. DEVELOPMENT OF A TENSILE TESTING METHODOLOGY.....	36
5.1. Standard Tensile Testing.....	36
5.2. SSRT: Slow Strain Rate Testing.....	36
5.3. Incremental Step Loading Technique.....	42
5.4. Constant Load Testing.....	47
6. EFFECT OF MICROSTRUCTURE ON HYDROGEN EMBRITTELEMENT.....	55
6.1. FB450.....	55
6.2. S700MC.....	58
6.3. DP600.....	60
6.4. DP980.....	63
6.5. DP1200.....	65
6.6. Overlay all materials & discussion.....	68
7. FRACTURE MECHANISMS STUDY.....	71
7.1. Tensile Testing.....	71
7.2. Sample preparation.....	73
7.3. SEM analysis.....	74
7.4. EBSD analysis.....	79
7.5. Discussion.....	84
8. CONCLUSIONS AND SUGGESTIONS FOR FUTURE WORKS.....	85
9. BIBLIOGRAPHIC REFERENCES.....	87

APPENDICE INDEX

1. OPTICAL MICROSCOPE IMAGES.....	II
2. SEM IMAGES.....	VII
3. EDX MAPPING.....	XV
4. EBSD IMAGES.....	XVI

MEMORY

1. INTRODUCTION

Hydrogen Embrittlement (HE) can be defined as a loss of mechanical properties, in particular ductility, due to the presence of hydrogen and stress. A significant decrease of ductility and/or fracture strength is typical features of HE. Another illustration of the detrimental effect of H is the delayed fracture phenomena. Understanding the fundamentals of HE is a key issue for numerous future material developments.

The major aim of this study was to obtain an optimized tensile testing methodology with in-situ H-charging to reveal the HE in various high strength steels.

This study has been done in OCAS, the research centre of ArcelorMittal for non-automotive product development, which is located in Gent, Belgium.

The various goals of this study were, in chronological order:

First, to define the most appropriate experimental parameters for H-charging:

- Sample geometry
- Electrochemical charging conditions:
 - Type of electrolyte
 - Galvanostatic or potentiostatic methods
 - Current density
 - Effect of steel type

The amount of hydrogen (ppm) introduced into the steel will influence the mechanical results.

Secondly, to define the most appropriate tensile test type that allows to differentiate C-steels in their sensitivity to H-embrittlement:

- SSRT “Slow Strain Rate Testing” :
 - Effect of pre-charging time
 - Effect of strain rate

- Incremental Step Loading:
- Constant Load Testing

For the first two parts of the research, a long variety of steels was studied (depending on specific internal project requests).

Finally, fundamental material knowledge was generated by characterizing a systematic set of steel grades in their sensitivity to hydrogen.

There, two steel families were investigated:

- Dual Phase steels, having a predominantly ferrite-martensite structure. (DP600 / DP980 / DP1200)
- Bainitic containing steels of various strength levels. (S700MC / FB450)

Afterwards, fracture surface analysis was done by means of SEM and crack propagation was studied by mean of EBSD technique.

2 LITERATURE REVIEW

2.1 Hydrogen Embrittlement

Hydrogen can enter into the material during manufacturing, e.g. welding, casting, annealing, and during service, e.g. when subjected to wet environments with simultaneous corrosion. In solid solution hydrogen at low concentration in the material does not affect the mechanical properties significantly except during the application of load. As a consequence of mechanical loading dislocations are generated with possibility of becoming hydrogen traps. There are different forms of degradation, one of which is the weakening of the material due to hydrogen.

The impact or degradation due to hydrogen may vary with composition, microstructure, and applied stress levels of the material in service in solution. The presence of hydrogen traps in the material influence the degree to which the material can suffer.

The latter is an important aspect that must be considered for the design of components. To understand the mechanisms of HE is necessary to evaluate via experiments the diffusion, the solubility (determinate by an H-analyzer) and hydrogen traps characteristic of the material.

2.2 Material Description

This study is focused on carbon steels materials with different microstructures.

The American Iron and Steel Institute (AISI) define carbon steel as follows:

- when no minimum content is specified or required for chromium, cobalt, columbium [niobium], molybdenum, nickel, titanium, tungsten, vanadium or zirconium, or any other element to be added to obtain a desired alloying effect;
- when the specified minimum for copper does not exceed 0.40 per cent;
- when the maximum content specified for any of the following elements does not exceed the percentages noted: manganese 1.65, silicon 0.60, and copper 0.60.

Steels can be classified by a variety of different systems depending on:

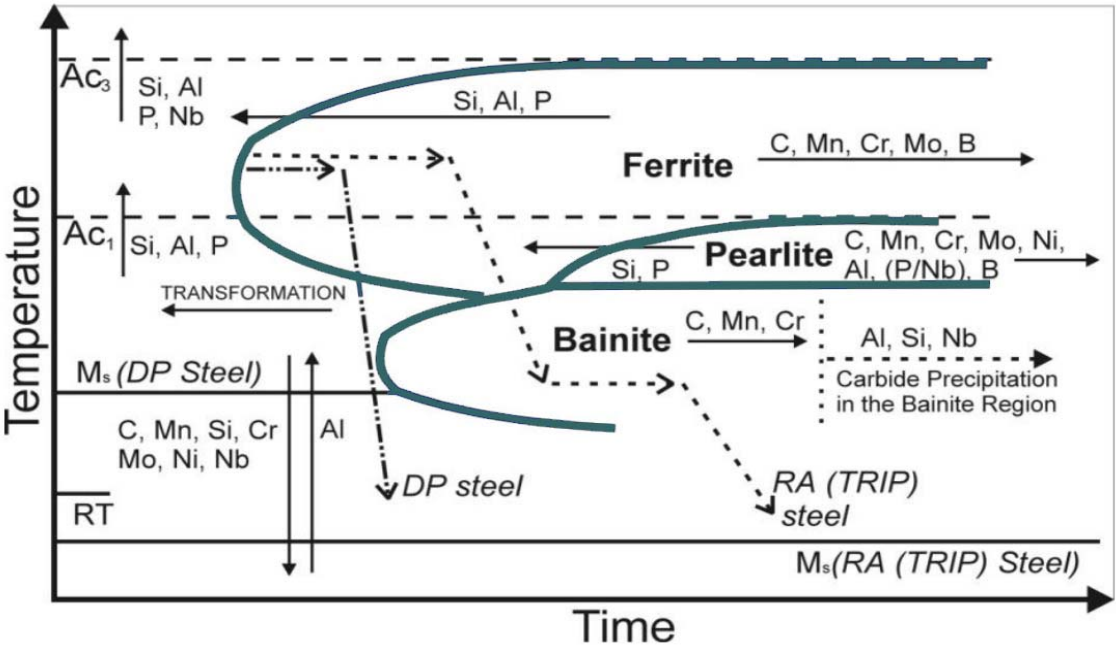
- The composition, such as carbon, low-alloy or stainless steel;
- The manufacturing methods, such as open hearth, basic oxygen process, or electric furnace methods;
- The finishing method, such as hot rolling or cold rolling;
- The product form, such as bar plate, sheet, strip, tubing or structural shape;
- The deoxidation practice, such as killed, semi-killed, capped or rimmed steel
- The microstructure, such as ferritic, pearlitic and martensitic
- The required strength level, as specified in ASTM standards
- The heat treatment, such as annealing, quenching and tempering, and thermomechanical processing
- Quality descriptors, such as forging quality and commercial quality.

For the better understanding of different steel microstructures formation, Dual Phase and TRIP steels have been explained:

Dual-phase steel (DPA) is a high-strength steel that has a ferrite and martensitic microstructure. DPA starts as a low or medium carbon steel and is quenched from above A_1 but below A_3 on a continuous cooling transformation diagram. This results in a soft microstructure; with a ferritic matrix containing islands of martensite in the secondary phase (martensite increases the tensile strength).

TRIP steel is a high-strength steel, stands for "transformation induced plasticity." TRIP steel has a triple phase microstructure consisting of ferrite, bainite, and retained austenite. During plastic deformation and straining, the metastable austenite phase is transformed into martensite. This transformation allows for enhanced strength and ductility.

The graph 1 shows the curve TTT (Temperature-Time-Transformation) for DP and TRIP steels and give an idea to how obtain them and which alloys modify the curves in time-temperature.



Graph 1: Influence of alloying elements on TTT behavior

3 EXPERIMENTAL

3.1 Materials

The materials used throughout this study are shown on the following *table 1*

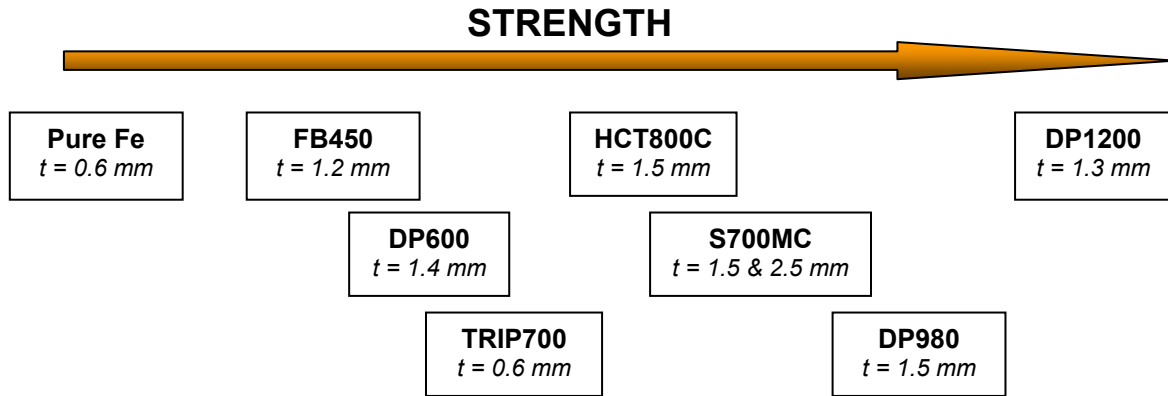


Table1: Strength distribution and thickness of the materials

- **PURE Fe**

○ **Chemical composition**

C	Si	Mn	P	S	Al	Cr	Ni	Mo	Cu	N	Ti	V	Nb
0.0015	0	0.0003	0.0017	0.0003	0.0019	0.0001	0	0	0.0007	0	0.0002	0	0

Table 2: Chemical composition in Wt% of the Pure Fe

○ **Microstructure**

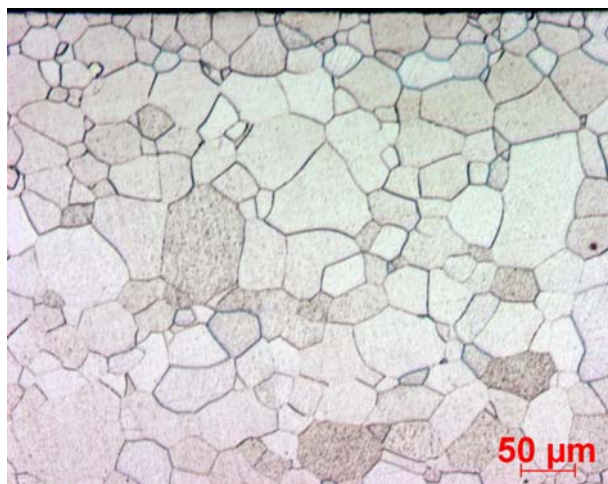


Fig.1: Pure Fe after salt bath at 750 °C during 30 seconds

- **HCT800C**

○ **Chemical composition**

C	Si	Mn	Al	OTHERS:
~0.1	~0.15	~2.2	~0.05	Nb

Table 3: Chemical composition in Wt% of HCT800C

○ **Microstructure**

The blue to grey colored areas is the ferritic fraction. The small white phase distinguishes the high carbon martensitic structure whilst the brown one is characterized as low carbon martensitic phase.

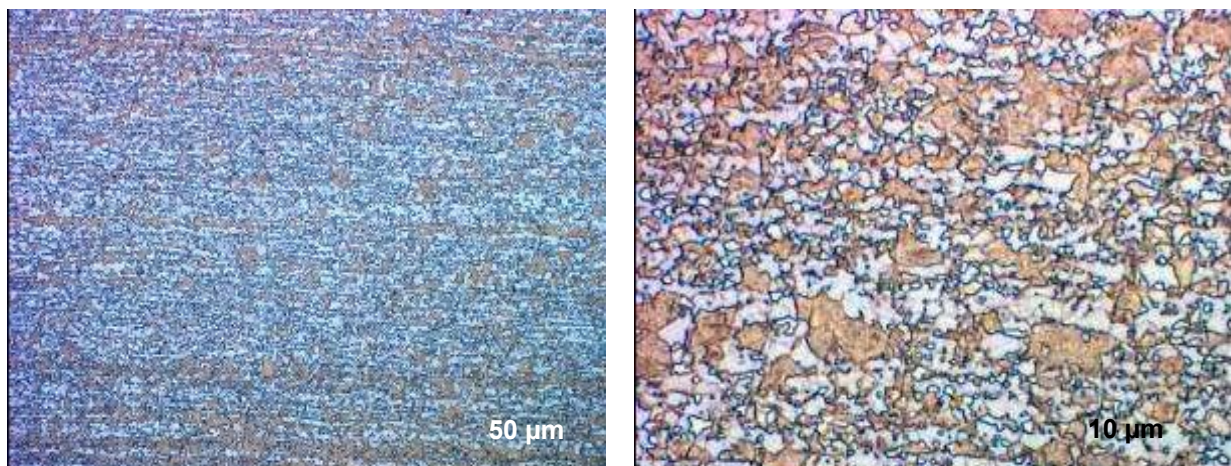


Fig. 2: Microstructure of HCT800C (Le Pera etching)

○ **Mechanical properties**

Direction	Rp 0.2 MPa	Rm MPa	Au %	A80 %
Longitudinal	715	892	8.1	14.6

Table 4: Mechanical properties HCT800C

- **TRIP700**

○ **Chemical composition**

C	Si	Mn	Al	OTHERS:
~0.15	~0.4	~1.5	~1.5	V

Table 5: Chemical composition in Wt% of TRIP700

○ **Microstructure**

The blue to grey colored areas is the ferritic fraction. The small white phase distinguishes retained austenite whilst the brown one is characterized as low carbon martensitic phase. The small dark brown grains are specified as bainitic phase.

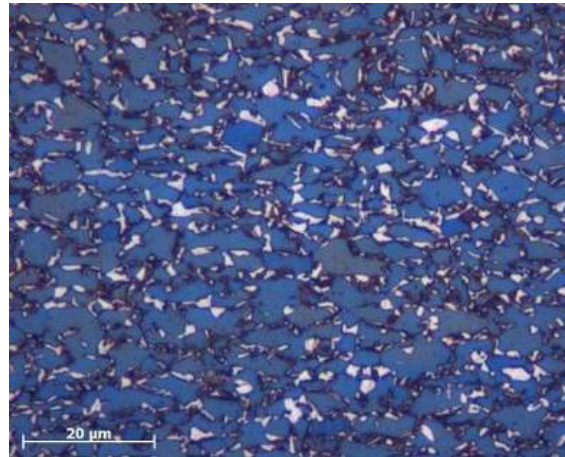


Fig. 3: Optical microstructures of the TRIP700

○ **Mechanical properties**

Direction	Rp 0.2 MPa	Rm MPa	Au %	A80 %
Longitudinal	478	705	23.5	31.6

Table 6: Mechanical properties of TRIP700

- **S700MC**

○ **Chemical composition**

C	Si	Mn	Al	OTHERS:
~0.05	~0.2	~1.7	~0.05	Ti, Mo, Nb

Table 7: Chemical composition in Wt% of the S700MC

○ **Microstructure**

Next to bainite the sample contained mainly Ti & Nb-rich precipitates (Ti,Nb,Si,O; Ti,Nb,C,N and Nb,Ti,C). The precipitates had a very varying shape (round, oval, angular or irregular) and covered a whole range of dimensions (20 – 550 nm).

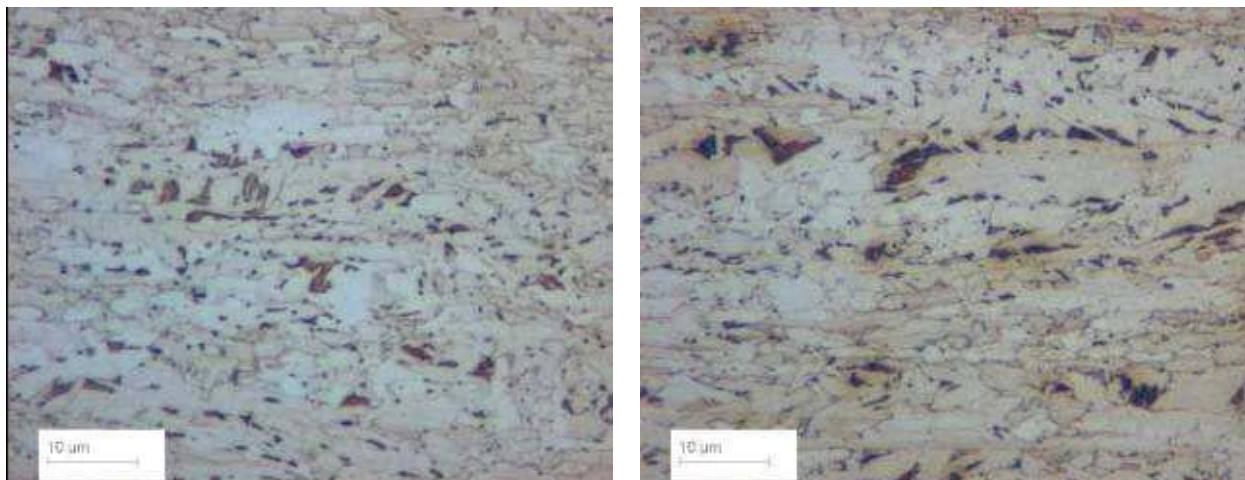


Fig. 4: Microstructure of S700MC

○ **Mechanical properties**

Direction	Rp 0.2 MPa	Rm MPa	Au %	A80 %
Longitudinal	782	819	9	18

Table 8: Mechanical properties of TRIP700

- **DP600**

○ **Chemical composition**

C	Si	Mn	Al	OTHERS:
~0.07	~0.13	~1.4	~0.05	Cr

Table 9: Chemical composition in Wt% of DP600

○ **Microstructure**

The smaller dark brown grains characterize the Martensite, the rest distinguishes the ferrite phase.

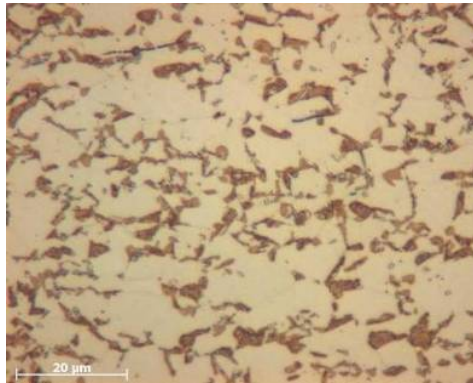


Fig. 5: Microstructure of the DP600 material.

○ **Mechanical properties**

Direction	Rp 0.2 MPa	Rm MPa	Au %	A80 %
Longitudinal	402	648	15.4	26.1

Table 10: Mechanical properties of DP600

- **DP980**

○ **Chemical composition**

C	Si	Mn	Al	OTHERS:
~0.14	~0.20	~1.9	~0.030	Cr

Table 11: Chemical composition in Wt% of DP980

○ **Microstructure**

Consists on low carbon martensitic and bainitic microstructure.

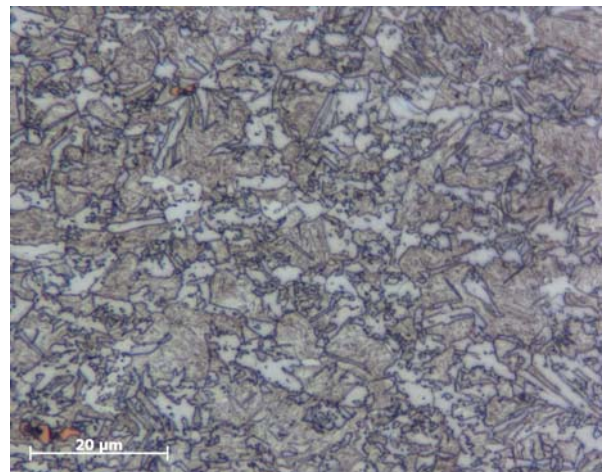
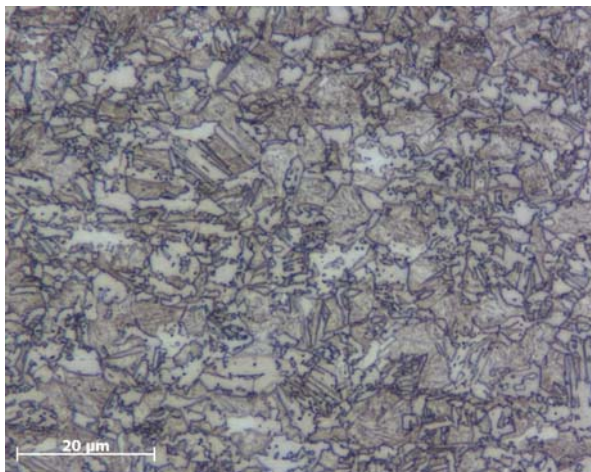


Fig. 6: Microstructure of the DP980 material. Etched with Le Pera 20 seconds

○ **Mechanical properties**

Direction	Rp 0.2 MPa	Rm MPa	Au %	A50 %
Longitudinal	687	966	8.5	14.7

Table 12: Mechanical properties of DP980

- **DP1200**

○ **Chemical composition**

C	Si	Mn	Al	OTHERS:
~0.15	~0.20	~1.9	~0.03	Cr

Table 13: Chemical composition in Wt% of DP1200

○ **Microstructure**

Consists in a mainly martensite with a small fraction of ferrite microstructure.

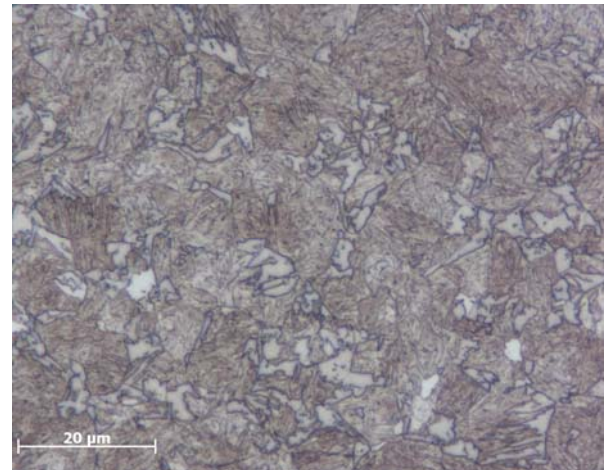
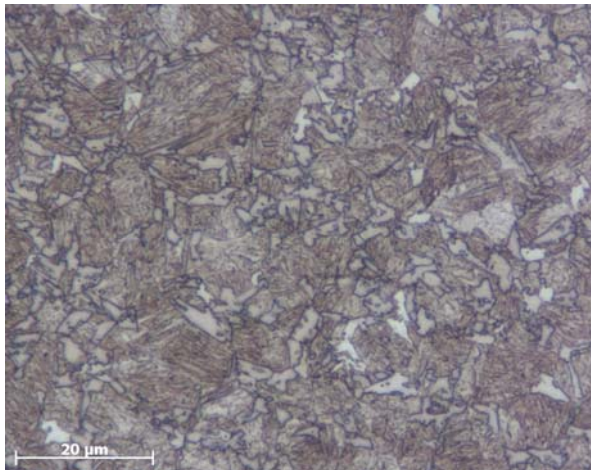


Fig. 7: Microstructure of the DP1200 material. Etched with Le Pera 20 seconds

○ **Mechanical properties**

Direction	Rp 0.2 MPa	Rm MPa	Au %	A50 %
Longitudinal	969	1212	4.5	7.8

Table 13: Mechanical properties of DP1200

- **FB450**

○ **Chemical composition**

C	Si	Mn	Al	OTHERS
~0.07	~0.13	~1.00	~0.07	Ti, Nb, Mo

Table 14: Chemical composition in Wt% of FB450

○ **Microstructure**

The FB450 has a ferritic-bainitic microstructure around the 11 %.

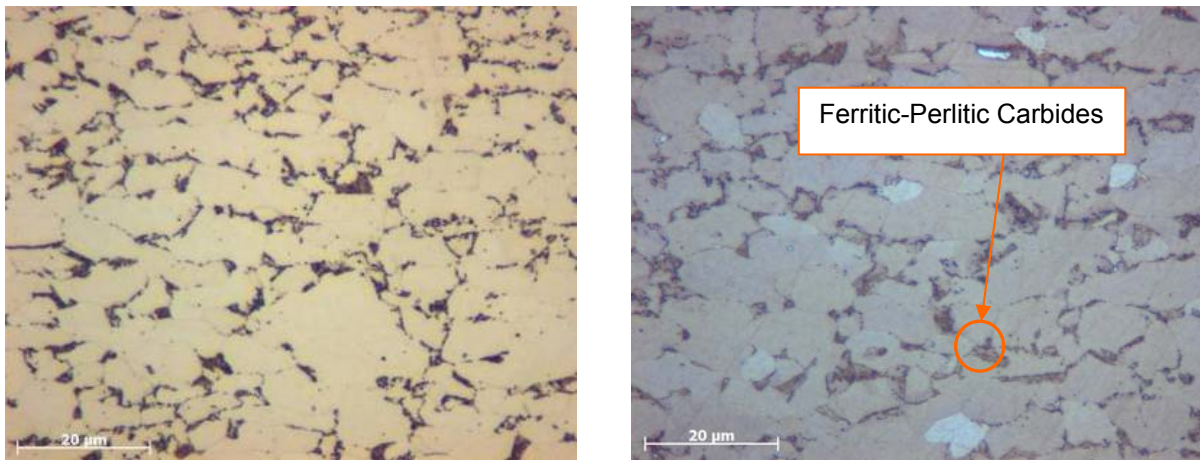


Fig. 8: Microstructure FB450 Ferrite-bainite

○ **Mechanical properties**

Direction	Rp 0.2 MPa	Rm MPa	Au %	A80 %
<i>Longitudinal</i>	360	485	16.6	24.3

Table 15: Mechanical properties of FB450

3.2 Equipments & techniques

3.2.1 H-MAT

The Hydrogen content of solid materials can be determined with the computer controlled analyzer system H-mat 2500.

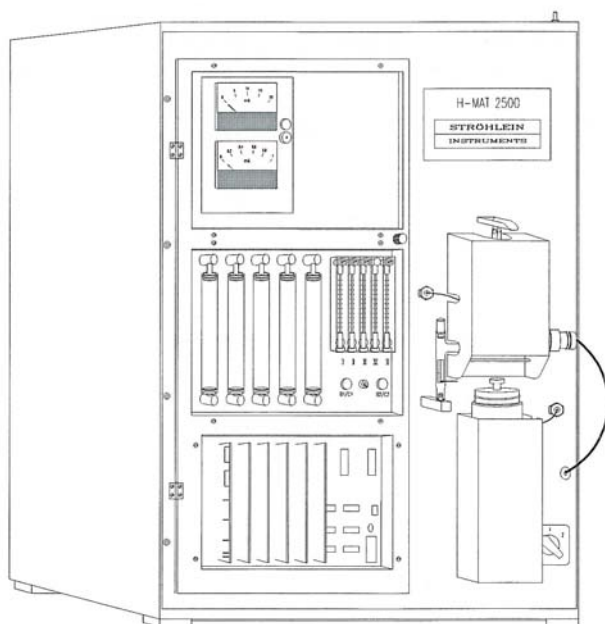


Fig.9: H-mat 2500

A wide range of different materials such as steel, iron, non-ferrous metals, alloys, ceramics, glass, semiconductor materials, special materials, powdered metals and inorganic compounds can be examined with this analyzer to determine their Hydrogen content.

The Hydrogen concentration is determined using the carrier gas procedure. Nitrogen or Argon with 99.995 % purity is used as

carrier gas.

The samples are heated in a graphite crucible in the pulse furnace. During this melt extraction Hydrogen and Carbon Monoxide are released from the sample and taken up by the carrier gas flow.

On passing the dust trap, oxidising agent and a molecular sieve, coarse particles are removed from the carrier gas and CO_2 as well as H_2O are retained. The thermal conductivity measuring cell of the H-mat 2500 operates as Hydrogen detector. Thermistors in a bridge circuit measure the thermal conductivity of the carrier gas flow and of a reference gas flow. A change of the thermal conductivity of the carrier gas flow due to the released Hydrogen produces a measurement signal on comparing the two gas flows. The magnitude of this signal is proportional to the Hydrogen content of the particular sample.

The central processing unit calculates the Hydrogen content to an accuracy of 0.01 ppm and displays the result digitally on the screen.

3.2.1.1 Reagent tubes

This reagent tubes (Fig.10 (b)) are filled with various chemicals to stop "impurities" such as water vapor and CO in the gas flow. The tubes 1 and 3 are used as a molecular sieve, the tube 2 is filled with Schuetze reagent for CO-oxidation, activated charcoal and glass wool.



Fig.10 (a): H-Mat

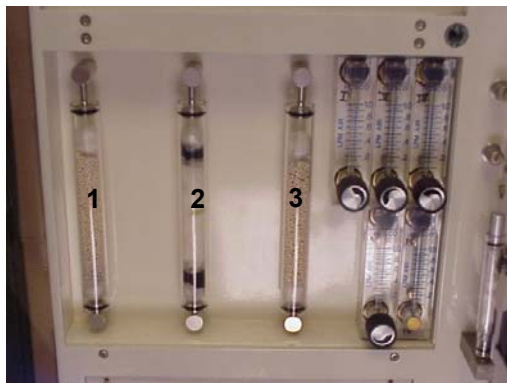


Fig.10 (b): Reagent tubes

The left molecular sieve (number 1 in Fig.10 (b)) is used to reference the N_2 to purify CO_2 and water vapor.

The test stream from the furnace contains nitrogen, hydrogen, CO and CO_2 . This stream is purified in a first tube number 2, where the Schuetze reagent to keep the moisture and CO turnover in CO_2 . All the CO_2 will then be recorded by the right molecular sieve (number 3 in Fig.10 (b)), and the measuring current only consists of nitrogen and hydrogen.

3.2.1.2 Thermal conductor sensor

The operation of this sensor is based on the thermal conductivity of gases and is used as a detector of hydrogen.

The upper meter indicates the bridge power again in our equivalent to 8.5 mA. The bottom meter gives us the change in voltage caused by a variation in the temperature of the gases entering the test cell.

The reference flow incorporates nitrogen, while the measuring current is a mixture of nitrogen and hydrogen. The more hydrogen the test current contains, the greater the difference in temperature between the reference flow and the flow measurement because of the large difference in thermal conductivity between hydrogen and nitrogen. This temperature difference is reflected in a change of voltage, reflecting the amount of hydrogen (ppm) can be determined.

3.2.1.3 Oven

The oven is the bottom of the cup holder in each analysis a new crucible of graphite inserted. Before we begin an analysis, the device is calibrated by using empty cups and reference materials. After sufficiently calibrated, a material inserted with a certain amount of hydrogen.

The oven of the H-mat ensures that the material is in the melt state at a temperature between 1000 ° C and 2500 ° C. When the material is melted, the hydrogen desorption is detected. A pump is used to ensure a vacuum above the melt. The amount of dissolved hydrogen in the melt is proportional to the square of the partial pressure of hydrogen. In this partial vacuum pressure to zero and thus the amount of dissolved hydrogen.

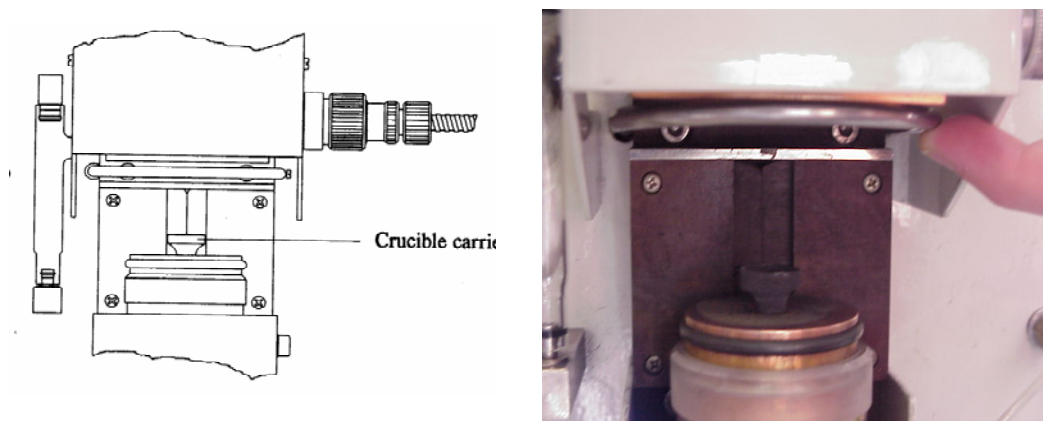


Fig. 11: H-Mat Oven

3.2.2 Universal Testing Machine INSTRON 5500R

Features:

- 250:1 force measurement range (i.e. use the load cell to down to 0.4% of full capacity with no loss of accuracy)
- Load accuracy of $\pm 0.5\%$ of indicated load
- 500 Hz synchronous data acquisition rate for all channels
- Hardware control panel for operator convenience
- Automatic transducer recognition for load cells and extensometers
- Bluehill® 2 software compatibility
- Extra height and width options available
- Second test space option
- Library of ASTM and ISO test methods
- Full CE compliance

MODEL 5500R

- 50 kN (11,250 lbf) capacity
- 0.001-500 mm/min (0.00004 – 20 in/min) speed range



Fig.12: Universal Testing Machine INSTRON 5500R

3.2.3 Scanning Electron Microscope, JEOL JSM-700F

The JSM-7001F, Thermal Field Emission SEM, is a platform for demanding analytical applications as well as those requiring high resolution and ease-of-use. The JSM-7001F has a large, 5-axis, fully eucentric, motorized, automated specimen stage, a one-action specimen exchange airlock, small probe diameter even at large probe current and low voltage, and expandability with geometry for EDS, WDS, EBSP, and CL. The specimen chamber handles specimens up to 200mm in diameter.



The JSM-7001F SEM also supports full integration of EDS, WDS, e-beam lithography, and an image database. Stage automation is standard with a 5-axis computer control of X, Y, Z Tilt and eucentric rotation.

3.2.4 EBSD Technique

Electron backscatter diffraction (EBSD) [12] is a technique for obtaining crystallographic information from samples in the scanning electron microscope.

In EBSD a beam of electrons is directed onto a tilted crystalline sample in a scanning electron microscope (SEM). The electrons undergo various interactions with the atoms in the crystal lattice and some of the electrons emerge from the sample. If a fluorescent phosphor screen is placed close to the

sample a pattern is formed on the screen because the intensity of the emerging electrons varies slightly with direction. This pattern is called a diffraction pattern and its appearance is very striking.

Unfortunately, there is no simple analogy in the everyday world for the physical phenomena of diffraction that causes the patterns. The symmetry and appearance of the pattern is related intimately to the crystal structure at the point where the beam meets the sample. If the crystal rotates (in other words its orientation changes) the diffraction pattern will be seen to move. If a different type of material is placed under the beam, the diffraction pattern will change completely. So the diffraction pattern can be used to measure crystal orientations and to identify materials.

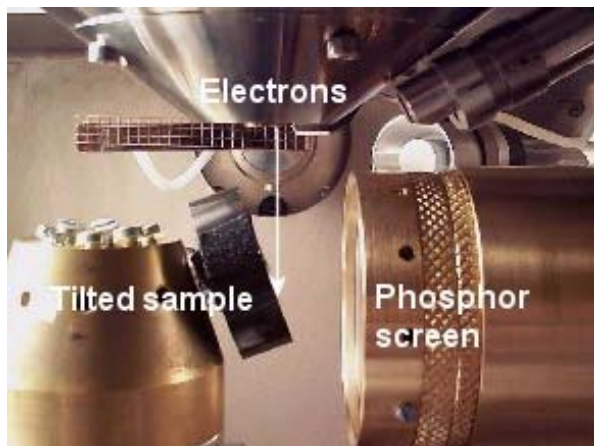


Fig 13: View showing tilted sample and phosphor screen in SEM chamber.

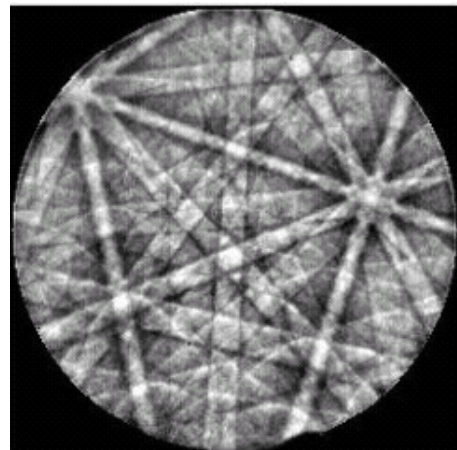


Fig 14: Electron backscattering diffraction pattern from nickel

Microstructural analysis with EBSD

Microstructure is important because it determines many of the physical properties of materials. For example, grain size can influence tensile strength and the properties of grain boundaries can determine the way in which materials fracture. Optical microscopy and scanning electron microscopy are both used to examine microstructure. Polishing and chemical etching can reveal the positions of grains and grain boundaries. However, these techniques may not reveal all the grains. This is where EBSD comes in - it measures crystal orientation and so must be able to show unambiguously the position of all grains and grain boundaries.



Fig.15: A scanning electron micrograph of the microstructure of a steel sample

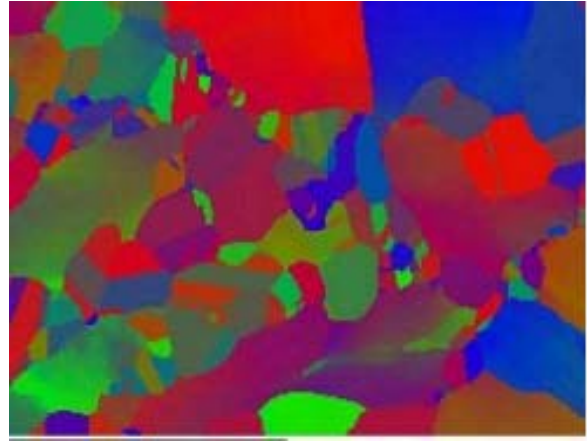


Fig.16: crystal orientation map from the same sample. Similar orientations are in similar colors

EBSD is used to form crystal orientation maps by scanning the electron beam over the sample and measuring the orientation from the diffraction pattern at each point. In a crystal orientation map points with similar crystal orientations are shown in similar colors. In these maps a grain is a region of the sample where the crystal orientation is the same within a certain orientation angle tolerance. The maps can be processed to show with certainty the position of all the grains and grain boundaries.

EBSD is unique in that it provides a link between microstructure and crystallography. It complements conventional analysis techniques by providing definitive information about the crystal orientations present in the sample.

4 H-CHARGING & SOLUBILITY

This chapter is divided in four points, i.e. the sample geometry, the charging method, the type of electrolyte and the optimal charging parameters.

4.1 Sample geometry

The sample geometries used for determinate the total H-content is as follows:

– HCT 800C

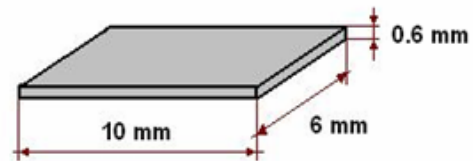
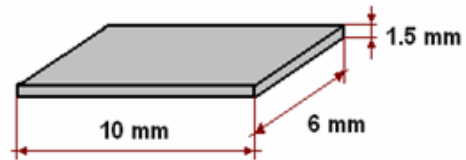
– S700 MC

– PURE IRON 0% deformed

– PURE IRON 15% deformed

– TRIP700 0% deformed

– TRIP700 17% deformed



The samples dimensions are specifically $(6 \times 10) \text{ mm}^2$ to allow easy introduction inside the graphite capsules (fig. 17), used for to measure the total hydrogen content (H-ppm) in the materials with the *H-mat* machine.



$\varnothing = 11.20 \text{ mm}$
Height = 14.20 mm

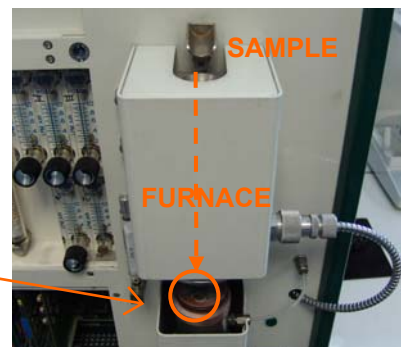
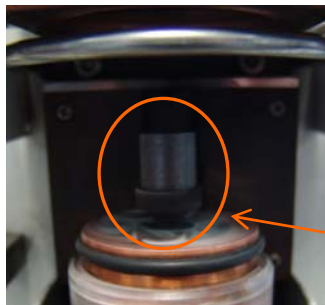


Fig. 17: Graphite Capsule

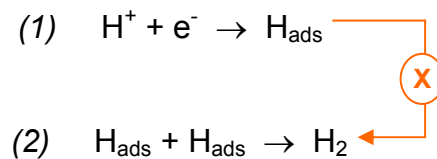
Fig. 18: Graphite Capsule holder

Fig. 19: H-mat furnace Schema

The geometry of the samples for the tensile testing are explained in the respective chapter of tensile testing (5.2).

4.2 Charging methods

As the intention is to charge a steel substrate (sample) with hydrogen, and for that a high surface coverage of the substrate with H_{ads} (1) is needed;

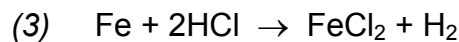


Therefore H_2 (2) recombination has to be prevented. Second reaction step has to be blocked as it causes a bubble wall on the sample surface preventing the hydrogen entry into the material and as more H_2 , less H available for entry. This can be done by adding a “poison” for the recombination reaction to the electrolyte: e.g. Arsenic, Thiourea [4]

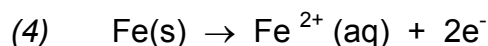
To charge the materials with hydrogen three methods have been applied:

i. Chemical method

The chemical method involves immersing the sample in a glass recipient filled with HCl 37% for specifies times, causing a chemical redox reaction (3) on the surfaces of the sample. This reaction generates the hydrogen in the atomic form (H_{ads}) (1) and also in gas state (H_2) (5) [2]:



When two H^+ ions collide at the surface of the steel electrode, an iron atom releases two electrons to the H^+ ion. The iron atom enters the solution as an Fe^{2+} ion. The oxidation half-reaction is:



Each H^+ from HCl solution captures one electron. These two ions form a Hydrogen molecule. The reduction half-reaction is:

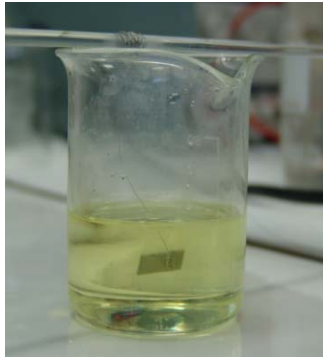
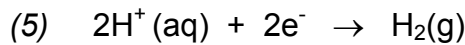


Fig. 20: Sample in HCl 37% solution

Sample preparation for chemical method:

- Grinding the surfaces with grind paper P120
- Cleaning with distilled water and acetone to have a surface free of oxide and dirt.
- Hanging the samples on a metallic wire to avoid the contact with the bottom of the glass to have an homogeneous distribution of the reaction on all surfaces

After the charging, the samples were cleaned again with distilled water and acetone to remove the rest of the HCl on the surfaces and dried with paper.

ii. Galvanostatic method

The galvanostatic technique is the more common technique in which a constant cathodic current is maintained in the circuit containing the test specimen. The constant current produces an electrode potential that changes with time as the concentration of the environment changes as the result of precipitation of reaction products and gas evolution [3].

Sample preparation and montage done to implement the galvanostatic method:

- Grinding the samples surfaces with grind paper P120
- Cleaning with distilled water and acetone to have a surface free of oxide and dirt
- Welding the sample to a metallic wire

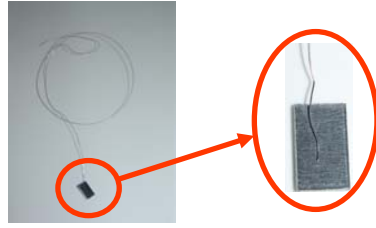


Fig. 21: Welded sample

- Introducing the wire in the plastic holder and place it in the cell ensuring that the sample is located exactly between the two platinum anodes.



Fig. 22: Detail of the sample between the two platinum disks

- Filling a glass recipient with the electrolyte until cover the sample and platinum disks.



Fig. 23: Overview of the cell ready

- To realize the connections between the galvanostatic source and the cell:

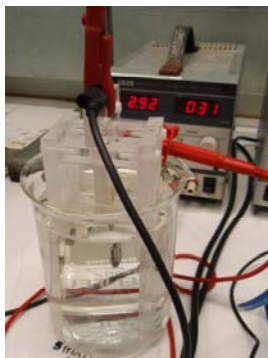


Fig. 23a: Shows the cell connected to the galvanostatic source

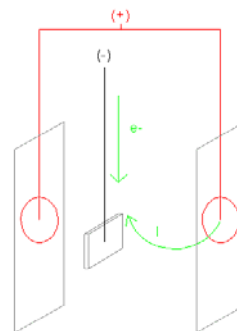
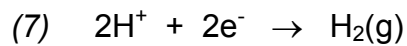
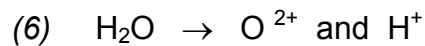


Fig. 23b: Working schema of the galvanostatic method in the cell

The two platinum disks located on the walls of the cell structure are acting as the anodes and the sample as the cathode. The cathode (sample) is connected to the ground or negative pole, and the anodes (Pt disks) are connected to the positive pole on the galvanostatic source.

When switching on the power source, flow from the anode to the cathode. It generates *redox* reactions on the material and electrolyte solution causing oxidation on the anode electrode (6) and reduction on the cathode electrode (7) which induces the adsorption and absorption of Hydrogen into the material.



After the necessary time, the sample is cleaned with distilled water and acetone to remove the rest of electrolyte solution on the surfaces. (Sometimes is needed to grind the surface after charging to remove deposits from the surface)

iii. Potentiostatic method

The potentiostatic technique maintains the electrode potential of the test specimen constant versus a standard reference electrode. The current path is maintained in the circuit containing the tension test specimen and the counter electrode, but it is not kept constant. Instead, the current is allowed to float and become the dependent variable. With this technique it is imperative that a reference electrode be used in the electronic circuit for continuous monitoring of the electrode potential of the test specimen [3].

Sample preparation and montage done to implement the potentiostatic method:

The sample preparation and the montage are exactly the same as for the galvanostatic method except for the reference electrode that must be used in potentiostatic method:

- To control the potential of corrosion a Saturated Calomel Electrode (SCE) with a reference voltage of +240 mV is used.



Fig. 24a: SCE reference electrode

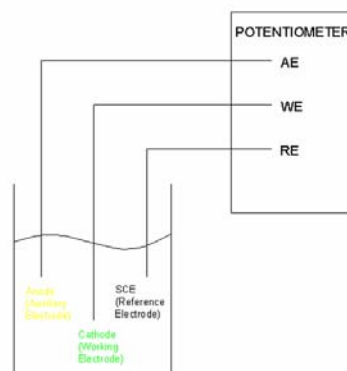


Fig. 24b: Schematic of the connections for potentiostatic method

After the charging, the sample is cleaned with distilled water and acetone to remove the rest of electrolyte solution on the surfaces.

4.3 Electrolyte solutions

The electrolyte is a medium that conducts an electric current when is dissolved in a solvent, usually water. Electrolytes are composed of positively charged species, i.e. “cations”, and negatively charged species, i.e. “anions”. For this study are needed electrolytes for the H^+ cation formation to achieve the Hydrogen adsorption.

Several types of compounds have been found to promote the entry of hydrogen into metals from both liquid and gaseous environments. The same types of compounds are known to poison catalysts for hydrogenation reactions in heterogeneous systems. Promoters and poisons show their full effect at relatively very low concentrations. Among the species found to promote hydrogen entry are [7]:

- 1) Certain compounds of the following elements:
 - Phosphorus, arsenic, and antimony belonging to the V-A periodic Group, sulfur, selenium, and tellurium belonging to the VI-A periodic Group.
- 2) The following anions:
 - CN^- (cyanide), CNS^- (rhodanide), and I^- (iodide).

3) The following compounds of carbon:

- CS_2 (carbon sulfide), CO (carbon monoxide), CON_2H_4 (urea), and CSN_2H_4 (thiourea).

Different electrolytes were used to see the effect on H-charging of the various steels.

The electrolytes used among the study were:

- 0.5 g As_2O_3 + 0.25 g HgCl_2 + 60 ml H_2SO_4 / l H_2O [4]
- 10 g CSN_2H_4 + 4 g NaOH / l H_2O [5]
- 5 g CSN_2H_4 + 4 g NaOH / l H_2O [5]
- 5 g CSN_2H_4 + 0.5 M H_2SO_4 / l H_2O [6]
- 1 g CSN_2H_4 + 0.5 M H_2SO_4 / l H_2O [6]
- 3.5 wt% NaCl in H_2O [9]

4.4 Results and discussion

4.4.1 Chemical method

A. H-discharging charts:

For the chemical charging method with HCL 37%, the effect of the discharging time was studied. The samples were charged during 10 and 30 minutes and, from 20 and 7200 seconds after charging, the H-content was analyzed with the H-mat.

The procedure can be better understood seeing the following schematic graph:

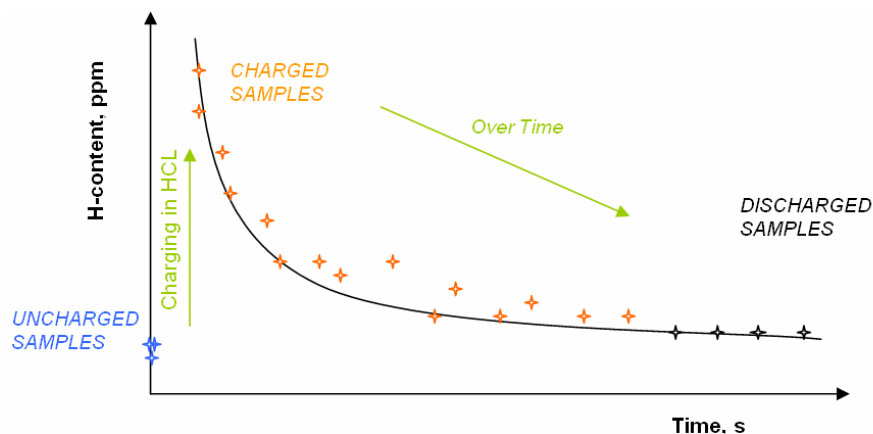
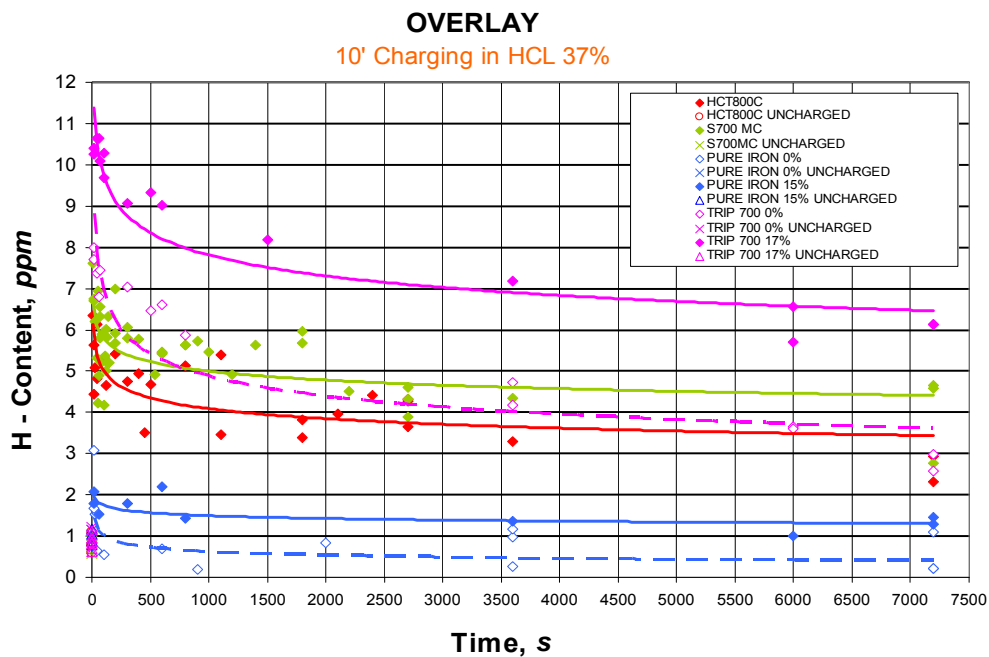


Fig. 25: schematic discharging time curve

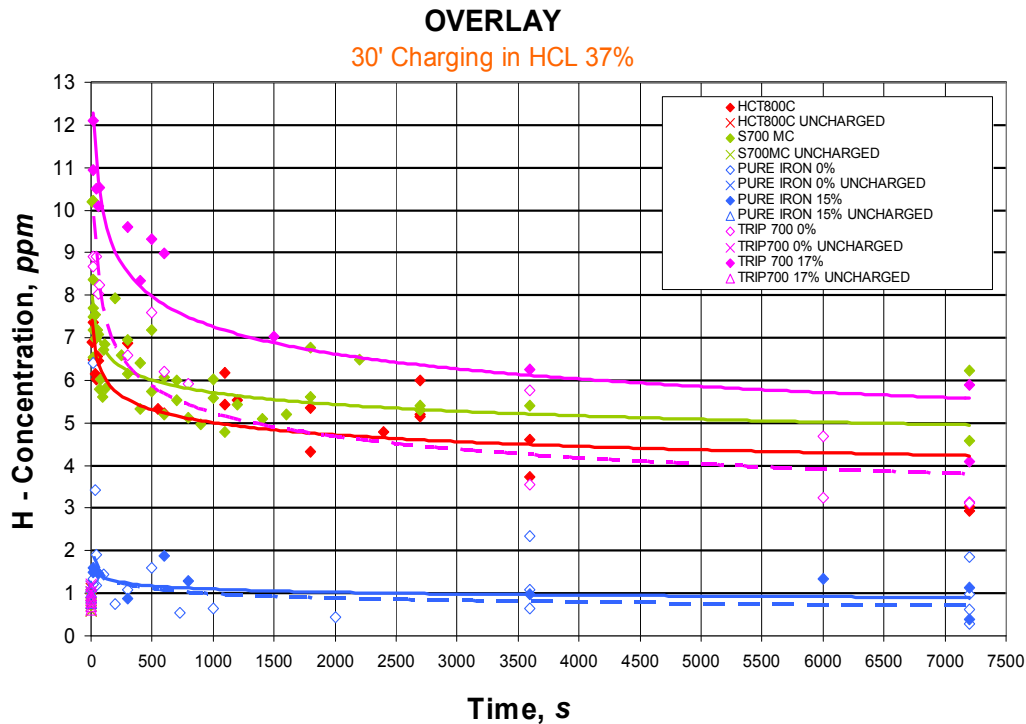
The blue points represent the samples without charge. Just after charging during 10 or 30 minutes, the H-content is represented with the orange points and with the passing time, the samples are diffusing out the hydrogen until reach the black points, where the H-content becomes almost constant, what means the material has discharged the most part of the hydrogen that was introduced, although part of it is trapped on the microstructure defects (dislocations, traps, etc).

Each material will have a different curve permitting to identify the H-discharging behavior e.g. which material adsorbs more hydrogen, which material diffuse faster and with which tendency, the effect of the microstructure, etc.

The following graphs show the H-discharging curves for the different materials.



Graph 2: Overlay of H-discharging time after 10 minutes ucharging on HCL 37%



Graph 3: Overlay of H-discharging time after 30 minutes charging on HCL 37%

B. Effect of charging time:

The differences between the two charging times (10 and 30 minutes) are not significant. Comparing the materials for each charging time, all of them (except pure Fe 15 % deformed) charging during 30 minutes are around 1 H-ppm higher than the ones 10 minutes charging.

The different charging times in HCL 37% don't have an essential influence on the H-discharging effect.

C. Effect of the microstructure:

The microstructure of the materials has a big influence on the H-diffusivity. The results can be seen on the previous graphs where each material has a different H-content after being charging in the same conditions and times. TRIP700 and PURE FE are the ones who have the highest and lower H-content, respectively, and it could be due to the microstructure.

The solubility of hydrogen in iron depends on the crystalline structure, and changes as the result of phase transitions. Hydrogen has a higher solubility in γ -Fe than in α -Fe.

The ferritic microstructure (α) has the property of the low solubility and fast diffusion property for hydrogen. The austenitic microstructure (γ) has the opposite property, high solubility and slow diffusion.

TRIP700 0% deformed contains a ferritic, retained austenitic (γ) and bainitic microstructure being the answer why is charging more than Pure Fe, that has an α -Fe matrix.

Another reason why TRIP700 is higher in H-content is because the grain boundaries, dislocations and phases boundaries retains the hydrogen and provoke a diminution of the H-diffusion.

D. Effect of the deformation:

When the TRIP700 is deformed (to 17% for this study), the retained austenite becomes martensite (α') staying the bainitic and ferritic phases. Also, to deform the material generates dislocations into the material that are traps for the hydrogen. With the Pure Fe happen the same, when is deformed (to 15% for this study) generates H-traps.

This is the reason why the curves of the deformed TRIP and Pure FE materials are higher than the non-deformed, the hydrogen can be adsorbed in more quantity and diffuse less because the traps generated during the deformation process.

The chemical method advantages/disadvantages are:

Advantages:

- possible to H-charging easily on the samples

Disadvantages:

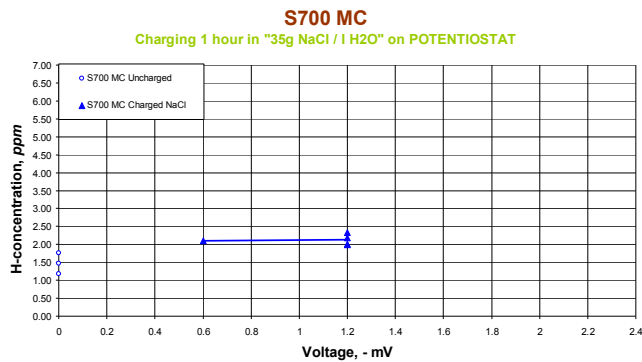
- is not possible to control the amount of the entering H-ppm
- the reactions occurring during H-charging between the steel and HCL causes an important decomposing of the material.

Basically for these two reasons, this method was not chosen for the future tensile testing.

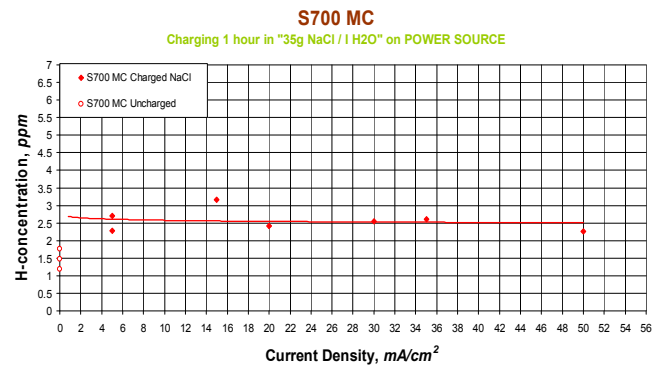
4.4.2 Potentiostatic & galvanostatic method

For the potentiostatic and galvanostatic method, S700 MC steel was used using two different electrolytes.

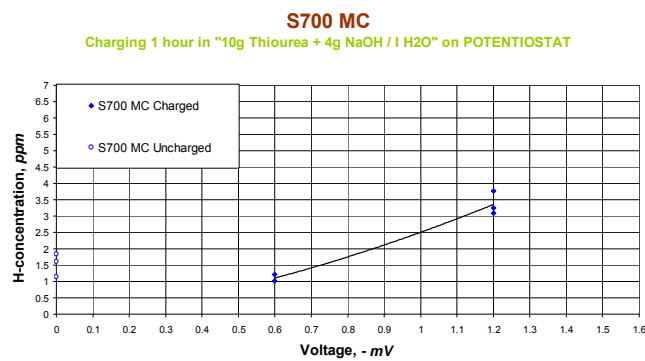
For potentiostatically charging curves (Graph 4a & 4c) there are just two voltage points represented, at -0.6mV and -1.2 mV (the reason is because on the references confines this voltage rang for hydrogen charging [8-9]). The correlation between these two voltages with a current value on the galvanostatic method is 0.1 and 1 mA/cm² for -0.6 and -1.2 mV respectively.



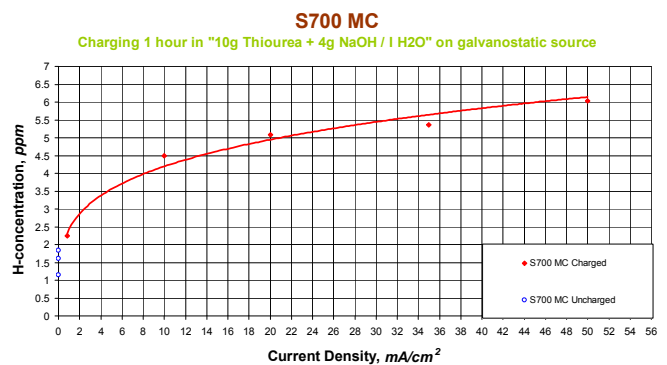
Graph 4a: S700 MC charged Vs SCE potentiostatically with "3.5 wt% NaCl" solution



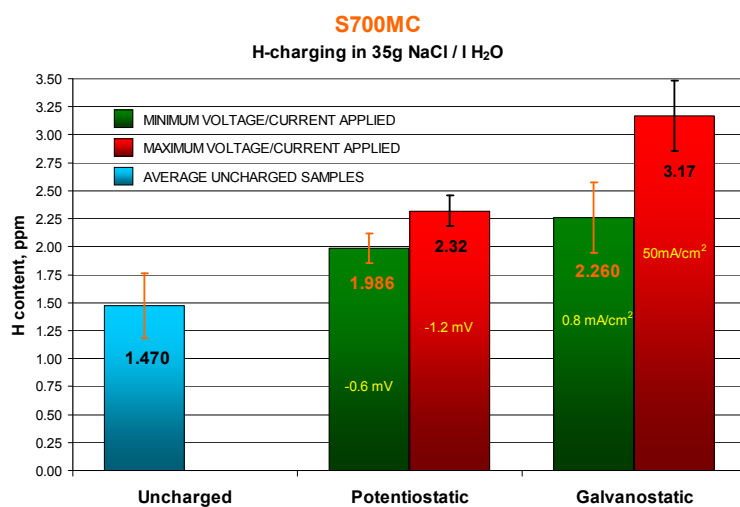
Graph 4b: S700 MC charged galvanostatically with "3.5 wt% NaCl" solution



Graph 4c: S700 MC charged potentiostatically with "10g Thiourea + 4g NaOH" solution



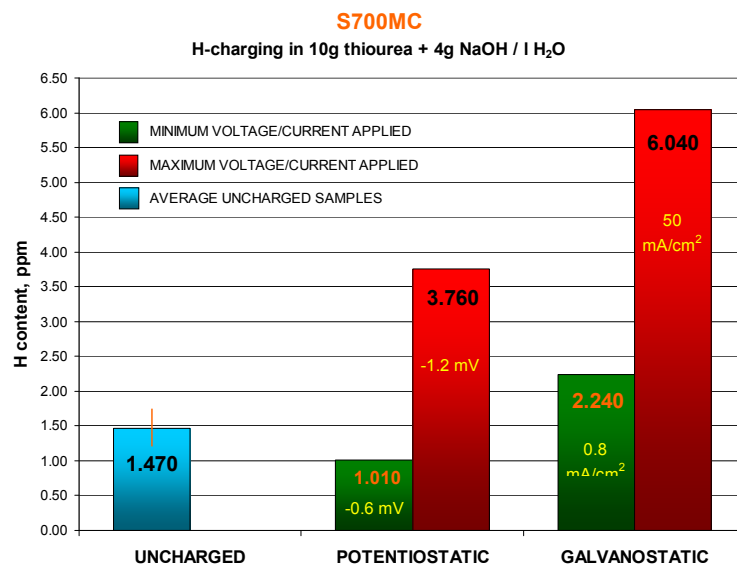
Graph 4d: S700 MC charged galvanostatically "10g Thiourea + 4g NaOH" solution



Graph 5: Comparison of the H content for each charging method

Graph 4a & 4b show the results of H-charging in 35g NaCl / l H₂O solution, applying potentiostatic and galvanostatic methods. When is applied the lowest or highest current/voltage value (depending of the method) the H-content doesn't changes in excess (Graph 5), what means this electrolyte is not valid to reach the aim of the study

therefore is not going to be used on the future tensile testing.

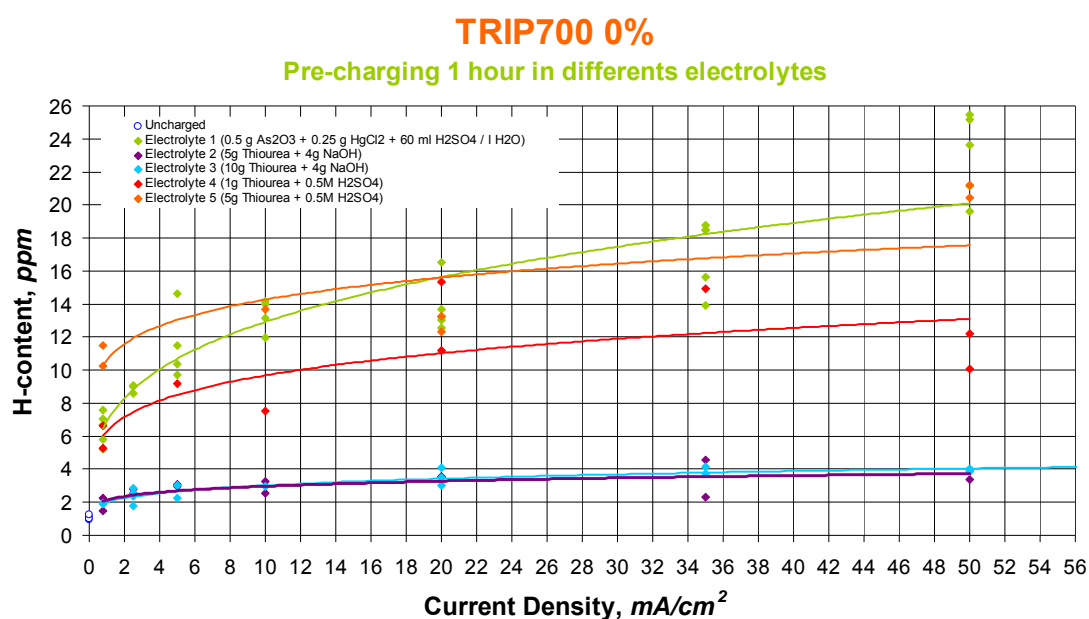


Graph 6: Comparison of the H content for each charging method

Graph 4b & 4d shows the results for the 10g Thiourea + 4g NaOH / l H₂O solution. This time the material is being higher H-charged. As the maximum voltage applicable with potentiostatic method corresponded around to 3 ppm of charged hydrogen, and the

galvanostatic method was selected for the future tensile tests. Indeed, The Graph 6 gives an easy way to understand how different are acting the two different electrolytes. galvanostatic method gives more charging options (from 2 to 6 H-ppm).

Once the optimal method is known for use on future experiments, TRIP700 (0% deformed) steel was tested with different electrolytes for obtain the optimal one which gives more options on the H-charging.



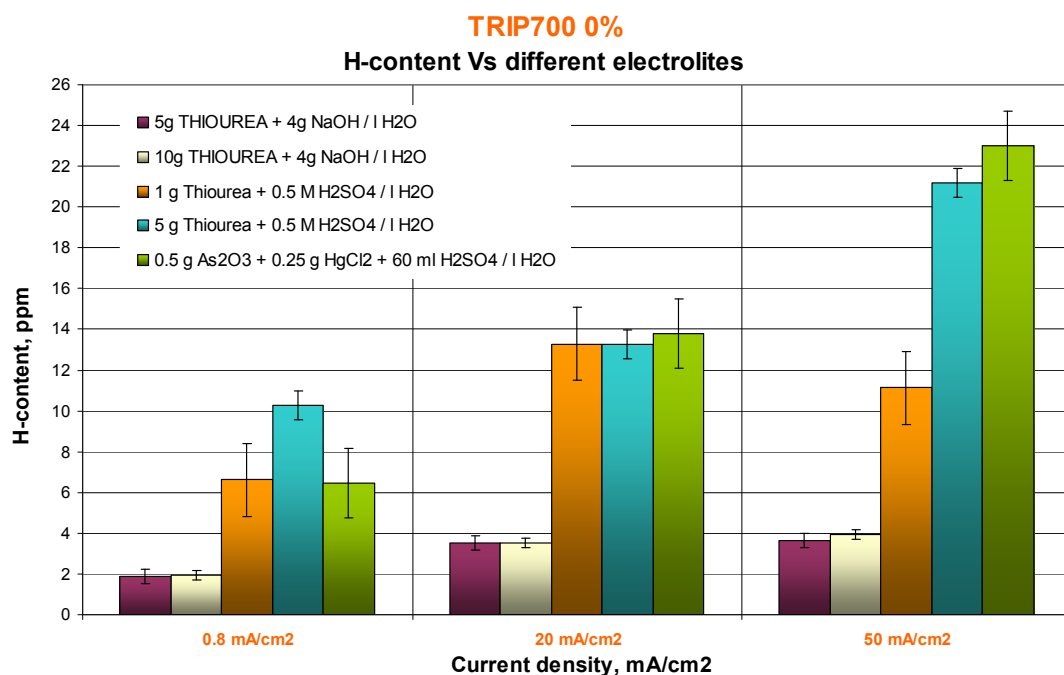
Graph 7: Overlay of H-concentration Vs current applied for TRIP700 in different electrolytes

Must be taken into account these different electrolytes were prepared and tested in a chronologic order during this study. It means for some tensile testing in the following chapters, will be used different electrolytes that, maybe, weren't the optimal in each case.

The previous chart (Graph 7) shows the H-charging effect on TRIP700 steel with five different electrolytes. All of them are commented in chronologic order of using as follows :

- “0.5g As_2O_3 + 25g HgCl_2 + 60 ml H_2SO_4 ” electrolyte was the one in use before start this study, but for healthy reasons has been searched for new ones on different bibliographies.
- were used the “thiourea + NaOH” electrolytes that in comparison with the first one, the H-content was much more lower allowing a maximum H-concentration value of 4 H-ppm either varying the amount of thiourea per liter of solution.
- For last, were tested the “thiourea + H_2SO_4 ” electrolytes, reaching values of H-content around the first electrolyte.

On the following graph (Graph 8), is shown, in a form of comparison, the H-content for 3 different applied current densities with the five different electrolytes for the same material:



Graph 8: Overlay of H-concentration Vs current applied for TRIP700 in different electrolytes

Doesn't give more information than the previous curves graph, but let more clear how the two electrolytes with NaOH are the ones that are charging lower, reaching a maximum value of 4 H-ppm when, for the same current density ($50\text{mA}/\text{cm}^2$), and replacing the 4g NaOH for 28ml (0.5M) of H_2SO_4 is reached 21 H-ppm.

The arsenic containing electrolyte is comparable with the 5g Thiourea + sulfuric acid due to the closed values reached. For that reason, was replaced the arsenic electrolyte for that one for future works.

5 DEVELOPMENT OF A TENSILE TESTING METHODOLOGY

This chapter will explain the different types of tensile testing on various steels and the methodology followed for each one to observe the effects of hydrogen on mechanical properties when stress is applied.

Depends on the test type applied, different samples geometries and preparation were used and will be defined in their respective test type chapter.

5.1 Standard Tensile Testing in air

The standard tensile testing provides information on the strength and ductility of the materials under uniaxial tensile stress in air. This test was done on the reference samples (without H-charging process applied) to compare with the hydrogen charged ones.

The tests were done according to the guidelines of the “Tension Testing of Metallic Materials” standard [10].

In the following chapters, the references curves are represented together with the H-charged samples curves to facilitate the comparison.

5.2 SSRT: Slow Strain Rate Testing

Slow strain rate testing, also known as constant extension rate testing (CERT), is a slight modification of the standard tension test. A more detailed description of this test method is given in ASTM G129 [11]. The benefit of SSRT testing is that it produces a result in a reasonably short time depending on strain rate. It also reduces incubation time to the onset of cracking in susceptible materials.

The material used for the SSRT was S700 MC and the sample dimensions were in *mm*:

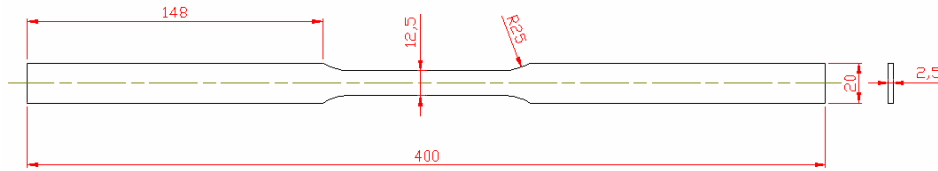


Fig. 26: S700MC sample dimensions for tensile testing

A. sample preparation:

- The edges of all the samples tested in the electrolytic cell were rounded with an special equipment in order to avoid defects in the corners which could help the crack initiation (Fig. 27a)
- The radius has a value of approximately 0.2mm
- The decrement of cross sectional area has not been considered due to its small value.



Fig. 27a: Rounding a sample's edges

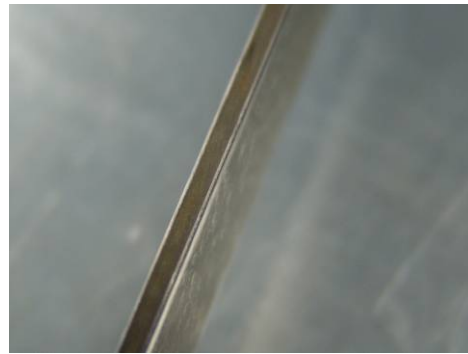


Fig. 27b: Detail from the rounded edges

- The samples were polished with grind paper P120, cleaned with distilled water and acetone to obtain a homogenous surface without surface contaminants.



Fig. 28: Grinding a sample

- To allow electrochemical charging with H, a glass cell was mounted on the tensile machine around the sample. This cell contains two platinum

flat electrodes which act as anode; the tensile sample acts as cathode.
(Fig. 29)

- Charging solution: 10g Thiourea + 4g NaOH / L H₂O



Fig. 29: Electrolytic cell

It was decided to test the samples with a hydrogen concentration of around 3.5 ppm.

To determine the current density, the graph shown in *graph 4d* was used. From this graph, it is clear that the current density of 4 mA/cm² must be applied.

The corresponding total current was calculated as follows:



$$4 \frac{\text{mA}}{\text{cm}^2} \times 65.50 \text{cm}^2 = 262 \text{mA}$$

$S = 65.50 \text{ cm}^2$ = The sample surface in contact with the electrolyte

Fig. 30: The orange lines delimit the surface in contact with the electrolyte.



To introduce 3.5 H-ppm is needed to apply 262mA on the tensile sample

B. Testing procedure:

The purpose of these tests was:

- to evaluate the effect of different pre-charging times
- to evaluate the effect of different strain rate

Due to the impossibility of using an extensometer inside the electrolytic cell, a reference sample (tested in air applied on it) was used to measure the strain as a function of the crosshead displacement. (Fig. 31)

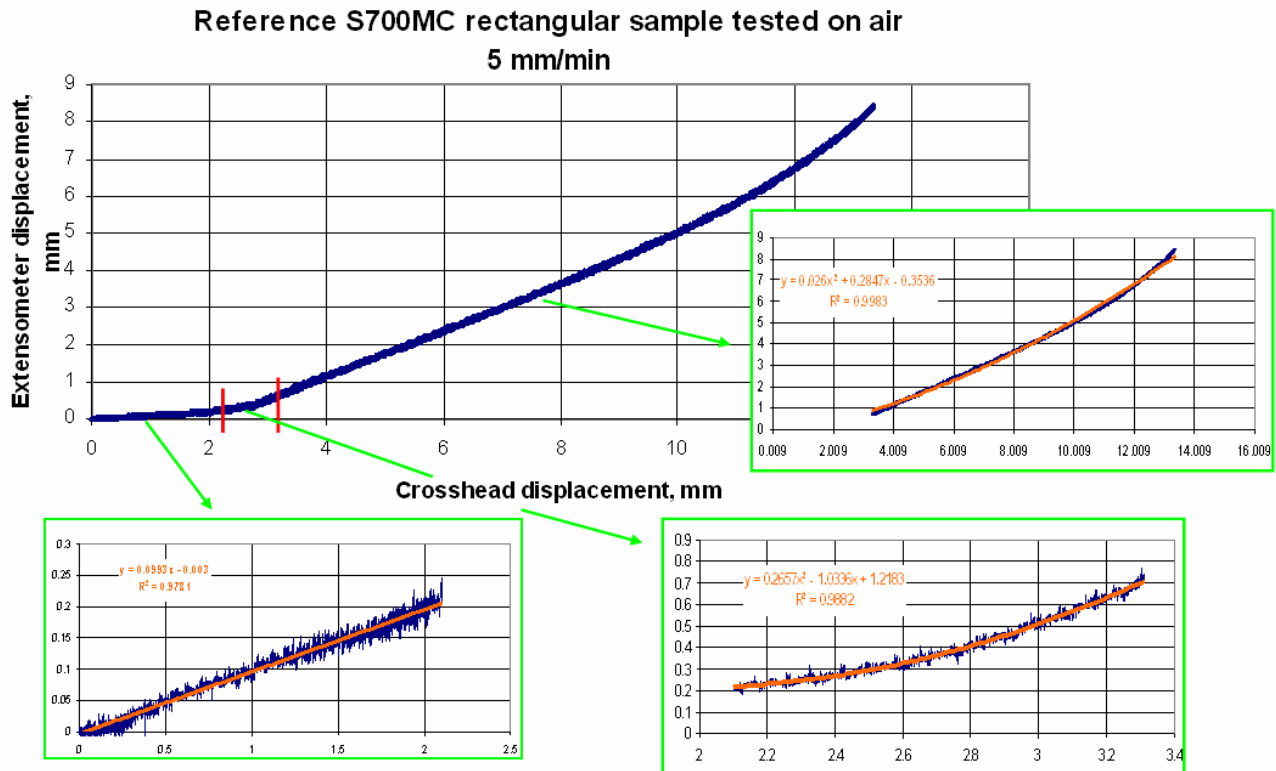


Fig. 31: Extensometer-Crosshead relation for S700MC

C. Strain rate effect:

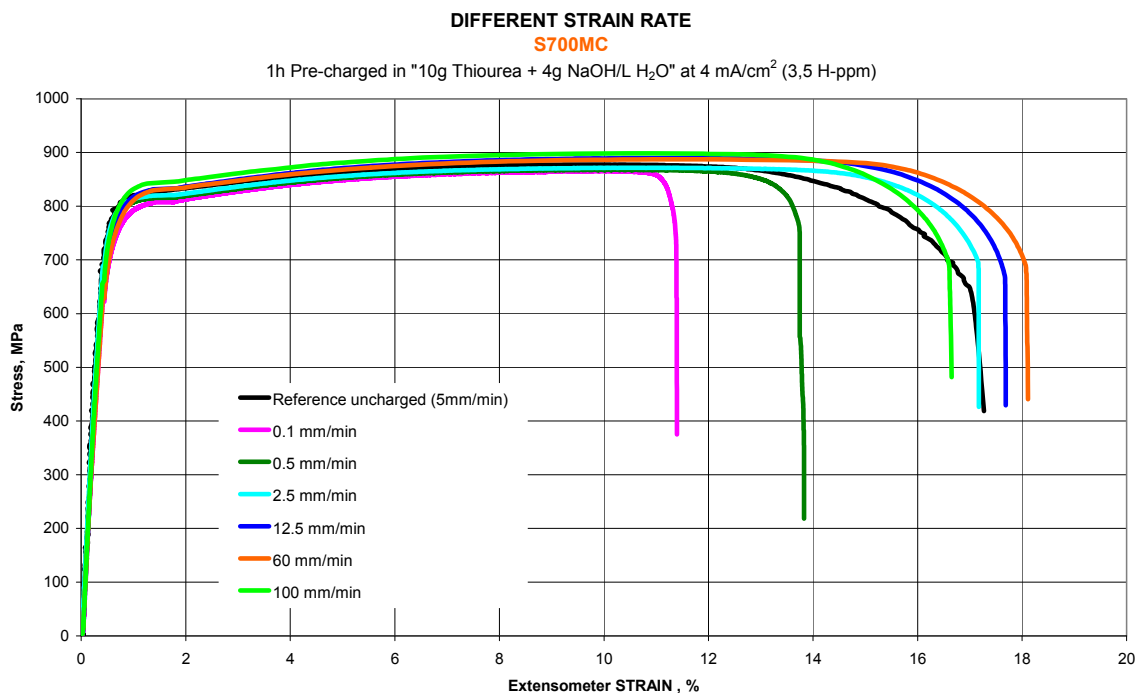
A reference sample was tested at 5mm/min in air using an extensometer. Subsequently the co-relation was made between the extensometer and crosshead displacement (Fig. 31) to recalculate the tensile data obtained for the charged samples.

6 samples were tested with the same pre-charging conditions:

- 1 hour pre-charging + continued charging during the test.
- Electrolyte: "10g Thiourea + 4g NaOH / L H₂O "

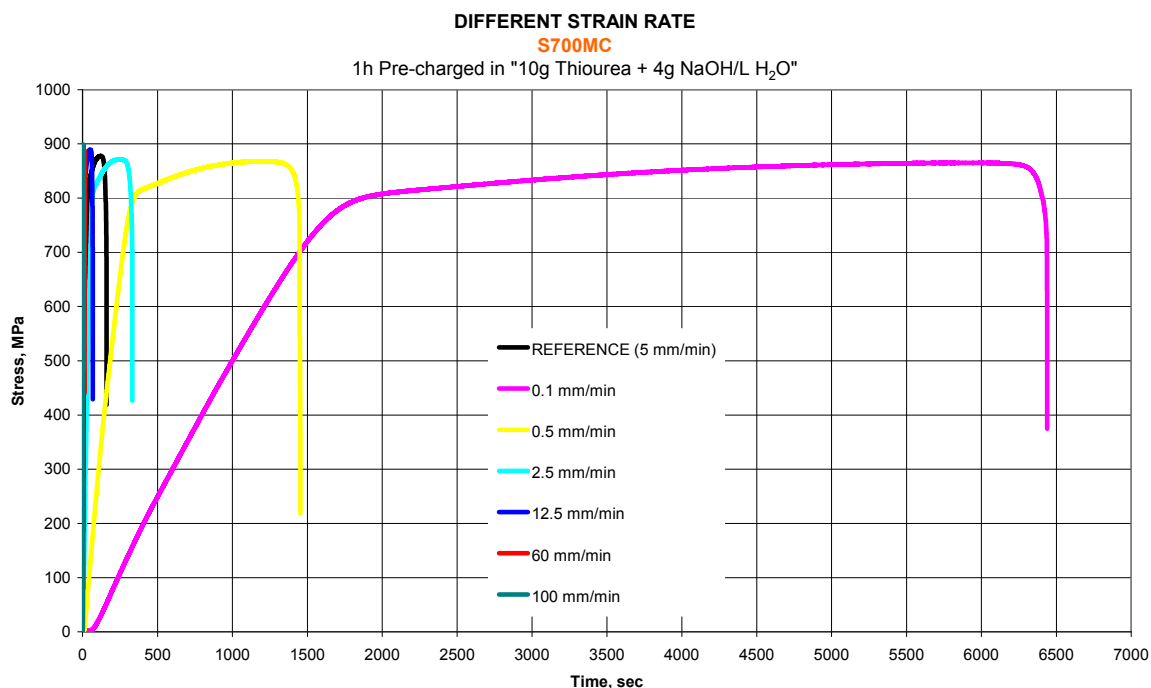
6 strain rates were tested 0.1, 0.5, 2.5, 12.5, 60 and 100 mm/min.

The following graph shows the results obtained:



Graph 9: S700MC different strain rate "Stress-Strain"

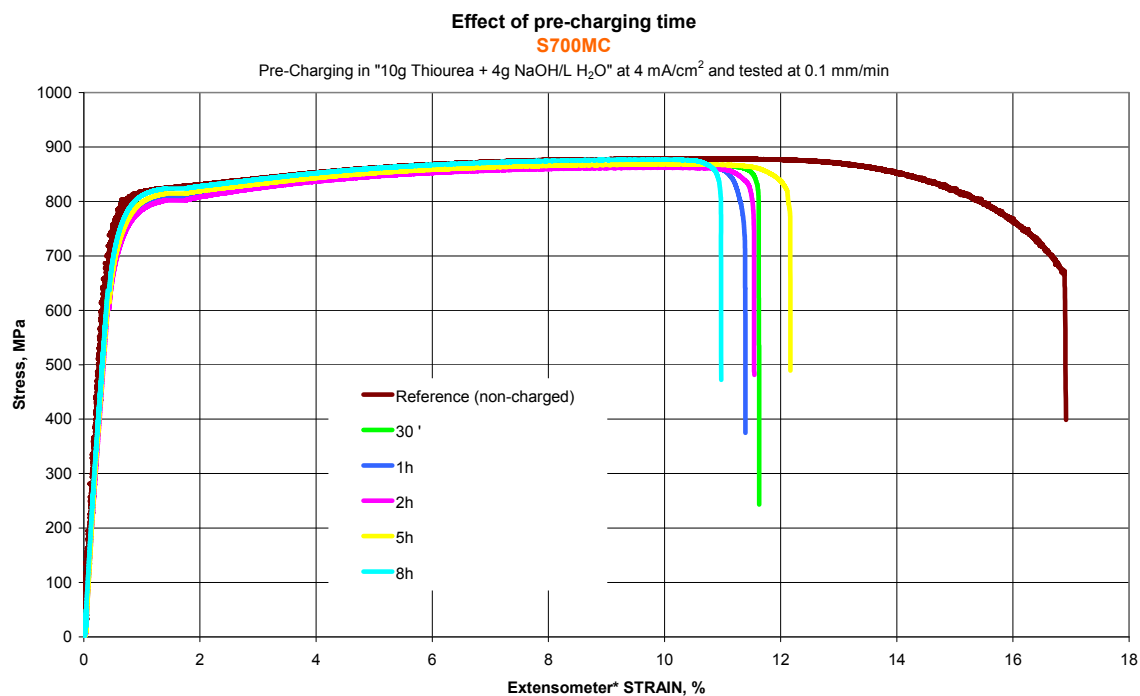
The curves (Graph 9) illustrate a reduced ductility for the slowest strain rates. This confirms that lower strain rates allow the entry the maximum amount of hydrogen into the material due to the longer testing time for low strain rates and. Apparently, seems correct to conclude that the H-charging time has a significantly effect on the results (Graph 10), but this will be detailed on the following sub-chapter "*D. Effect of pre-charging time*".



Graph 10: S700MC different strain rate "Stress-Time"

D. Effect of pre-charging time:

A reference sample was tested in air at 0.1 m/min. This strain rate was then applied for all tests with in-situ charging. The time of pre-charging was varied: 0.5, 1, 2, 5 and 6 hours. The electrolyte used was again “10g Thiourea + 4g NaOH / L H₂O”. The following graph shows the results obtained:



Graph 11: S700MC different pre-charging times “stress-strain”

The results show no clear effect of the pre-charging time on the rupture strain:

The rupture strain points for the different pre-charging times are not the expected ones. The samples that were pre-charged longer times, were expected to break at lower strain values, more brittle than the ones pre-charged for shorter times. It means that the reference sample tested in air, which had no H-charging, should have the highest rupture strain value, and decreasing on the strain axis direction followed by the one pre-charged 30', after 1 hour, 2h, 5h and arriving to the most brittle sample: the one pre-charged 8 hours.

The curves obtained didn't show that expected behavior, all the samples have broken at the same strain level of 11 ~ 12 % meaning the pre-charging time doesn't influence on the losing of ductility of the material.

CONCLUSION SSRT:

- This method of testing reveals hydrogen effect on the results
- Contradiction on the H-charging time influence:
 - for different strain rates, the time has a notable influence on the losing ductility.
 - for the same strain rate but different pre-charging times doesn't have almost any influence.

5.3 Incremental Step Loading Technique

This method is extracted from the standard test method “Measurement of Hydrogen Embrittlement Threshold in Steel by Incremental Step Loading Technique” [8] and establishes a procedure to measure the susceptibility of steel to a time-delayed failure by hydrogen. It does so by measuring the threshold for the onset of subcritical crack growth using standard fracture mechanics specimens or irregular-shaped specimens such as notched round bars. The applied stress-time curve is shown in the *graph 12* and is explained further.



Fig. 32: Notch detail of a S700MC round sample

This method measures the load necessary to initiate a subcritical crack in the steel at progressively decreasing loading rates.

The test is performed in a controlled environment, to measure the effect of hydrogen introduced into the steel as a result of external sources of hydrogen.

The material used for this test was S700MC and the sample dimensions are (mm):

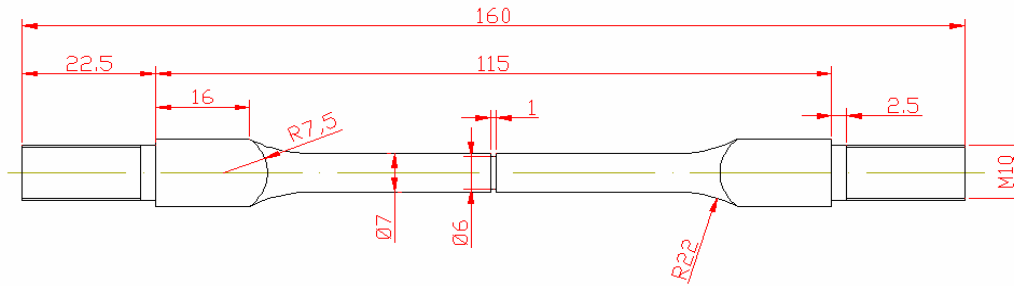


Fig. 33: S700MC round notched sample dimensions for tensile testing

The heads of the sample are threaded to add an extension on each head, which allows to fix the samples on the gripping devices of the tensile machine.

Apparatus:

- **Testing Machine:** Universal Testing Machine INSTRON 5500R {A1.2}
- **Test environment:** 10g Thiourea + 4g NaOH / L H₂O (~3.5 ppm of charged H)
- **Galvanostatic control:** The intensity to apply to the electrolyte can be controlled directly from the power source without needing a reference electrode. Depending the current applied is entering different amount of hydrogen into the steel, ranging from 0.0 to 4.0 A.

It was decided to test the samples with a hydrogen concentration of 3.5 ppm, which means the current density of 4 mA/cm² must be applied. The total applied current was calculated as follows (taking into account the contact area between sample and electrolyte):

Sample preparation:

- The samples were cleaned with distilled water and acetone
- The extensions were mounted on the samples.
- The sample was introduced into the electrolytic cell which was then filled with the electrolyte.
- Pre-charging during 1 hour before the start of the test and in-situ charging during the test.



$$4 \text{ mA/cm}^2 \times 35 \text{ cm}^2 = 140 \text{ mA}$$

$$S = 35 \text{ cm}^2$$

Fig 34:: The orange lines delimit the surface in contact with the electrolyte.

→ To introduce 3.5 H-ppm is needed to apply 140 mA on the tensile sample

Testing procedure :

- A reference test (ASTM E-8) to rupture was done to establish the maximum fracture load (P_c) in air.
- Another sample P_{i1} was tested with H-charging by applying an stepwise load increments under displacement control in tension, programmed to attain P_c .
- Another sample was tested using stepwise load increments to attain P_c at a slower loading rate, by using the same load increment and doubling the time increment. This load sequence will establish the value designated as P_{i2} .
- Subsequent specimens are tested at progressively decreasing loading rates to attain P_c . This testing sequence will continue until a significant drop in load is detected that will establish the value designated as e.g. P_{i3} .

It is suggested that with the subsequents tests the time increment is doubled, only for stress values in excess of $0.5P_i$. The procedure shall be continued until an invariant value (P_{th}) is obtained.

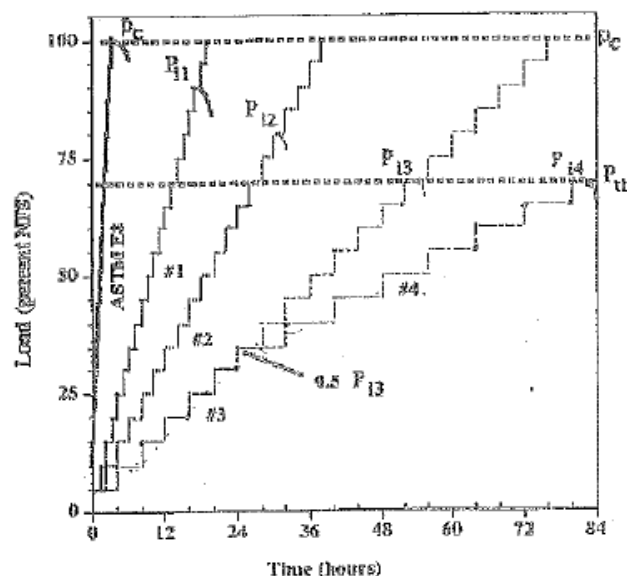


Fig. 35: Schematic of suggested protocol for a step loading profile to determine threshold

To program these steps, the following step profile was applied:

Test Number of Steps ($\pm 5\%$ Accuracy) / % Pc/ Time increment (h).

- For specimen #1 :
 - $20 / 5 / 1 = 20 \text{ steps} / 5\% \text{ Pc} / 1 \text{ hour}$
- For specimen #2:
 - $20 / 5 / 2 = 20 \text{ steps} / 5\% \text{ Pc} / 2 \text{ hours}$

...

Results

The reference sample gives a value of maximum tensile stress of 820 MPa (on the notched geometry). After that it is possible to program the rest of steps:

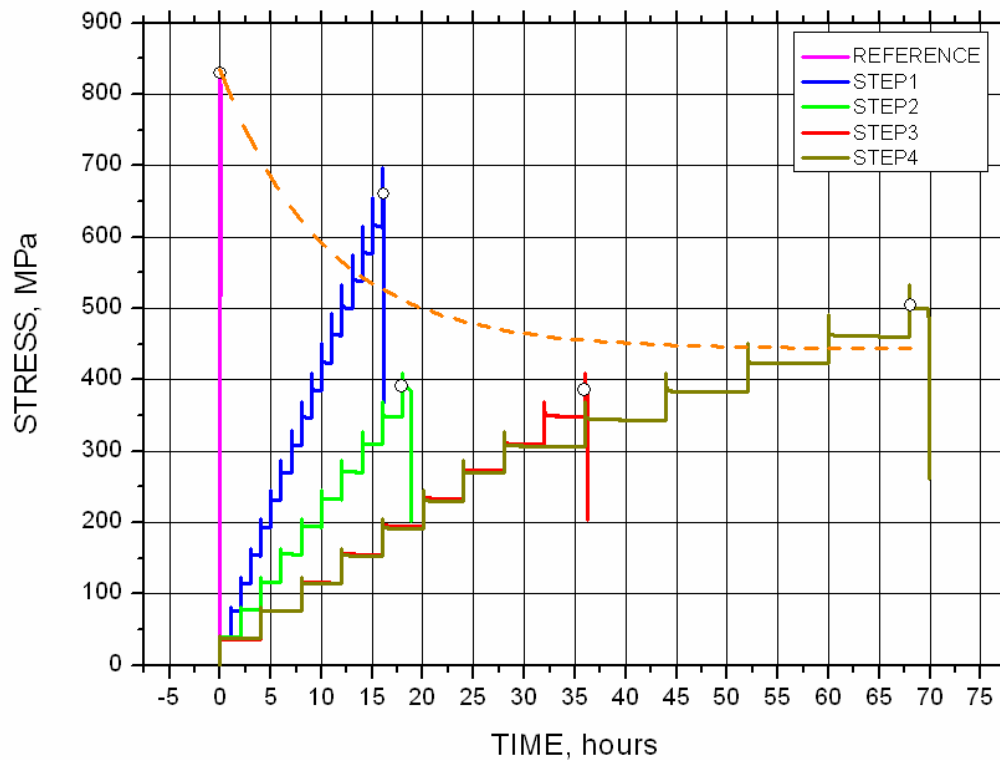
Step 1: Each step must be 5 % of the maximum stress of the reference, which means $820 \text{ MPa} \times 0.05 = 41 \text{ MPa}$.

$20/41/1 = 20 \text{ steps of } 41 \text{ MPa increasing remaining at constant load during } 1 \text{ hour between each step.}$

Step 2: The same stepwise increase but remaining 2 hours between two increments.

Step 3: The same stepwise but remaining 4 hours between two increments.

Step 4: was applied a different increasing mode: $(7/41/4) + (13/41/8)$.



Graph 12: Incremental steps loading for S700MC round notched samples pre-charging 1 hour in 10g Thiourea + 4g NaOH / l H₂O and during the test.

A tendency might be observed in the curves, although there's a significant scatter, the trendline associated to the breaking points gives us an approximation of the threshold stress for the material S700MC, which is around 450 MPa.

In the following picture is shown the broken samples, permit to see that all of them have broken on the notch:



Fig. 29: S700MC notched round broken samples for incremental steps loading

CONCLUSION ISLT:

- + As is an standardized test, the acceptance is correct
- + Seems a powerful test for future studies.
- - Extensive sample preparation to fabric the round bars and the notch.
- - Is Needed a minimum thickness of material, not possible for flat plates
- - Potentiostatic procedure is not straightforward

5.4 Constant Load Testing

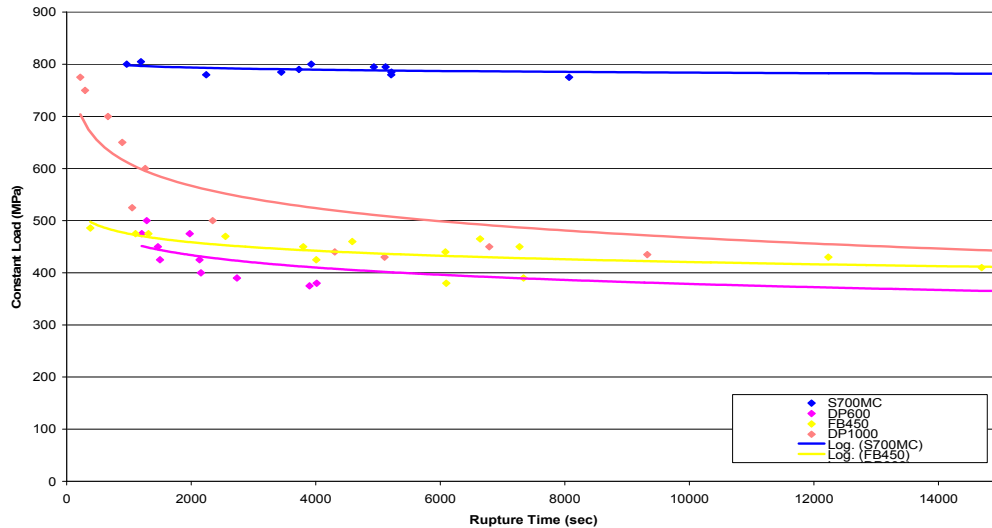
For this test type, instead of keeping a constant crosshead velocity (mm/min) during the test, a fixed tensile stress (MPa) must be applied to the samples.

The aim of this paragraph was twofold. On the one hand, to develop a useful methodology to do this type of testing (e.g. notches with different profiles can be introduced); On the other hand, to evaluate the effect of microstructure and strength level on the H-embrittlement of carbon steel.

The first step was to evaluate some results of constant load testing done prior to this study began to have an idea of the things that should be modified:

- The materials tested in 2008 were: S700MC, DP1000, DP600, FB450

- The charging parameters were: 10 mA/cm² in “0.5 g As₂O₃ + 0.25g HgCl₂ + 60 ml H₂SO₄ / l H₂O” electrolyte. (without pre-charging time), introducing around 13 ppm of hydrogen (Graph 7).



Graph 13: Constant load testing for non-notched samples. (2008 results, cfr. J. Galan Lopez)

As shown on the graph, a threshold value could be observed for each material below which no fracture occurred. However, some scatter exists on the data points, and when observing the broken samples after the tests (Fig. 30), it is possible to see that all the samples are broken at different sites.

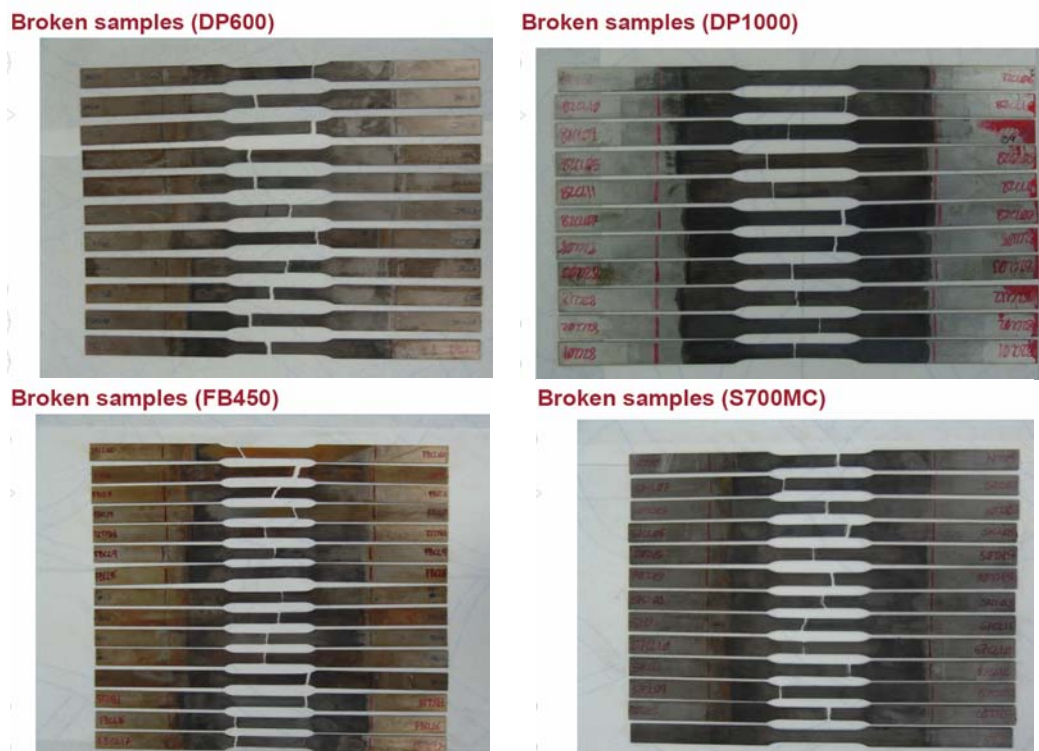


Fig. 30: Images of broken samples (2008 results, cfr. J. Galan Lopez)

To decrease the scatter a notch was introduced on the samples to force the crack initiation on it.

Two different materials (F6 and F7) high-strength martensitic steels were notched to reach the objective.

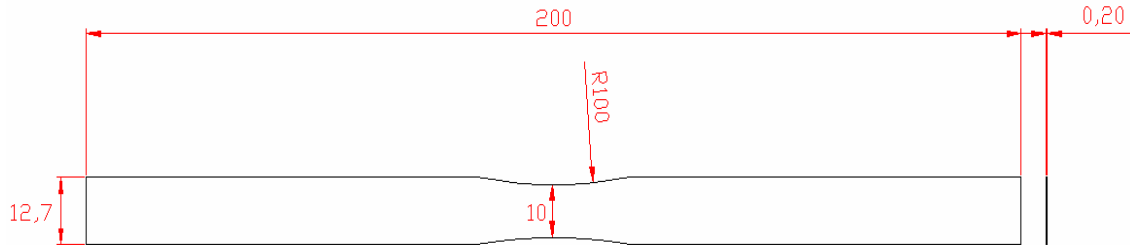
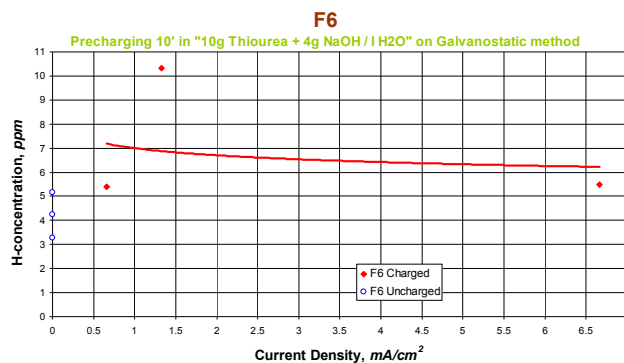


Fig 31: F6 & F7 rectangular notched sample dimensions for constant load testing (mm)

With the H-mat the approximate amount of hydrogen was checked for various current densities:



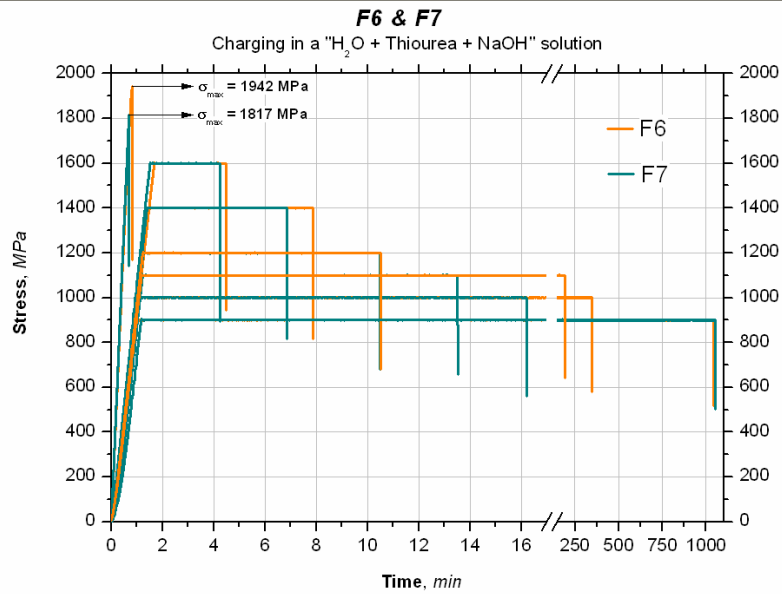
Graph 14: F steel H-concentration Vs Current density

Applying 1 mA/cm² on the sample inside a “10g Thiourea + 4g NaOH / L H₂O” electrolyte introduced over 6 ppm of hydrogen into the material. Samples were pre-charged 30 minutes before the start of the testing.

Constant loads were applied.

The sample preparation before testing was the same as for the previous samples.

After all testing, only 2 samples were found to be broken at the notch; the others were broken at different locations outside the notch. Therefore, the curves were recalculated changing the values of the notched sections to the real broken sections. The curves are shown in the Graph 15:



Graph 15: Constant load curves for F6 and F7 steels based on the broken section

A slightly different sensitivity can be seen between both materials, where F7 brakes slightly faster than F6 for identical loading conditions. Extra testing with lower constant loads, would allow revealing the threshold stress value. However, no more samples were available.

The next step was introduced another kind of notch that would concentrate the stress even more. The same rectangular constant load samples that were used for the previous study were notched as shown below:

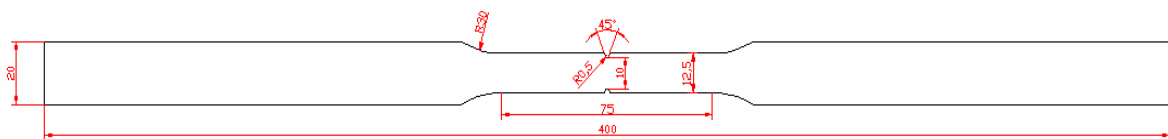


Fig. 32: rectangular notched sample dimensions for constant load testing (mm)

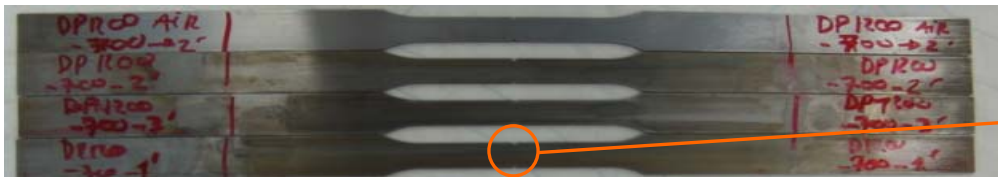


Fig. 33: Notched samples

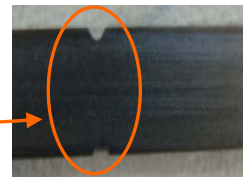


Fig. 34: Detail of the notch.

6 EFFECT OF MICROSTRUCTURE ON HYDROGEN EMBRITTLEMENT

The materials were the same as for the previous study, adding one more grade: FB450, S700MC, DP600, DP980 and DP1200.



Fig 35: DP1200 sample with Zn coating removed.

The sample preparation was the same as for the previous testing (SSRT) except for the DP1200 that had a Zn coating which was removed with a grinder in order to avoid any effect on the hydrogen absorption. The thickness reduction due to this grinding process was approximate by 20 μ m (10 μ m each side).

The charging conditions were:

- Current density applied: 10 mA/cm² \approx 10 H-ppm introducing.
- For a surface in contact with the electrolyte of 38.38 cm² x 10 mA/cm² \approx **768 mA**
- Electrolyte used: 1g Thiourea + 28 ml H₂SO₄ / L H₂O
- Precharging time: 15 minutes

Some of these samples were tested charged and in air in a constant load test to observe if were breaking on the notch, and proceed with this geometry in affirmative case. All of them did and.

Then, as the first aim of this chapter was reached, the next objective was testing the materials to obtain an approximation of the threshold stress level and observe the different sensitivities due to the H-effect.

PROCEDURE:

Before starting the constant load tests, reference slow strain rate tests were done in air at 5 mm/min to determinate the mechanical properties on the notched samples. The strain data was obtained directly from an extensometer without recalculate any curve.

The stresses were calculated on the smaller surface of the sample, by reason of is the surface with higher stress concentrate:

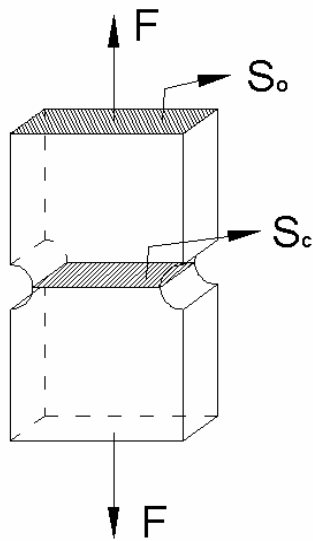
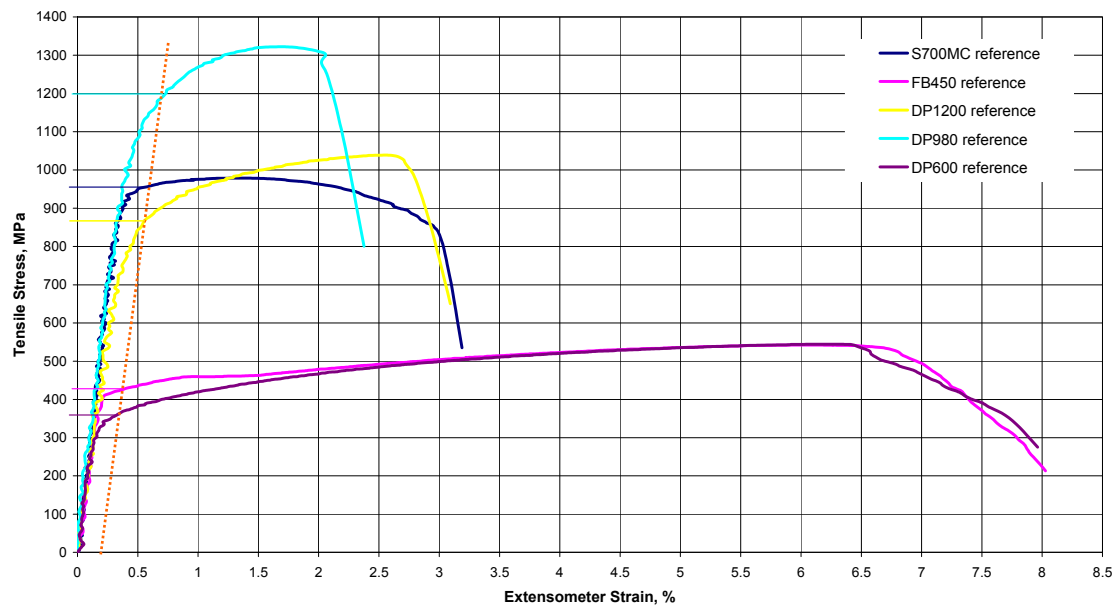


Fig. 36: Tensile sample section

As is shown on the Fig. 36, the forces applied are vertically opposites generating stress on the sample. The stress can be defined as:

$$\sigma = \frac{F [N]}{S [mm^2]}$$

The stress will increase when the surface decrease. Therefore, for the study, the stresses were calculated using the critical surface (S_c) of the notch where will be the maximum stress concentrate.



Graph 16: Reference curves and offset yield strength.

MATERIAL	R _{p0.2} (MPa)
FB450	430
S700MC	960
DP600	345
DP1200	1200
DP980	870

Table 16: Yield S

Once the $R_{p0.2}$ was known, the materials were tested at constant load. For each material the following stress levels were tested:

	350		400				200
	400		450		400		220
	420		500		425	100	275
	425		550		437	200	350
FB450	437	S700MC	600	DP600	450	300	450
(MPa)	450	(MPa)	650	(MPa)	463	400	500
	463		675		475	500	550
	475		700*		485	600	600
	485		750		500	700*	650
	500		800			800	700
							750
							800

* Some extra-tests were done at these stress levels, stopping the tests after different times before rupture. The aim was to analyze the microstructure and the crack propagation with SEM / EBSD.

As indicated before, inside the electrolytic cell it is not possible to use an extensometer, and hence just the crosshead displacement is measured. For this reason, again, the co-relations were made between the crosshead displacement and extensometer strain on reference samples of each material.

In the following graph there's an example for DP600 steel (the rest materials can be found on the appendix):

Crosshead-Extensometer relation:

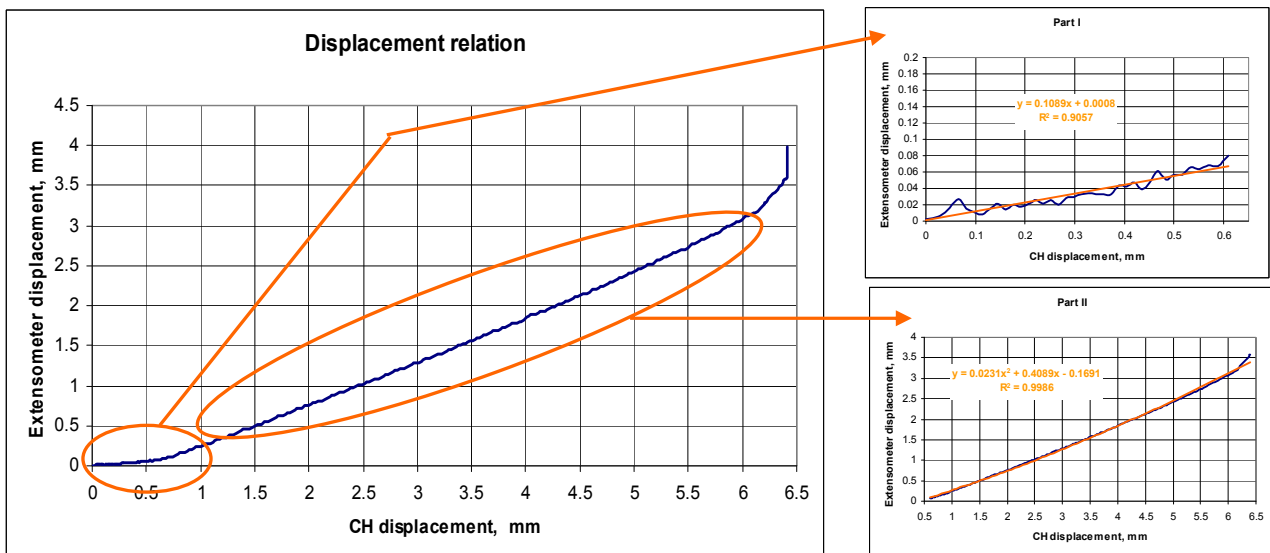


Fig 37: Example of Crosshead-Extensometer relation.

The following graph shows, as a general example, a typical creep curve graph that on the following constant load results will be obtained:

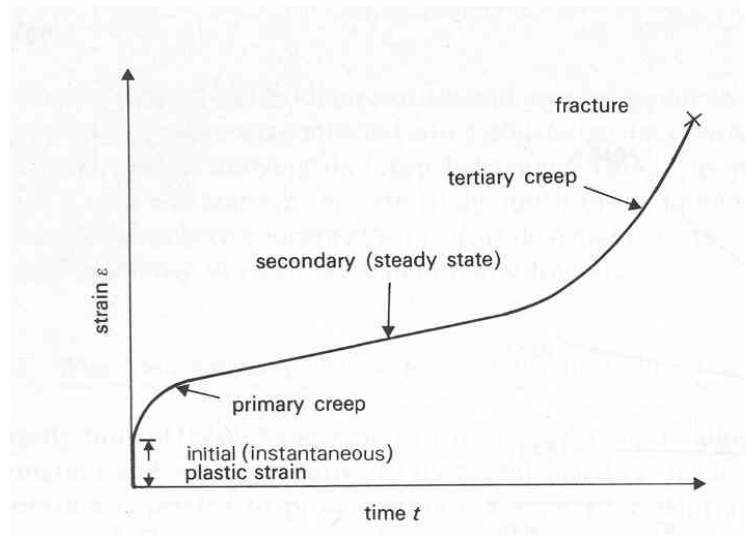


Fig 38: Stages in a typical creep curve

Creep in metals is defined as time dependent plastic deformation at constant stress (or load). The form of a typical creep curve of strain versus time is shown in Fig 38. The slope of this curve is the **creep rate** $dt/d\varepsilon$. The curve may show the instantaneous elastic and plastic strain that occurs as the load is applied, followed by the plastic strain which occurs over time.

Three stages to the creep curve may be identified:

Primary creep: in which the creep resistance increases with strain leading to a decreasing creep strain rate.

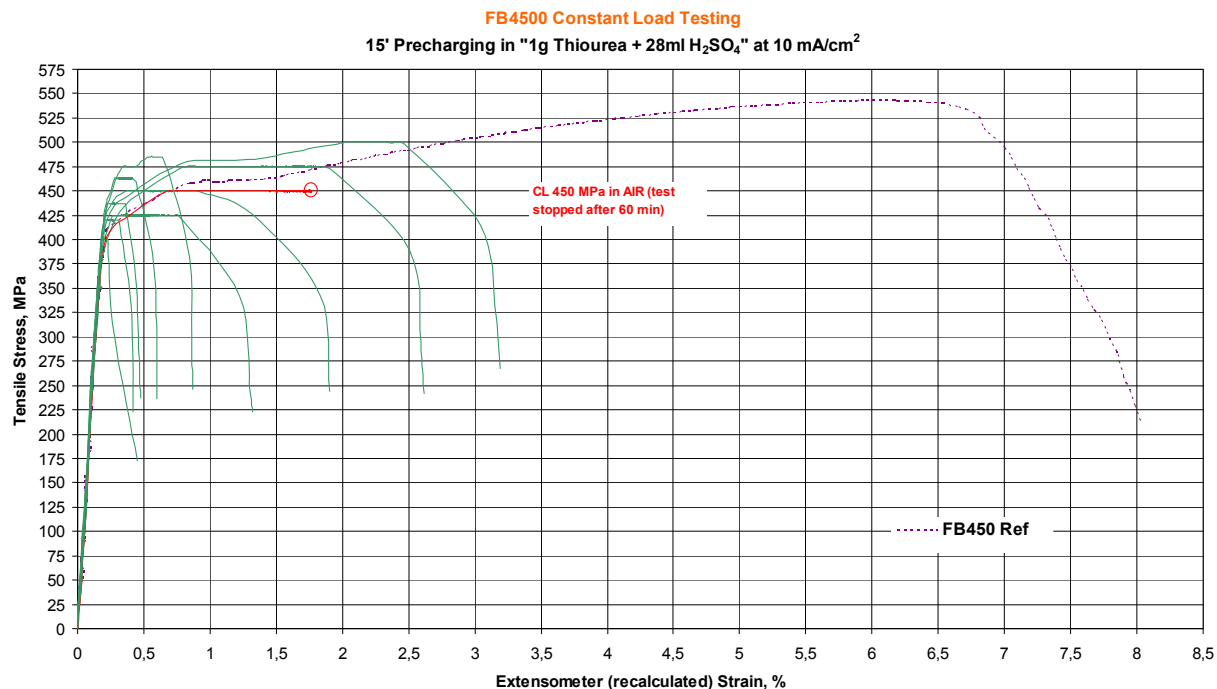
Secondary (Steady State) creep: in which there is a balance between work hardening and recovery processes, leading to a minimum constant creep rate.

Tertiary creep: in which there is an accelerating creep rate due to the accumulating damage, which leads to creep rupture.

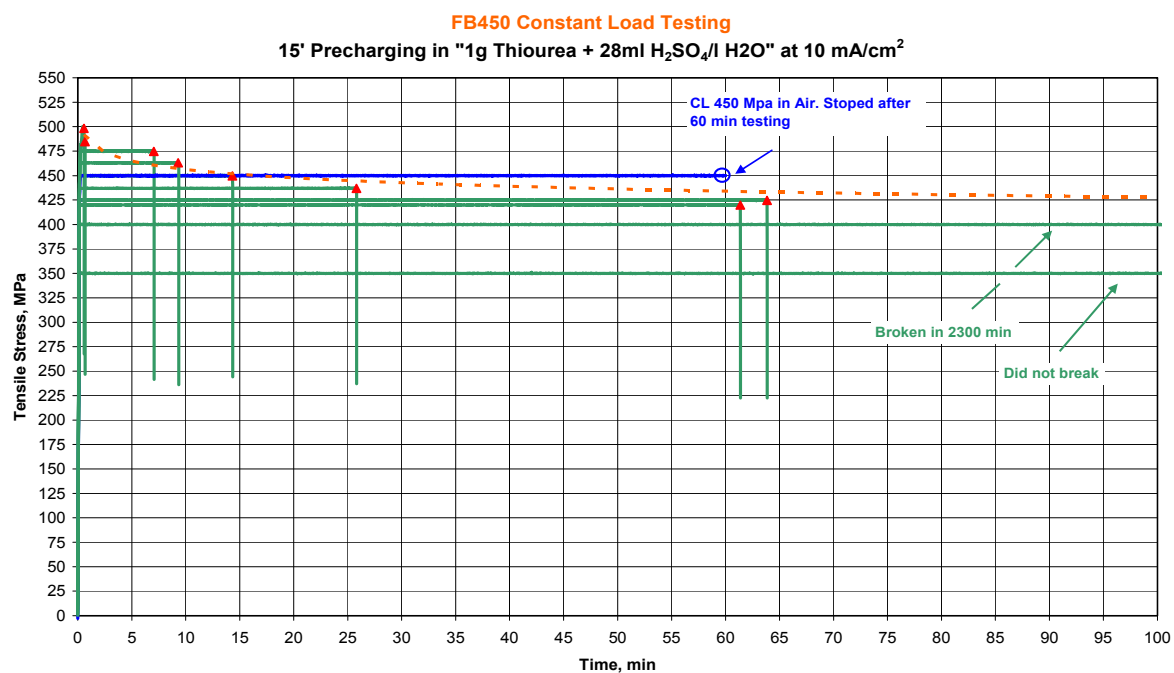
6.1 FB450

Graphs 17 to 20 summarize the results of the constant load tests for F450:

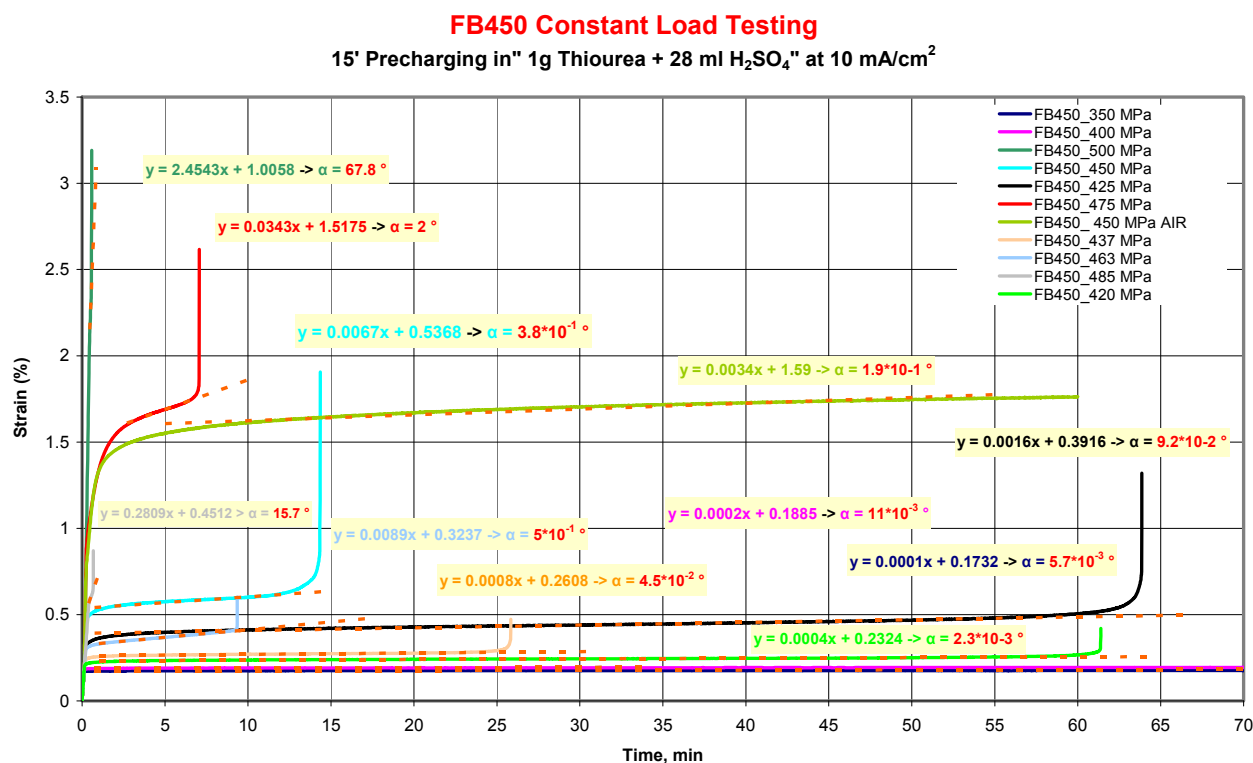
Stress Vs Strain:



Stress Vs Time:

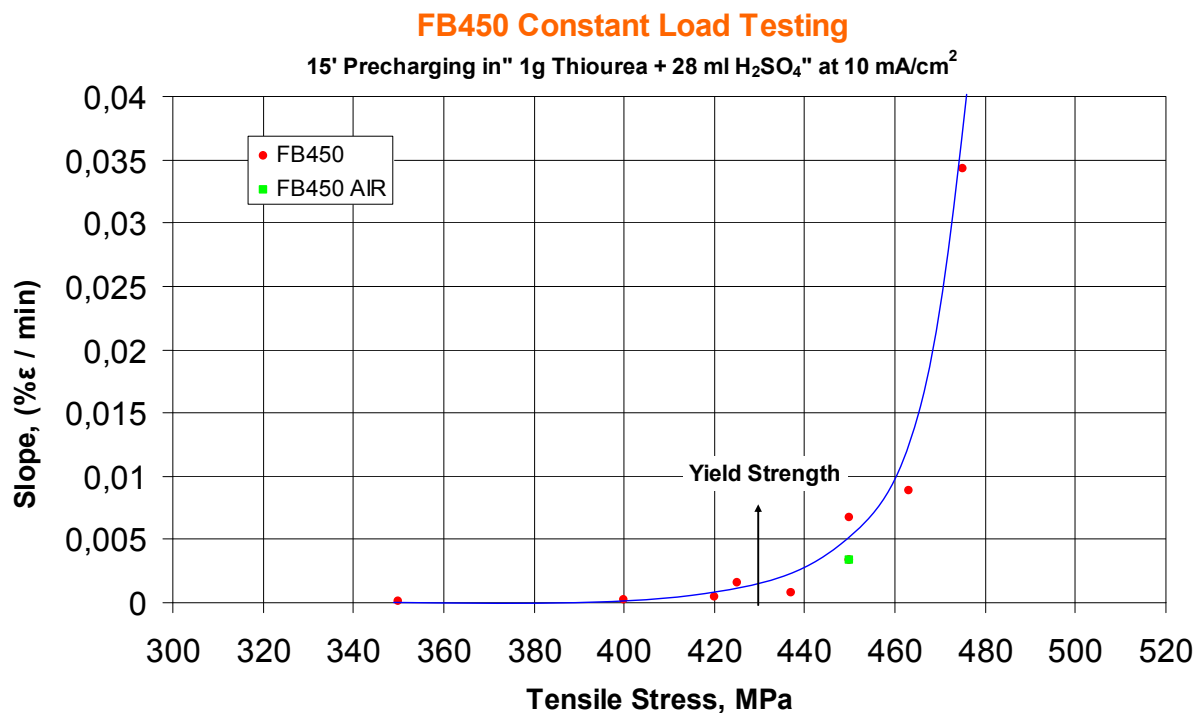


Creep:



Graph 19: Strain vs time for FB450 steel.

Creep Vs Stress:



Graph 20: Slope Vs Stress for FB450 steel.

The stress-strain graph shows that for a higher applied stress higher strain values are obtained in general. The red curve at 450 MPa tested in air confirms that hydrogen has an influence on the results. This influence is more clear in the graph where two samples, one charged and the other tested in air at 450 MPa, can be compared. The charged one breaks in less than 15 minutes and the one tested in air was stopped after 60 minutes testing without rupture.

From the stress-time graph an approximation can be done of the threshold stress for FB450 in these charging conditions. It appears to be around 400 MPa. Above this level the samples are breaking faster the higher the stress level is. Below, a very big difference of breaking time occurs: for 420 MPa → 63 min and for 400 MPa → 2300 min, which means that on decrease of 20 MPa increases the breaking time to 2240 minutes (≈37 hours).

The strain-time graph basically gives an idea of the creep phenomena. Creep is the tendency of a solid material to slowly move or deform permanently under the influence of stresses. It occurs during exposure to levels of stress that are below the yield strength of the material. The creep can be identified as the slope of the curves Strain-Time (*% strain/min*).

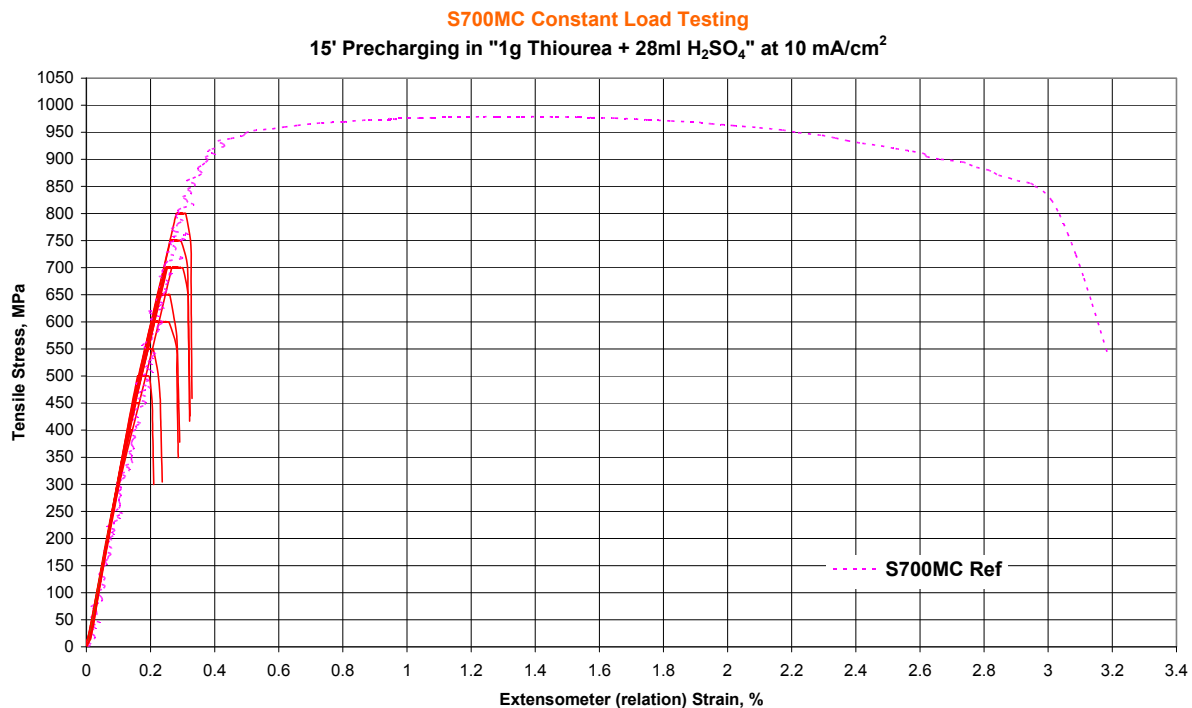
For the lowest levels of stress, the curves are almost straight, flat lines, which mean the creep phenomenon is almost neglectable. But as the stress increases, the slope increase too (and in a short range of time the strain of the material increase very high).

To better understand the creep of this material, the creep rates were represented as a function of the applied stress it is very clear how the creep increases exponentially.

6.2 S700MC

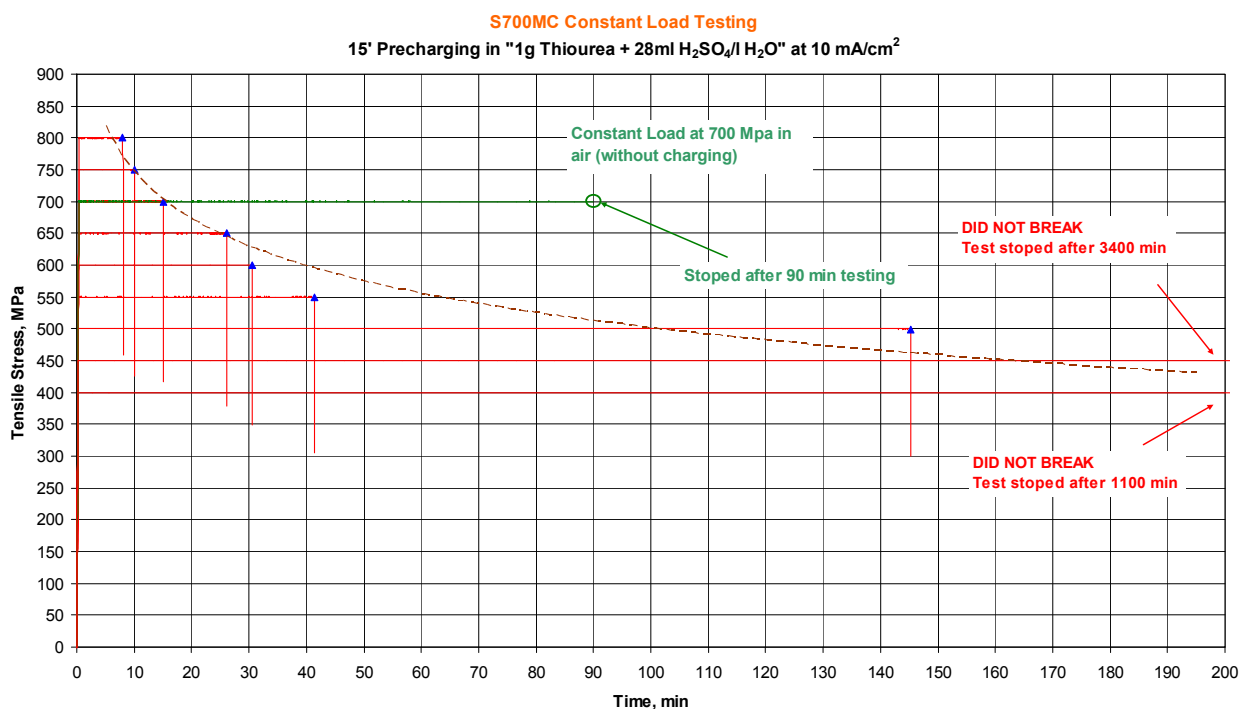
Graphs 21 to 24 summarize the results of the constant load tests for S700MC:

Stress Vs Strain:



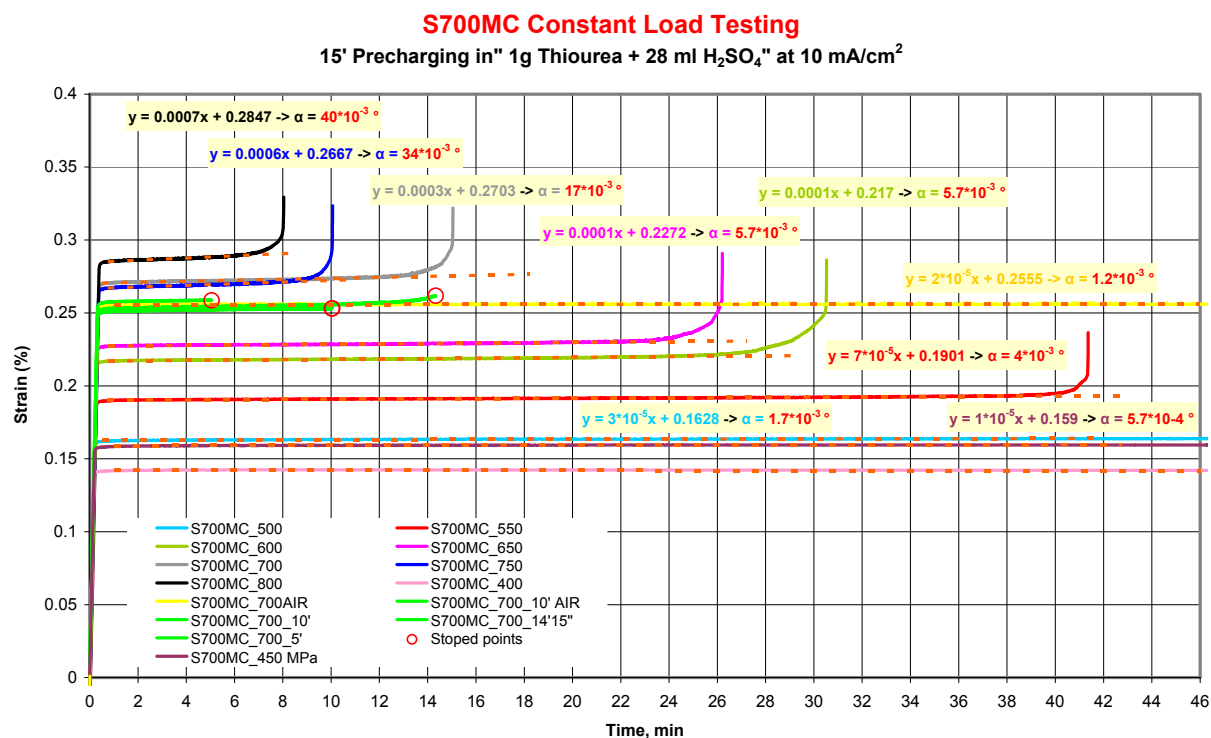
Graph 21: Stress Vs Strain for S700MC steel.

Stress Vs Time:

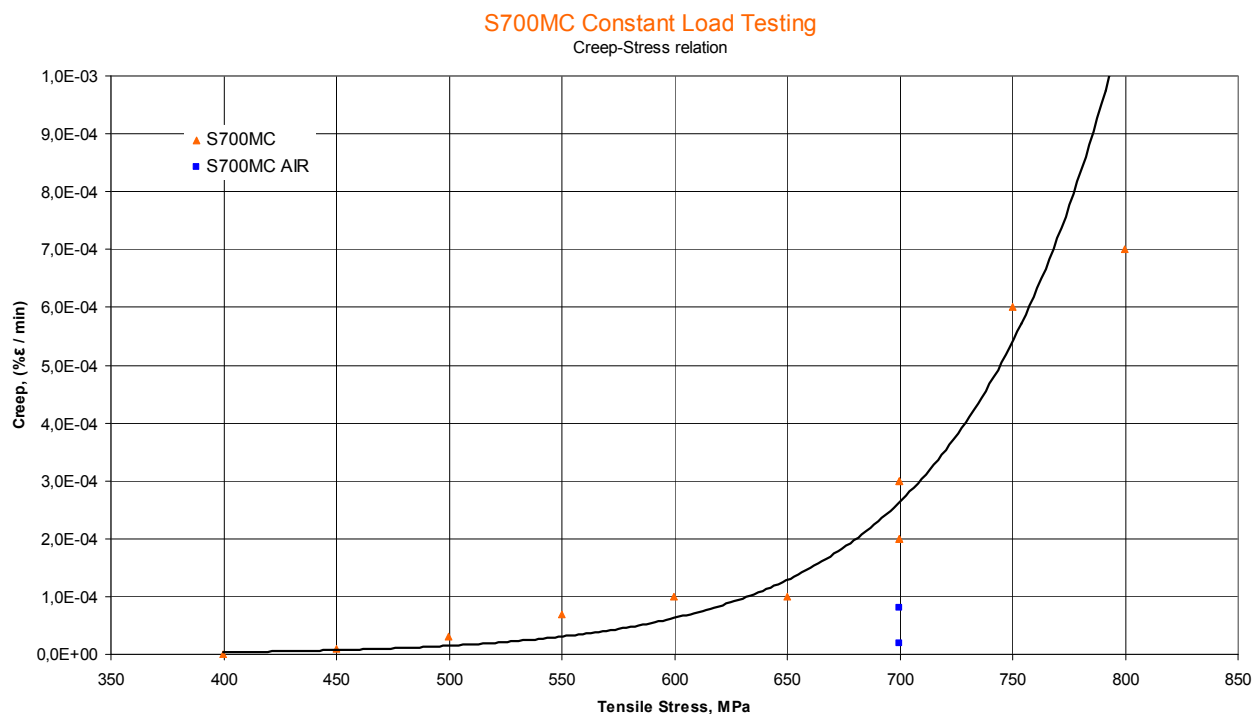


Graph 22: Stress Vs time for S700MC steel. .

Creep:



Creep Vs Stress:



The stress-time graph shows the breaking points with a clear tendency that corroborate the notch in the samples helps to obtain reproducible results

with less scatter comparing to the ones for the same material without notch from the previous study (Graph 13).

Is it possible to do an approximation off the threshold stress being around 450 MPa where there's a difference of time of 3250 minutes (≈ 54 hours) between the sample tested at 500 and the one at 450 MPa.

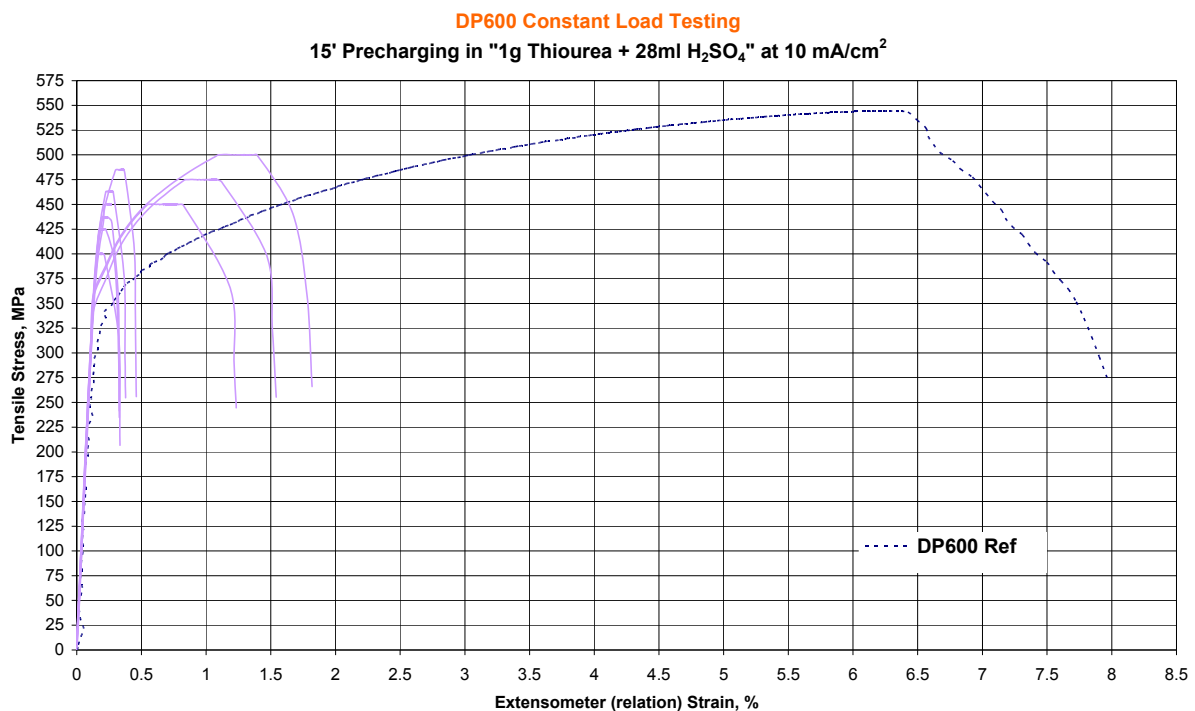
On the creep-stress graph there's again an exponential tendency after 700 MPa. Is it possible to see the sample tested at 700 MPa in air and the one charging that in air the creep value is lower, as in the FB450 450MPa in air comparing to the charging one.

On the strain-time graph three green curves were represented on the 700MPa stress level stopped at different times, and the reason was to analyze with SEM the crack initiation and EBSD technique to observe the microstructure if the cracks are propagating intergranular or by the grain boundaries, or if it's due to dislocations in the material during a test with charging.

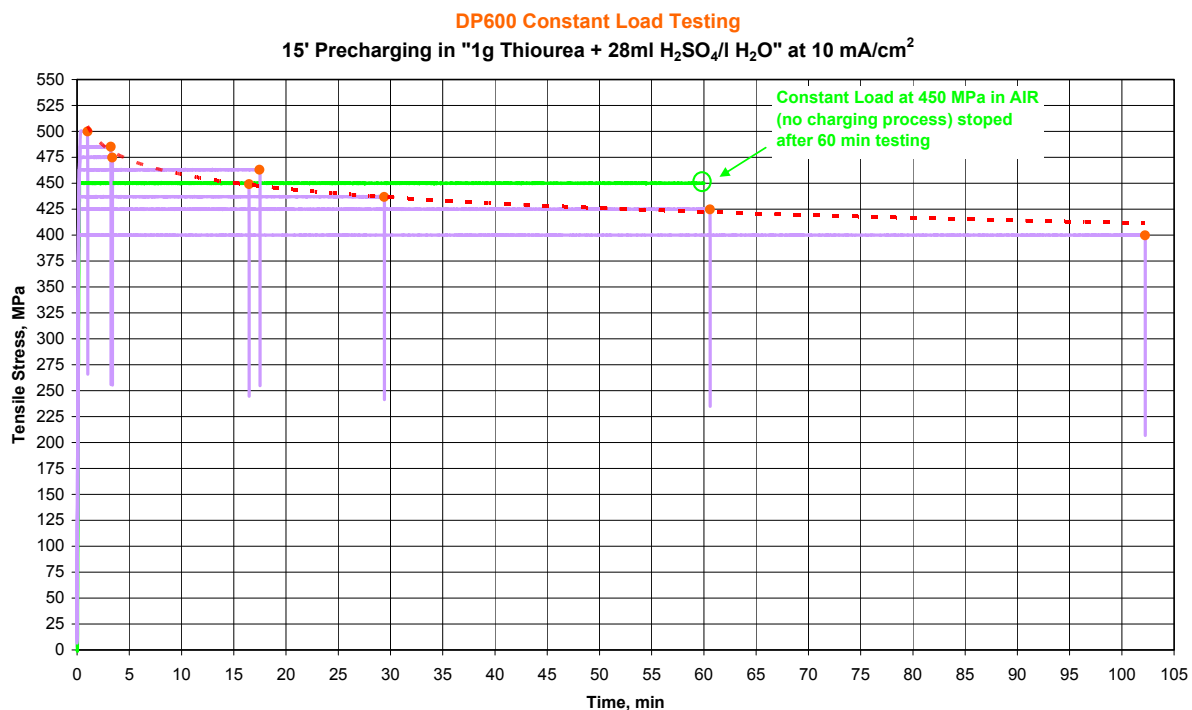
6.3 DP600

Graphs 25 to 28 summarize the results of the constant load tests for DP600:

Stress Vs Strain:

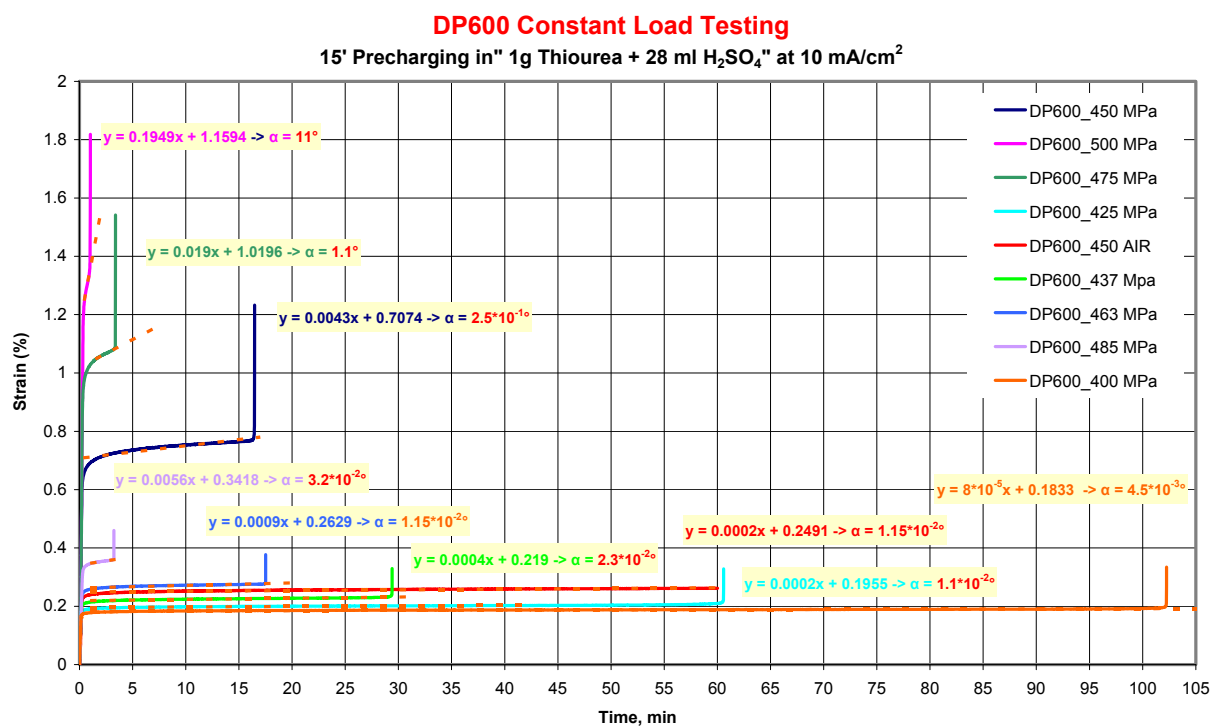


Stress Vs Time:

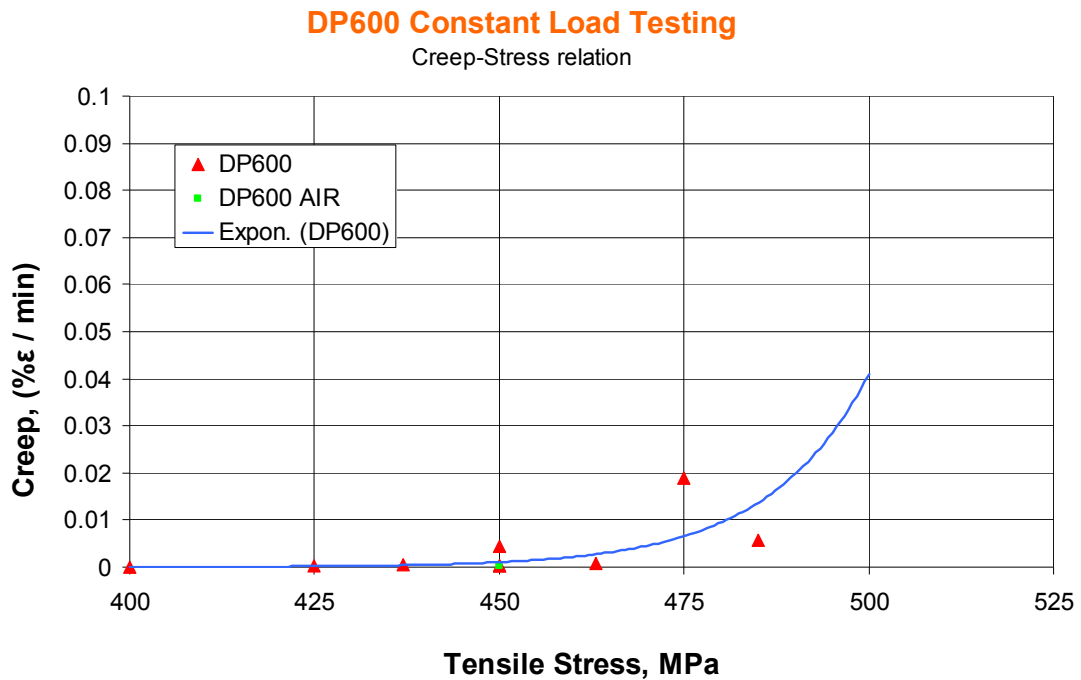


Graph 26: Stress Vs time for DP600 steel. .

Creep:



Graph 27: Strain Vs time for DP600 steel.

Creep Vs Stress:**Graph 28:** Creep Vs Stress for DP600 steel. .

On the references tested samples graph, the DP600 is the only material that the UTS (Ultimate Tensile Stress) is lower than the expected. For the rest of materials, e.g. DP1200, the UTS is around 1300 MPa or FB450 is near 550 MP.

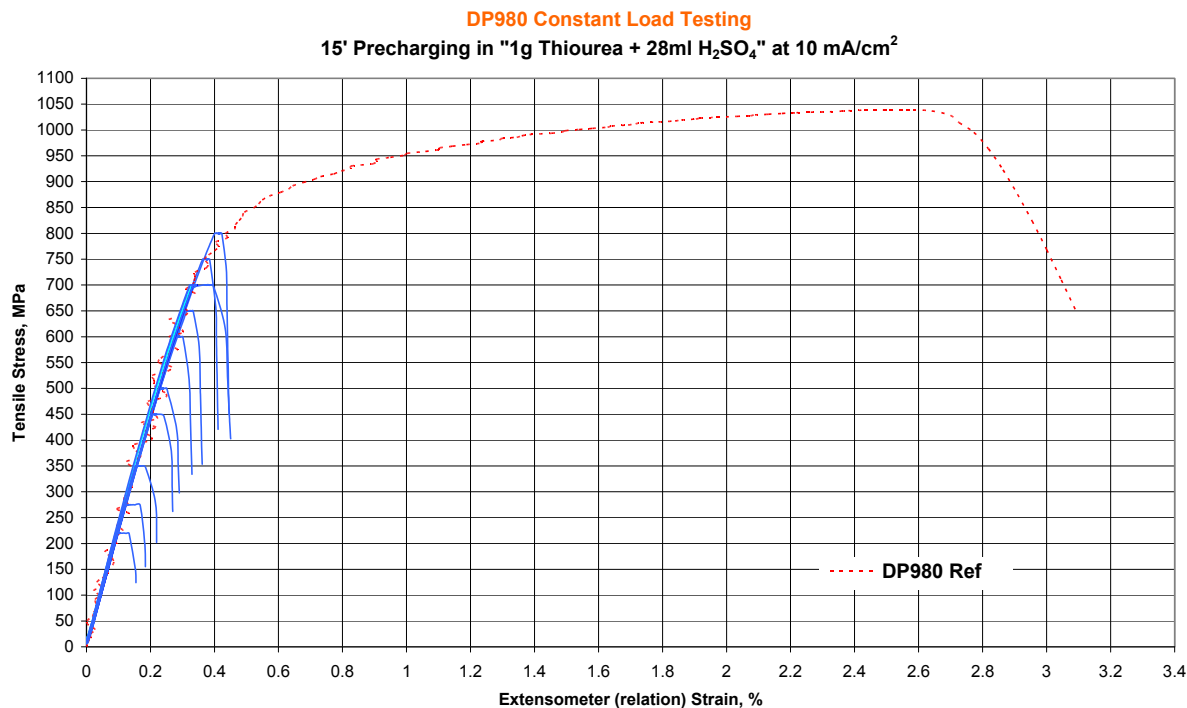
The stress-time graph shows that in the range from 400 to 500 MPa the behavior of the material due to the H-charging process changes fast, comparing to some other materials, e.g. S700MC needed a range of 400 MPa (from 800 to 400 MPa) to start seeing a considerable difference of breaking times.

An uncharged sample was tested at 600 MPa to observe how the hydrogen makes brittle the material and to see after the creep difference between the same material in different conditions (charged – uncharged). This test was stopped at 60 min being enough to obtain the results.

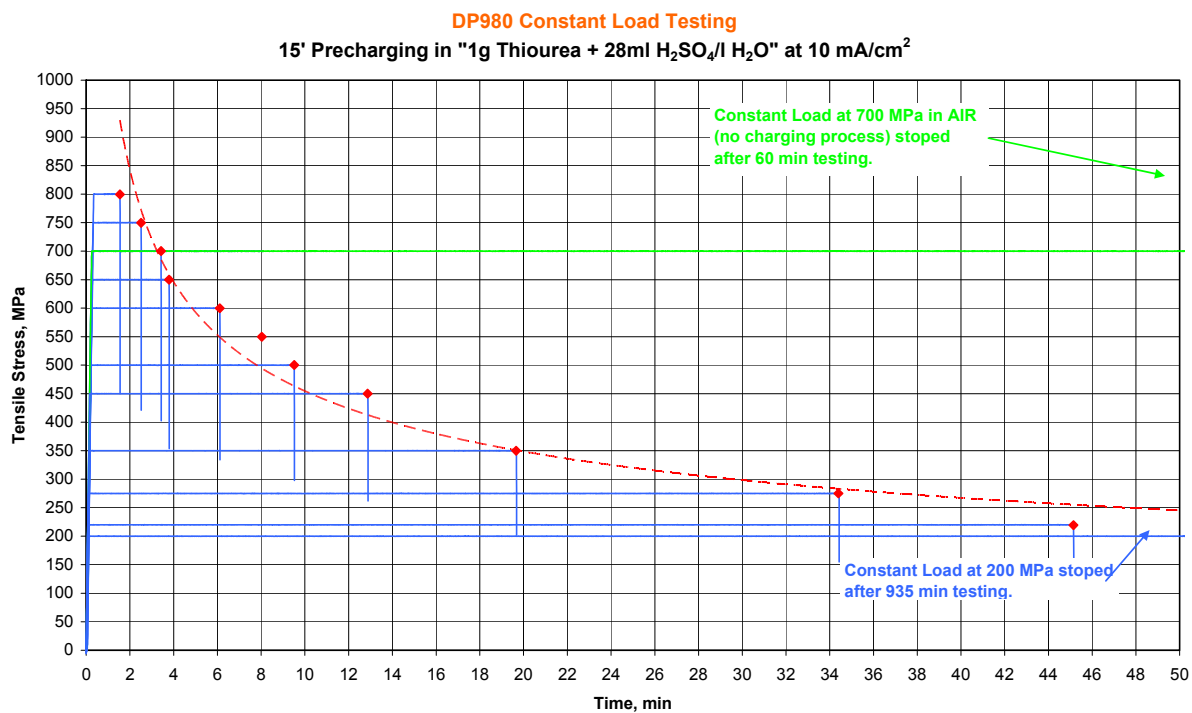
6.4 DP980

Graphs 17 to 20 summarize the results of the constant load tests for DP980:

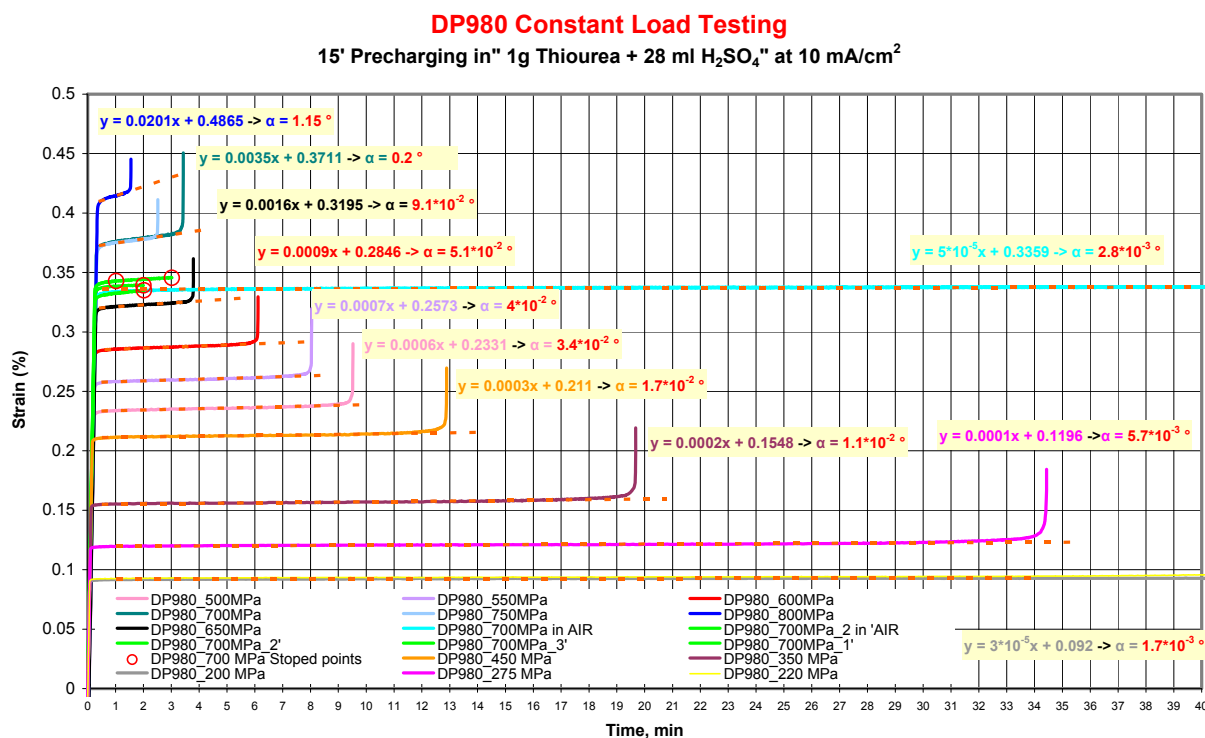
Stress Vs Strain:



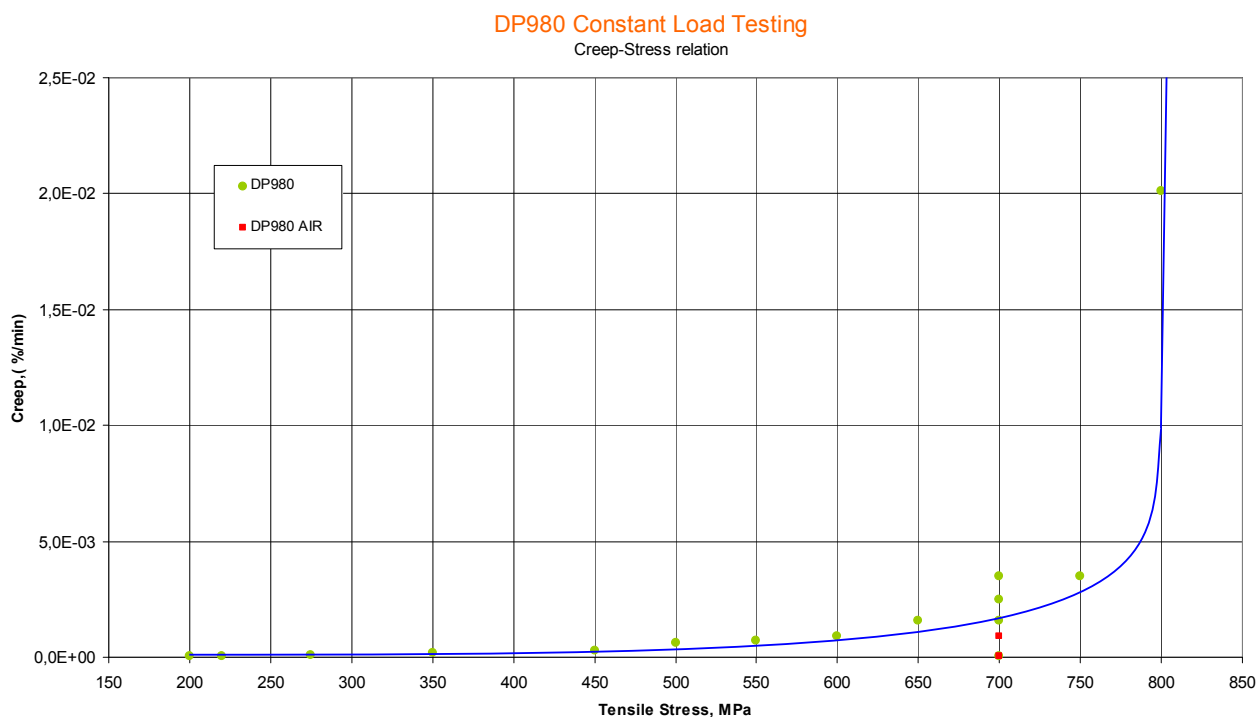
Stress Vs Time:



Creep:



Creep Vs Stress:



The DP980 material is the one with the most reproducible results and it can be seen on the stress-time test, were all the breaking points follow a tendency with almost no scatter. The threshold stress should be around 200

MPa because the breaking point from 800 to 450 MPa were increasing in time approximately of 2 minutes but for the stress level of 220 MPa is 45 minutes and the one of 200 MPa is more than 935 minutes, hence can be considered as the threshold stress level for DP980.

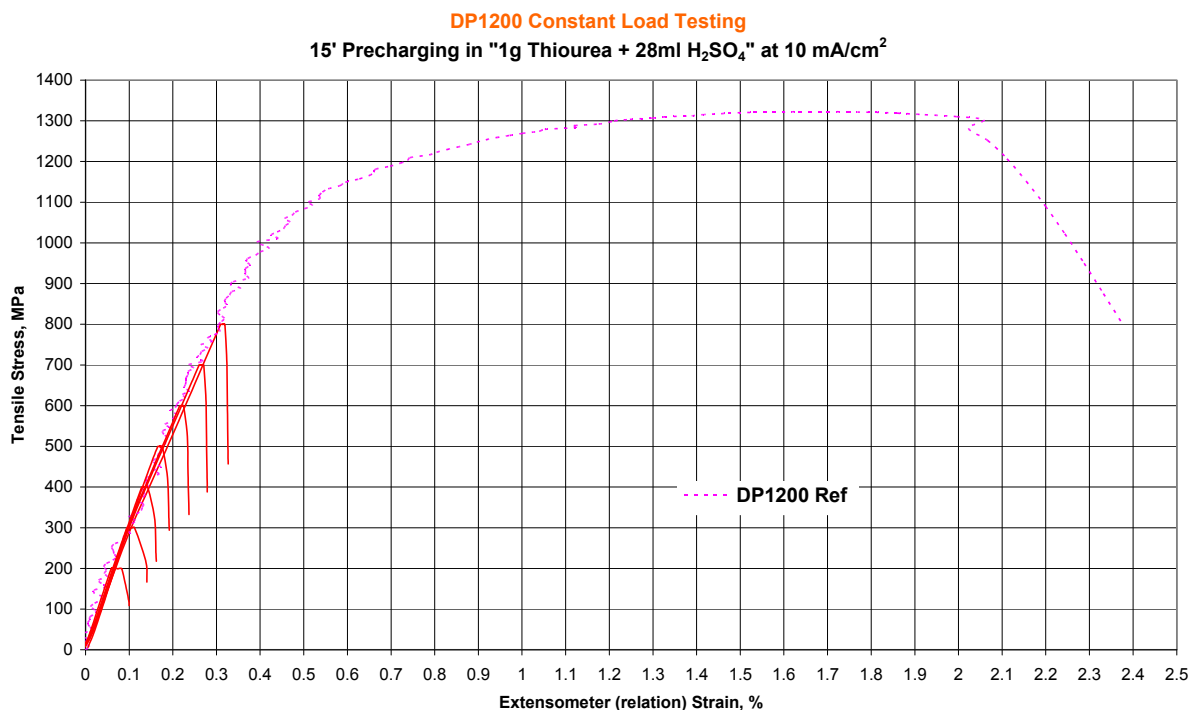
The creep graph shows as for the other materials, that the samples tested in air have a lower creep value than the charged ones.

For this material the same was done than for S700MC, four samples at the same constant load level (700 MPa) were tested in the same conditions and stopped the test at different times before the rupture to analyze those microstructures to understand the apparition and cracks propagation with SEM. It is detailed on the respective chapter.

6.5 DP1200

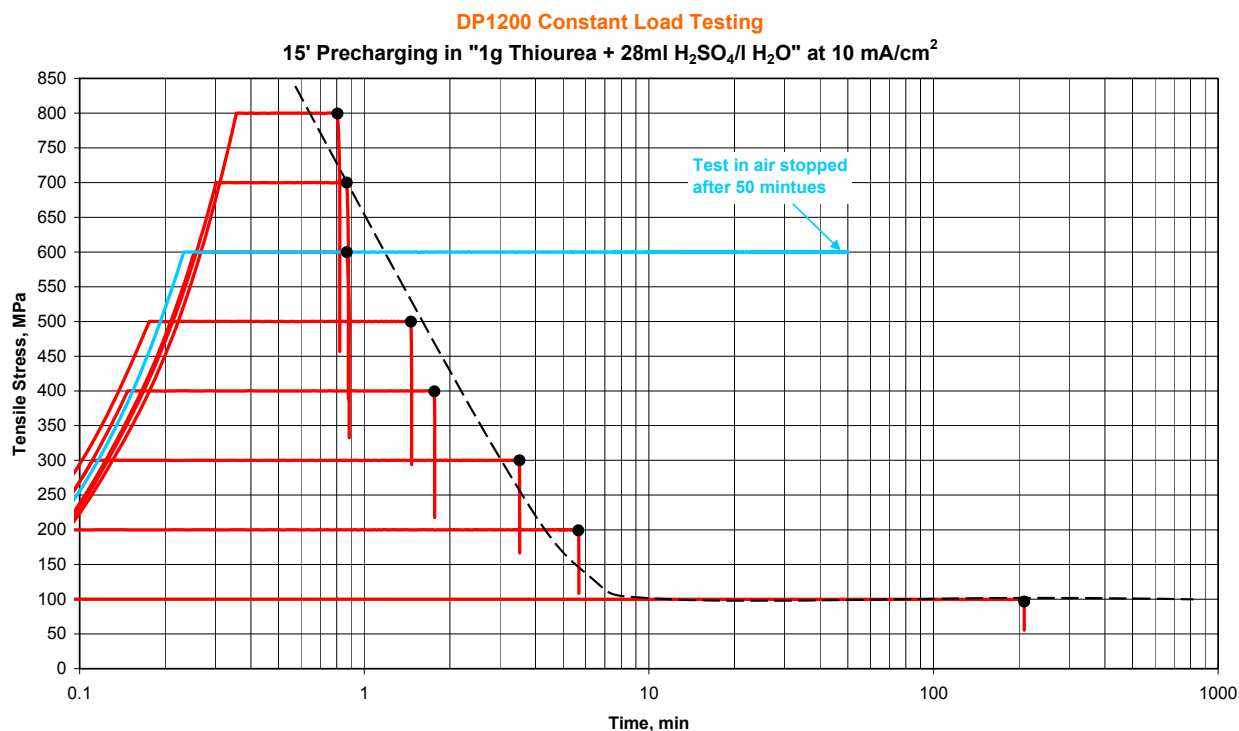
Graphs 17 to 20 summarize the results of the constant load tests for DP1200:

Stress Vs Strain:



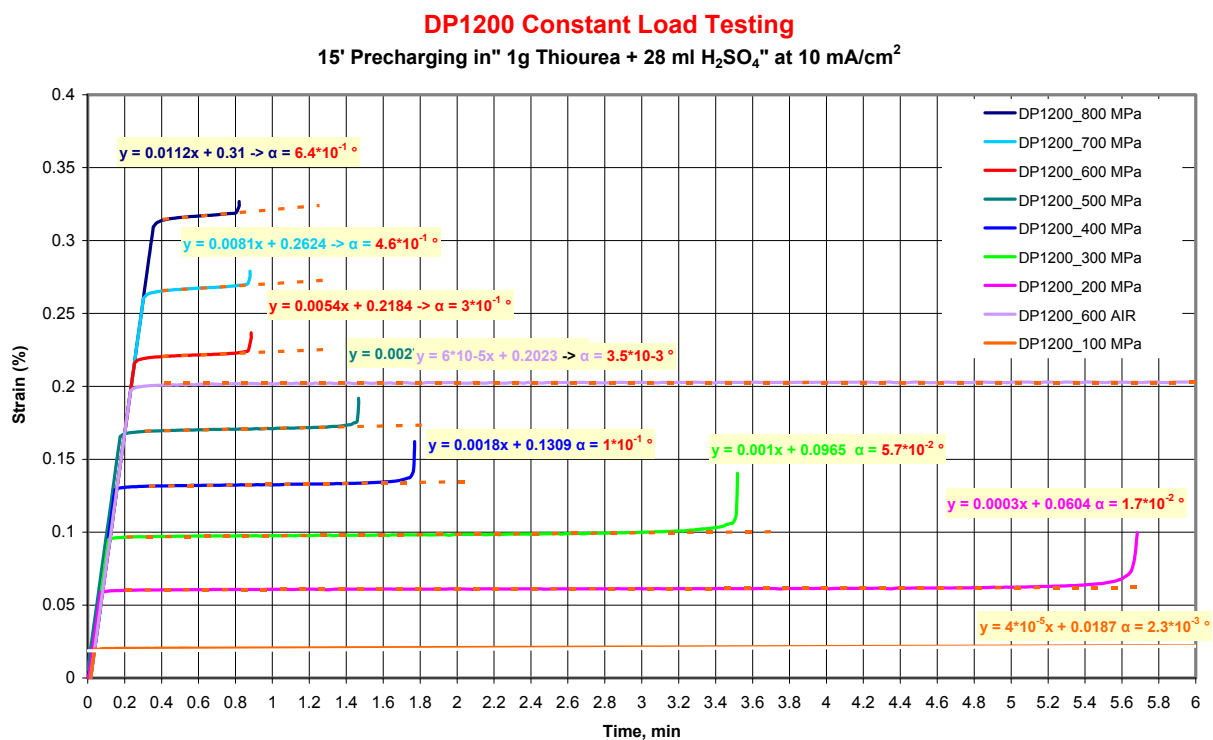
Graph 33: Stress vs Strain for DP1200 steel.

Stress Vs Time:



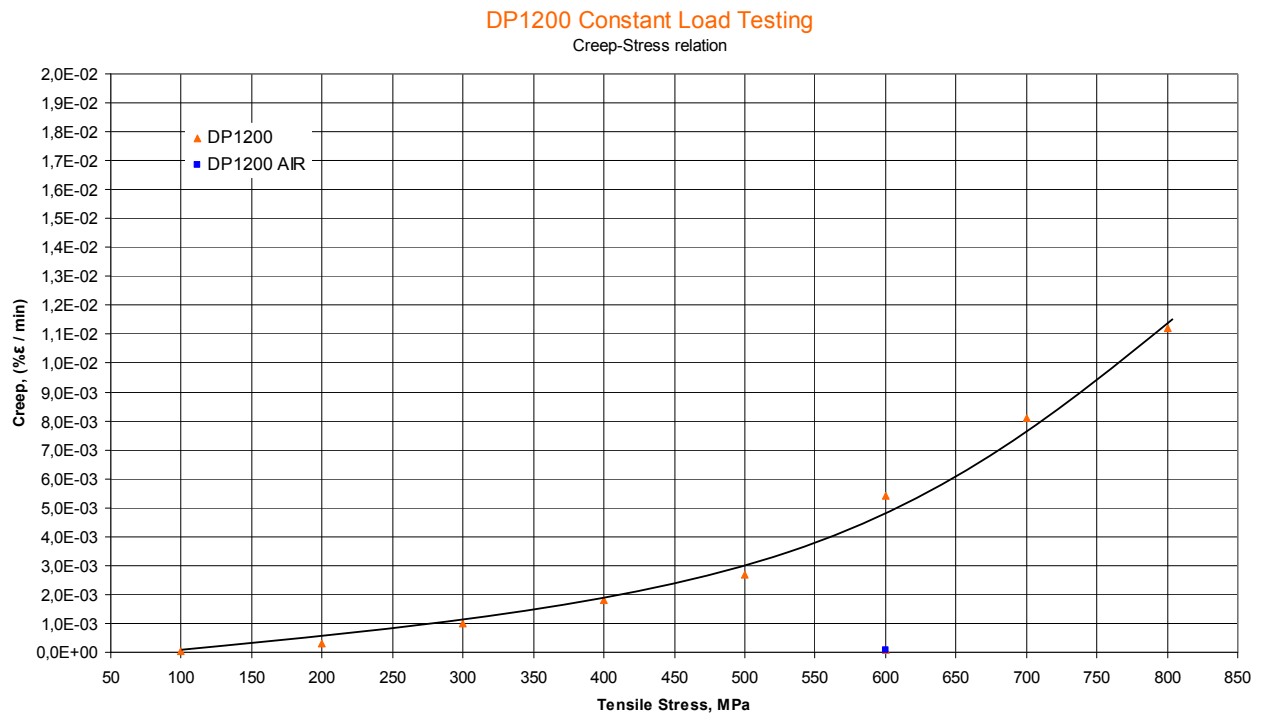
Graph 34: Stress Vs time for DP1200 steel.

Creep:



Graph 35: Strain Vs time for DP1200 steel.

Creep Vs Stress:



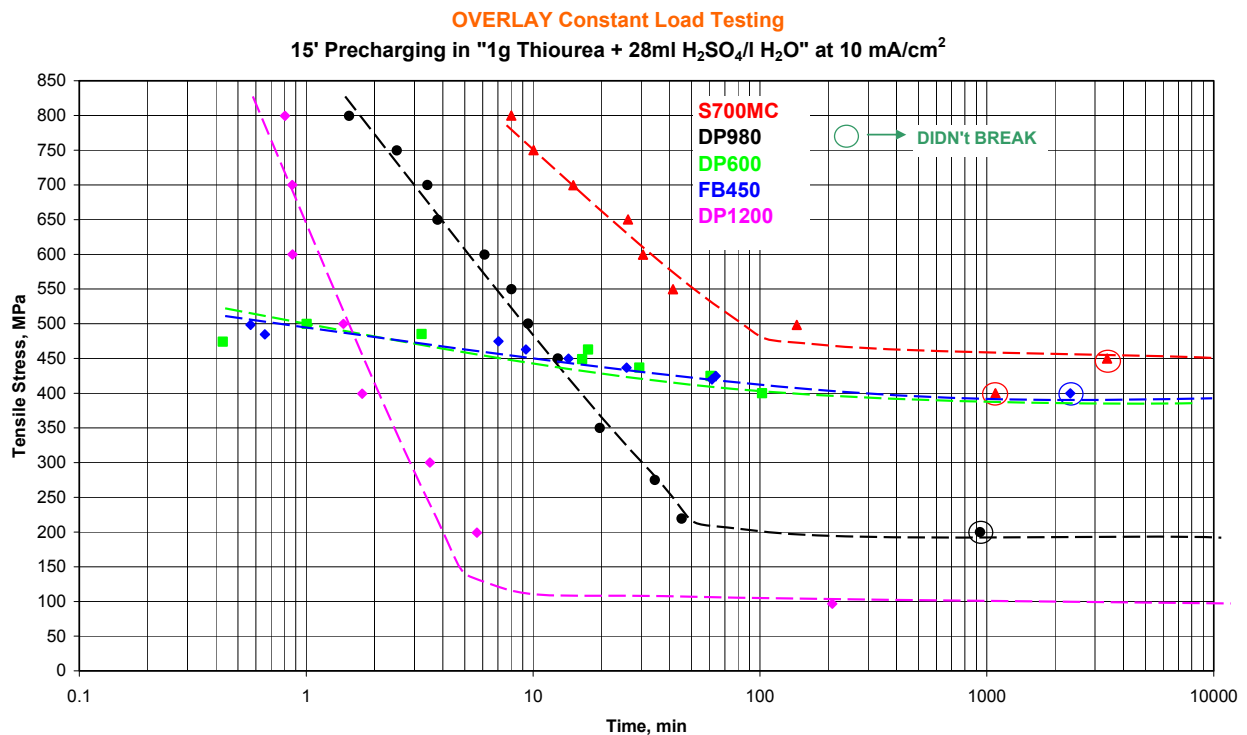
Graph 36: Creep Vs Stress for DP1200 steel.

DP1200 is the most sensitive material among all tested; as can be seen on the stress-time graph. All the samples had broken in less than 6 minutes (for all stress levels above 200 MPa), the threshold level is very low taken in account that the UTS of the material is 1300 MPa on notched samples.

6.6 Overlay all materials & discussion

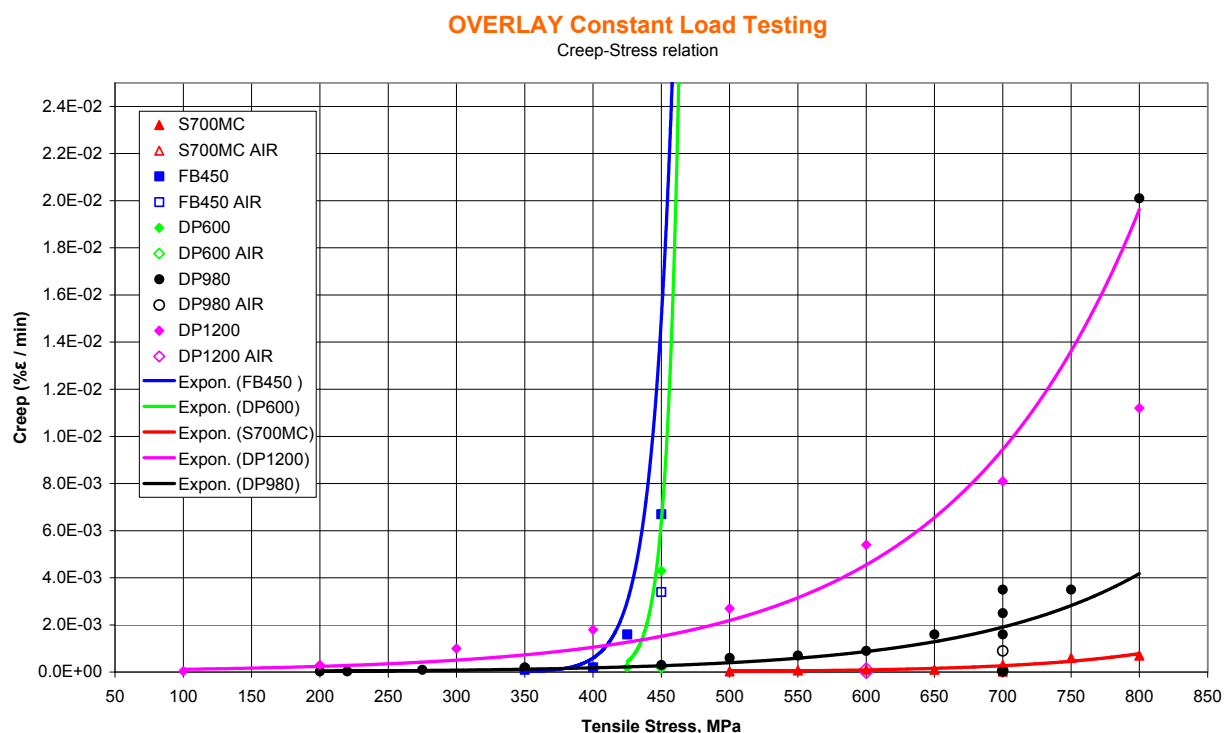
Graphs 17 to 20 summarize the results of the constant load tests for all materials:

Stress Vs Time:

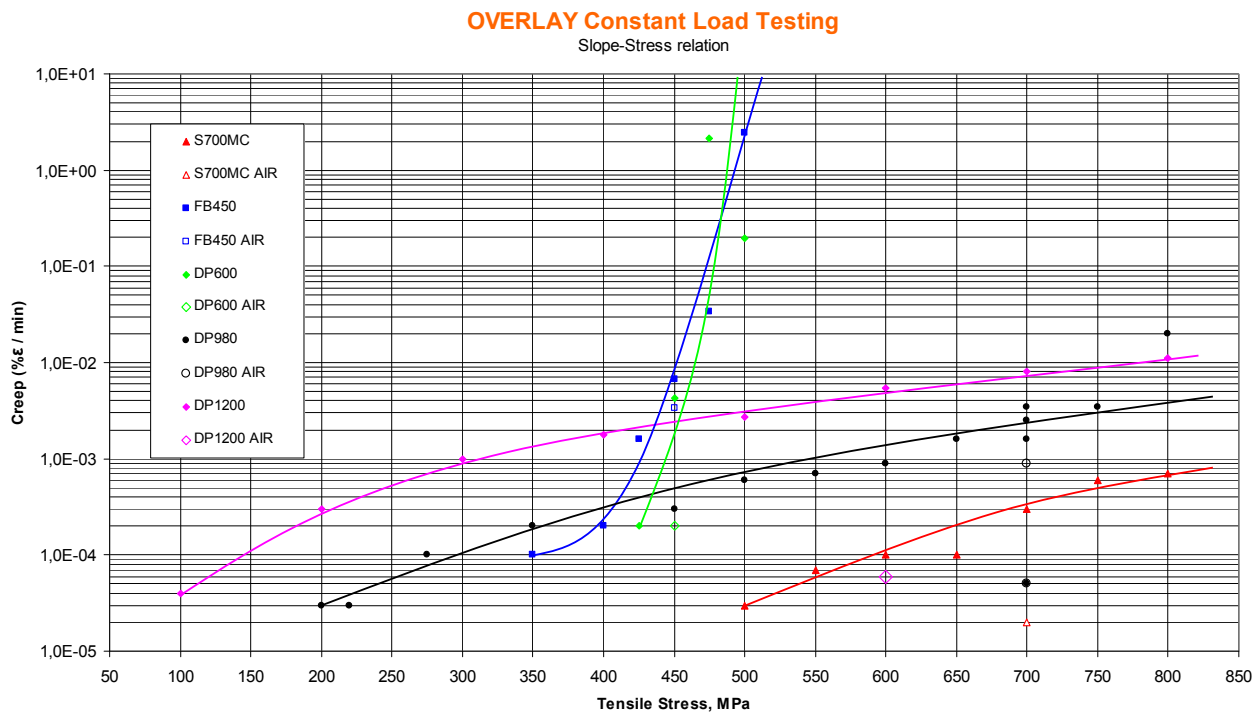


Graph 37: Stress Vs time for all materials.

Creep Vs Time:



Graph 38: Stress Vs time for all materials.

Creep Vs Time (Logarithmic scale):

The UTS (maximum tensile reached) showed in the stress-strain graph (Graph 16) for all materials except for DP600 is higher than the expected; for DP1200 is reached 1330 MPa, for the DP980 is 1040 MPa, for S700MC is 980 MPa, for FB450 is 550 MPa, but for the DP600 is 500 MPa, when the expected was at least 600 MPa.

The open symbols on the stress-time graph (Graph 37) indicate tests that were stopped without rupture of the sample.

DP600 and FB450 materials can be considered as the most ductile and the DP1200 the most fragile but has higher tensile resistance. On the graph creep-stress (Graph 38) those two materials have the same behavior; both have a fast exponential growth between 400 and 450 MPa while the rest of materials have a softer growth. It means DP600 and FB450 have a strong tensile resistance, almost no strain until approximately 400 MPa and after pass this point the materials start to strain a large amount per unit of time, and the rest of materials have a progressive creep rate since the start of tensile application.

S700MC steel is the one with lower creep rate; the strain keeps very low during all the stresses applied.

The graph 39 has the creep axis in a logarithmic scale to allow have an overview of all the points because with the graph 38 in normal scale was not possible to see all of them, but to have an idea of the tendency was correct.

All the samples from all materials have broken on the notch as follows in the picture:

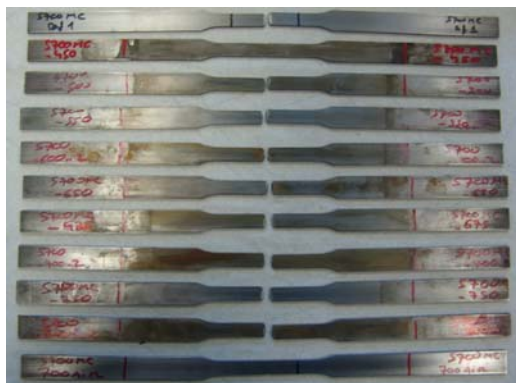


Fig 38: S700MC broken samples

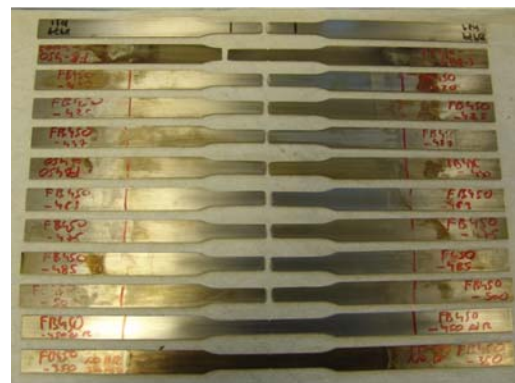


Fig 39: FB450 broken samples



Fig 40: DP600 broken samples



Fig 41: DP980 broken samples (wrong written)



Fig. 42: DP1200 broken samples (wrong written)

7 FRACTURE MECHANISMS STUDY

The aim of this chapter is the better understanding of:

- | | | |
|-----|---|--|
| SEM | { | ▪ the initial cracking on the sample's notches during the constant load testing with in-situ H-charging. |
| | | ▪ the amount of cracks appear for each material. |
| | | ▪ the distinction of the different phases. |
| EBS | { | ▪ the crack propagation type (intergranular, by the grain boundaries, etc.) |
| D | | ▪ the different deformation on the microstructure: close and far away to the crack |
| | | ▪ the grain orientation |

Samples of S700MC and DP980 were chosen to reach these objectives. Four samples of each were tested at 700 MPa constant load, stopping the test before rupture.

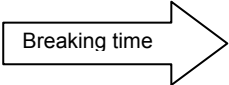
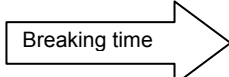
The consecutive steps were:

- Tensile testing
- Sample preparation
- SEM analysis
- EBSD analysis
- Discussion

7.1 Tensile testing

The purpose of this chapter is to obtain samples tested in air and samples tested with in-situ H-charging (before breaking) to analyze the cracks appearing throughout the test.

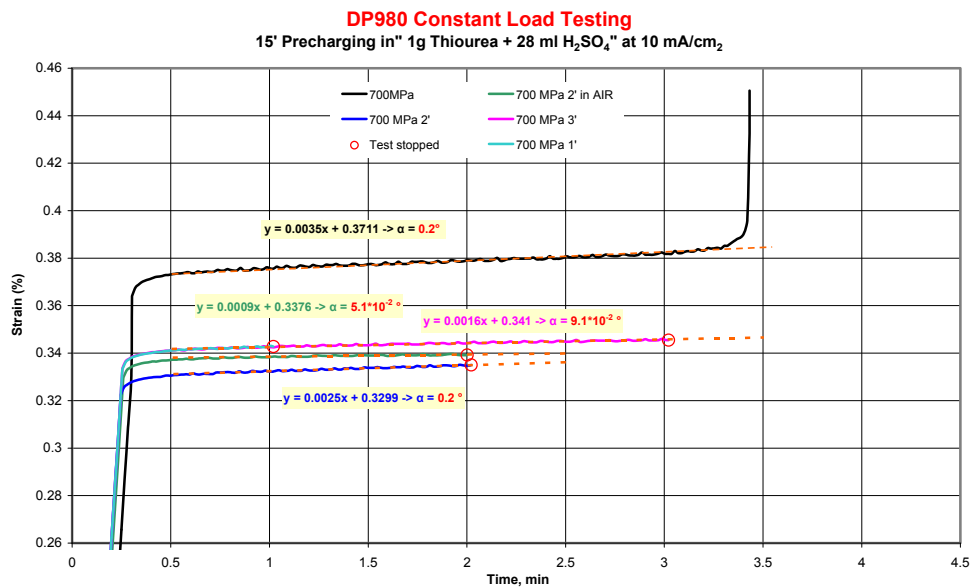
For that reason, the data generated in the previous chapter 6, needed to be considered:

S700MC at 700 MPa		15.00 minutes
DP980 at 700 MPa		03.40 minutes

For each steel four samples were tested at 700 MPa, stopped at different times below the rupture time:

DP980 tested samples:

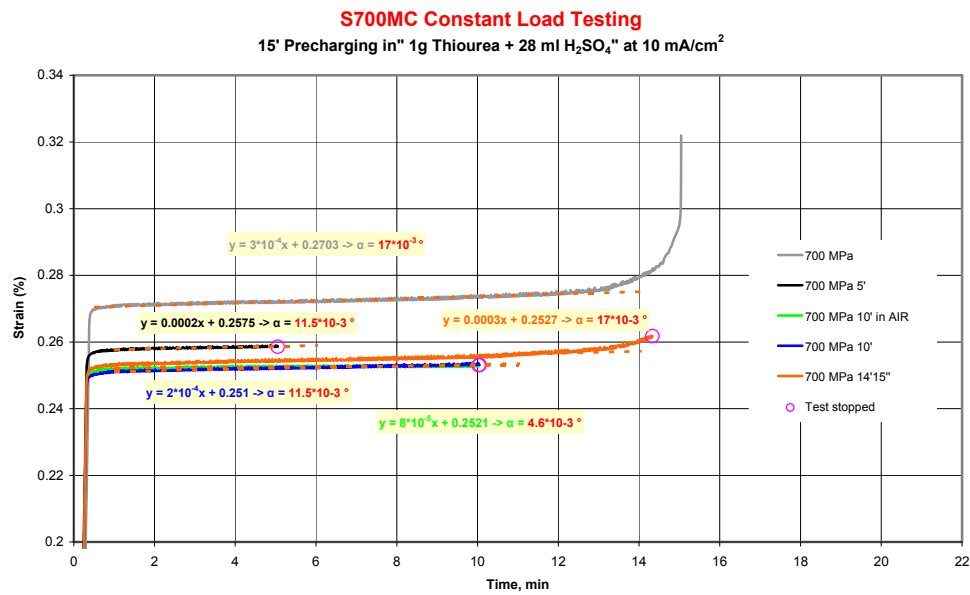
1. in air and stopped after 2 minutes testing
2. pre-charging 15 minutes in “1g Thiourea + 28 ml H_2SO_4 / L H_2O ” and stopped after 1 minute testing with in-situ H-charging.
3. pre-charging 15 minutes in “1g Thiourea + 28 ml H_2SO_4 / L H_2O ” and stopped after 2 minutes testing with in - situ H-charging.
4. pre-charging 15 minutes in “1g Thiourea + 28 ml H_2SO_4 / L H_2O ” and stopped after 3 minutes testing with in - situ H-charging.



Graph 40: DP980 Strain Vs Time for SEM samples

S700MC tested samples:

5. in air and stopped after 10 minutes testing.
6. pre-charging 15 minutes in “1g Thiourea + 28 ml H_2SO_4 / L H_2O ” and stopped after 5 minutes testing with in-situ H-charging.
7. pre-charging 15 minutes in “1g Thiourea + 28 ml H_2SO_4 / L H_2O ” and stopped after 10 minutes testing with in-situ H-charging.
8. pre-charging 15 minutes in “1g Thiourea + 28 ml H_2SO_4 / L H_2O ” and stopped after 14 minutes and 20 seconds testing with in-situ H-charging.



Graph 41: S700MC Strain Vs Time for SEM samples

Both materials present cracks on the charged samples, concretely starting from the notches and propagating perpendicularly to the tensile direction that could be seen by human view.

7.2 Sample preparation

For SEM, the samples:

- were cut to have just the zone with the notches
- were cleaned with acetone to remove the dirt on the surface
- were embedded on a resin matrix.
- were grinded and polished up to remove $\frac{1}{4}$ of the thickness.
- n° 3 and n° 7 were etched with NITAL 2% to see the different phases.
- were covered by a layer of Au on the samples surfaces to increase the conductivity for using in the SEM.



Fig 43a: DP980 sample embedded on a resin matrix



Fig 43b: S700MC sample embedded on a resin matrix

For EBSD, the samples:

- were cut to have just the zone with the notches
- were cleaned with acetone to remove the dirt on the surface
- were embedded on a resin matrix.
- were mechanical and chemical by polished.
- in order to remove the dirt on the surfaces, Coloidal Silica was used.

7.3 SEM analysis

Only the tested samples which were given more information were selected and commented as follows:

Sample 1.- DP980 tested in air at 700 MPA and stopped after 10 minutes:

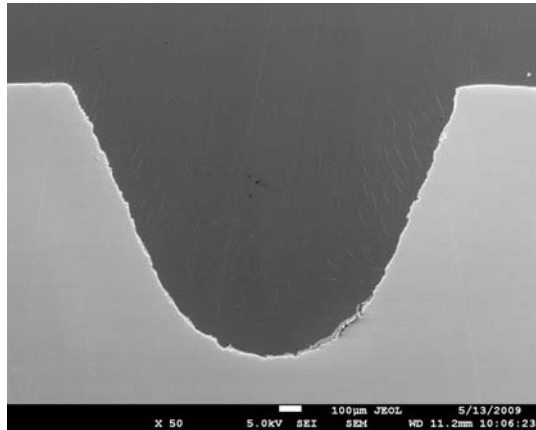


Fig.44: No cracks are present on the notches of DP980 sample

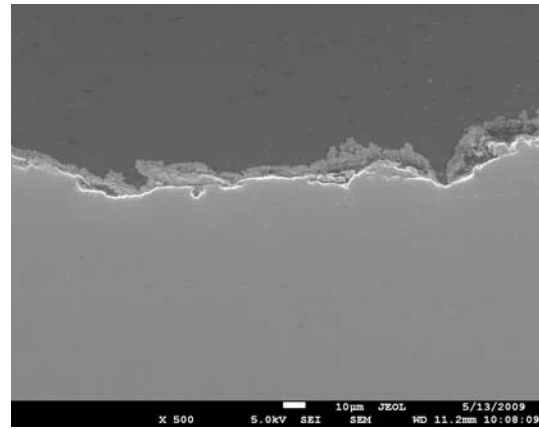


Fig.45: Detail on the notch boundary, free of cracks of DP980 sample

No cracks were observed on the sample tested in air, i.e. Fig 44 at magnification X50 doesn't show any crack and even at X500 magnification no cracks were observed.

Sample 2.- DP980 pre-charging 15 minutes in “1g Thiourea + 28 ml H₂SO₄ / L H₂O” and stopped after 1 minute testing with in-situ H-charging:

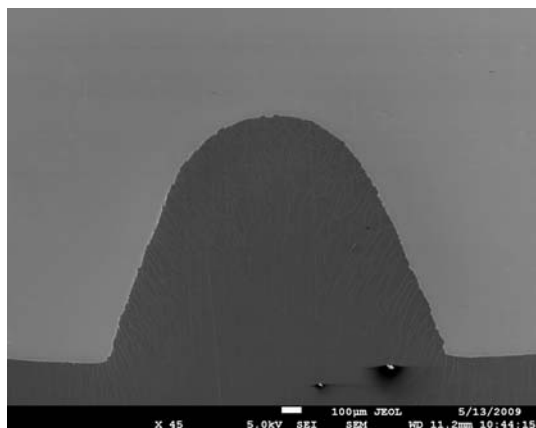


Fig.46: left notch of DP980 sample

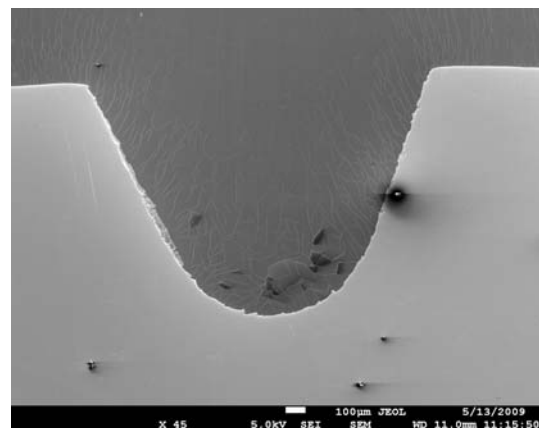


Fig.47: right notch of DP980 sample

On these two previous images X45 magnification is not possible to perceive any crack presence.

More in detail was scanned the notch boundaries and to appreciate some cracks was possible:

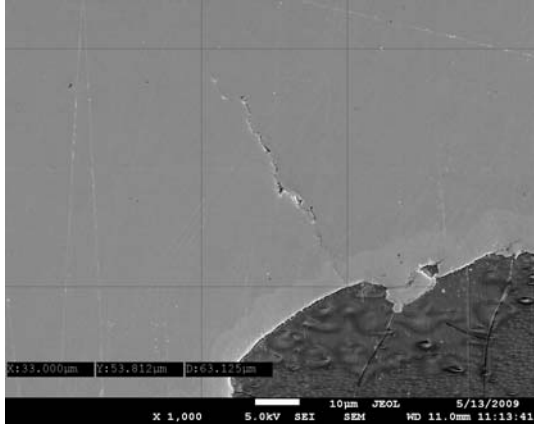


Fig.48: Detail of a crack on the left notch boundary of DP980 sample

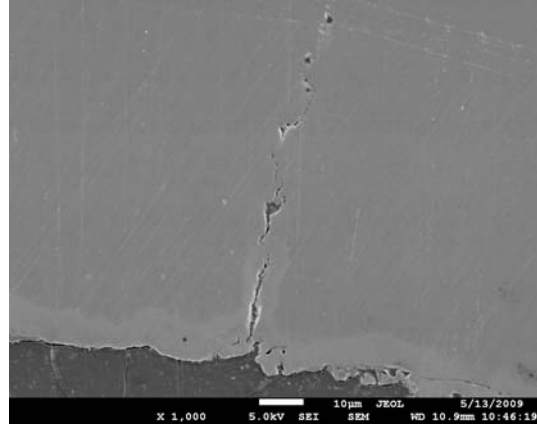


Fig.49: Detail of a crack on the left notch boundary of DP980 sample

In this case initial cracks can be seen, starting on the notch boundaries. The lengths of them are between 20 to 65 μm .

The first conclusion is to confirm if hydrogen has a real effect on the materials behavior.

Sample 3.- DP980 pre-charging 15 minutes in “1g Thiourea + 28 ml H_2SO_4 / L H_2O ” and stopped after 2 minutes testing with in-situ H-charging.

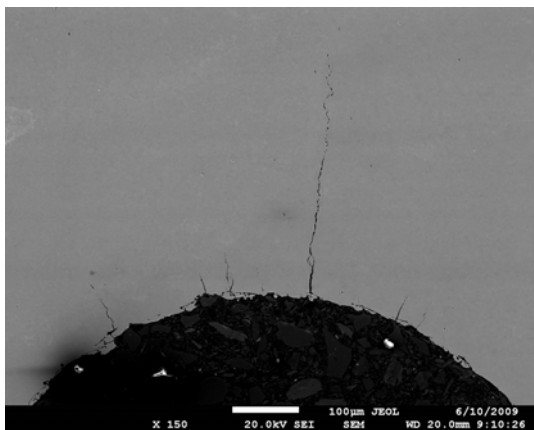


Fig.50: cracks in the left notch of DP980 sample

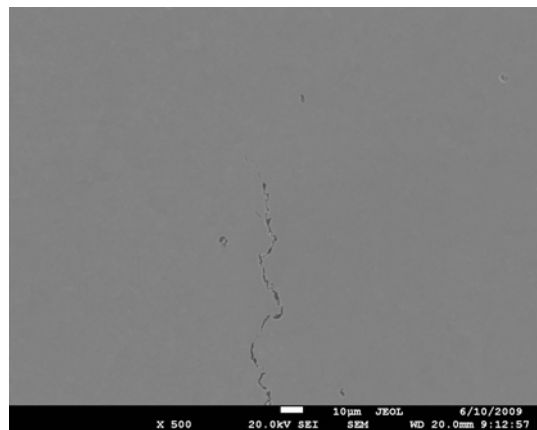


Fig.51: detail of crack tip on left notch of DP980 sample

Fig 50 shows a high amount of appearing cracks, and one big crack (around 0.5 mm length) can be seen. With more detail, in fig 51, is shown the crack tip of the largest crack.

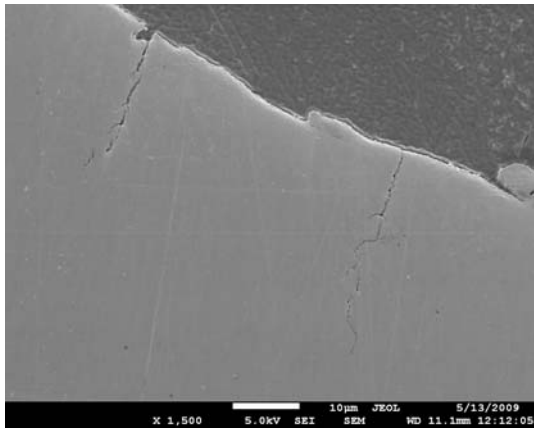


Fig.52: Detail of a crack on the right notch boundary of DP980 sample

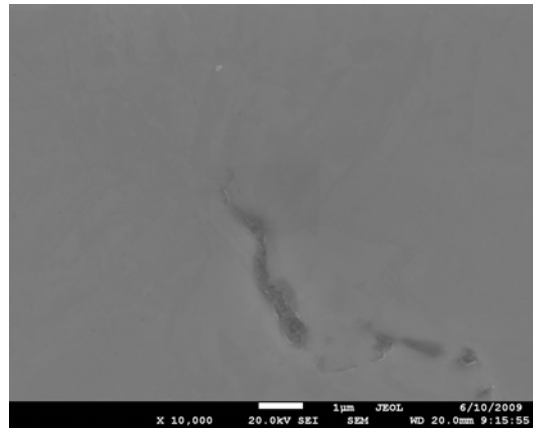


Fig.53: Detail of a crack tip on right notch of DP980 sample

The amount of cracks is higher than for the previous sample that was stopped after 1 minute testing.

The next sample to study was supposed to be the n°4, being 3 minutes charging instead of 1 and 2 minutes as the previous, but was decided to continue with sample 7 of S700MC because the previous DP980 results were enough to study the cracking behavior.

For S700MC, two samples were analyzed, i.e. those stopped after 10' & 14'20" testing respectively.

Sample 7.- S700MC pre-charging 15 minutes in “1g Thiourea + 28 ml H_2SO_4 / L H_2O ” and stopped after 10 minutes testing with in-situ H-charging

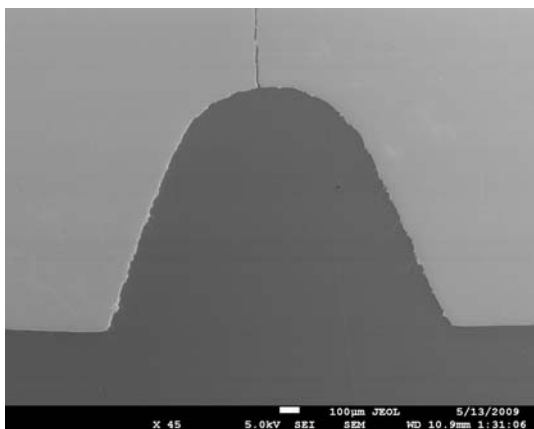


Fig. 54: crack on the left notch boundary of S700MC

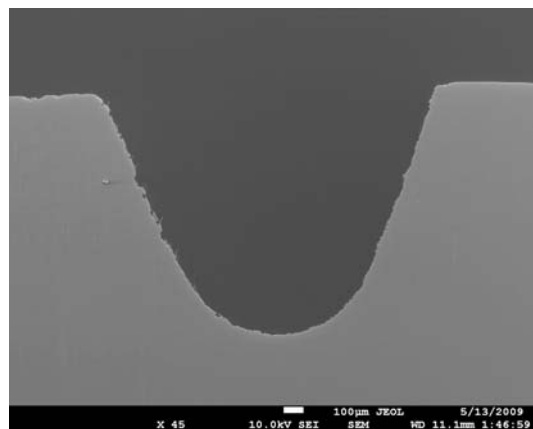


Fig.55: right notch boundary of S700MC

A visible crack at “x 45” is shown on the left notch. Apparently on the right notch there are not cracks, but more detailed analysis at the notch boundaries: revealed one small crack.

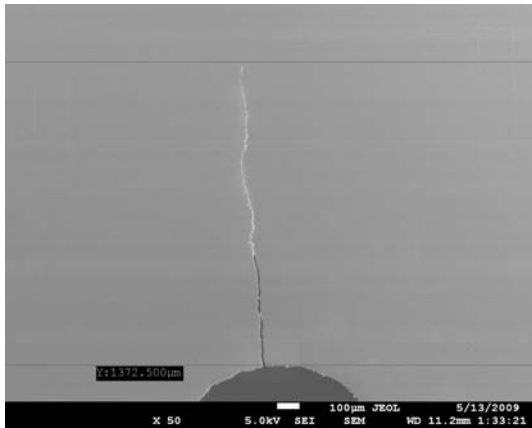


Fig.56: Detail of a crack on the left notch boundary

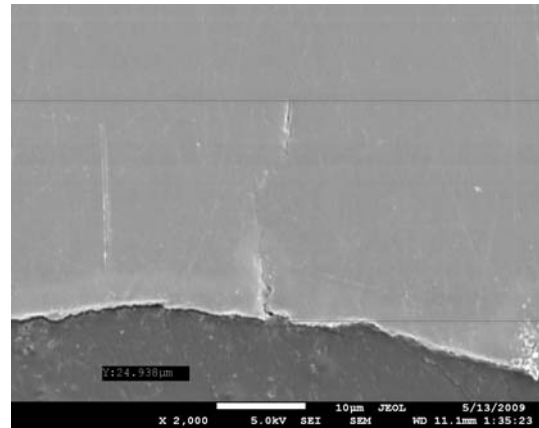


Fig.57: Detail of a crack on the left notch boundary

Comparing to the DP980 steel, S700MC present less amount of cracks. The biggest crack is around 1.30 mm and just another smaller of 24 µm was found.

Sample 8.- S700MC pre-charging 15 minutes in “1g Thiourea + 28 ml H_2SO_4 / L H_2O ” and stopped after 14 minutes 20 seconds testing with in-situ H-charging



Fig. 54: crack on the left notch of S700MC sample

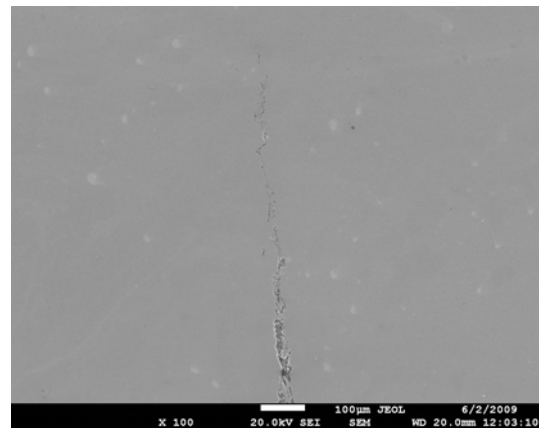


Fig.55: Detail of crack tip on left notch of S700MC sample

Fig 54 demonstrates the S700MC (bainitic containing steel) has only one remarkable crack but bigger than DP980.

Observing these images and studying the tensile tests result graphs, can be concluded DP980 steel is much more sensitive to the hydrogen than S700MC.

To observe the cracks being in relation to the different phases of samples n°3 (DP980) and n°7 (S700MC), they were etched with Nital 2%.

Sample 3.- ETCHED DP980 pre-charging 15 minutes in “1g Thiourea + 28 ml H_2SO_4 / L H_2O ” and stopped after 2 minutes testing with in-situ H-charging.

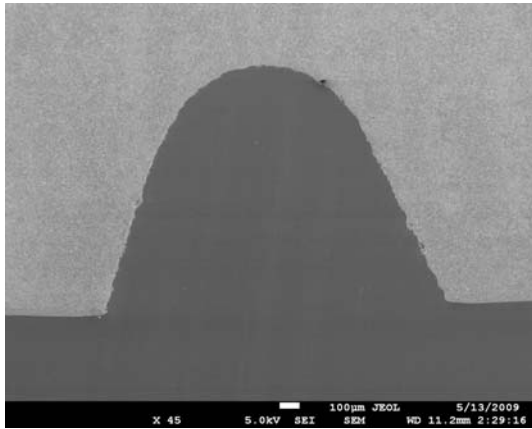


Fig.58: left site of the notch of DP980 sample

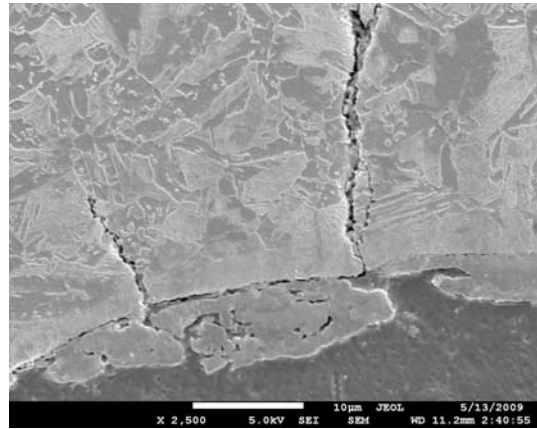


Fig.59: Detail of the cracks on the notch boundary in etched DP980 sample

From these images, two phases could be differentiated; the white zones can be related to martensite and the grey ones to Ferrite.

Is not possible to know if the crack is intragranular or propagating along the grain boundary propagating, will be needed the EBSD technique.

Sample 7.- ETCHED S700MC pre-charging 15 minutes in “1g Thiourea + 28 ml H_2SO_4 / L H_2O ” and stopped after 10 minutes testing with in-situ H-charging:

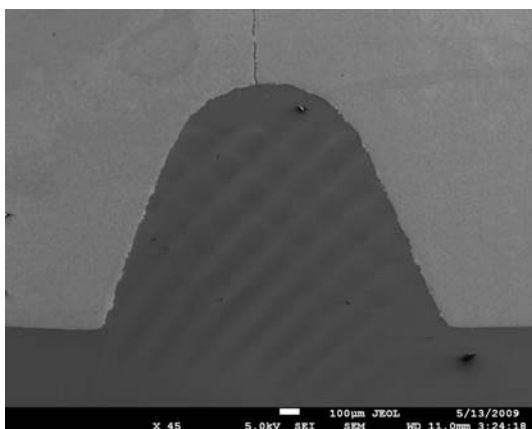


Fig.60: Detail of a crack on the notch boundary of S700MC etched

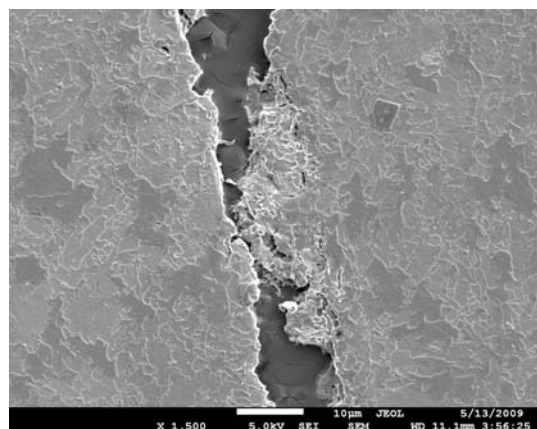


Fig.61: Detail of the crack near the notch boundary

The Fig 60 shows the whole notch and the crack on the top clearly appreciable. The Fig 61 shows a detailed zone of the crack and the different

phases; the bainite are the white particles around the grains on the ferrite matrix.

The same as DP980, to try to identify if the crack is intergranular or grain boundary propagating, a EBSD technique must be applied.

7.4 EBSD analysis

EBSD gives a way to better understand the crack propagation, the different crystallographic orientation near and far away from the crack and the distinction of the different phases on the tested samples.

The different types of results that could be obtained with this technique are shown as follows:

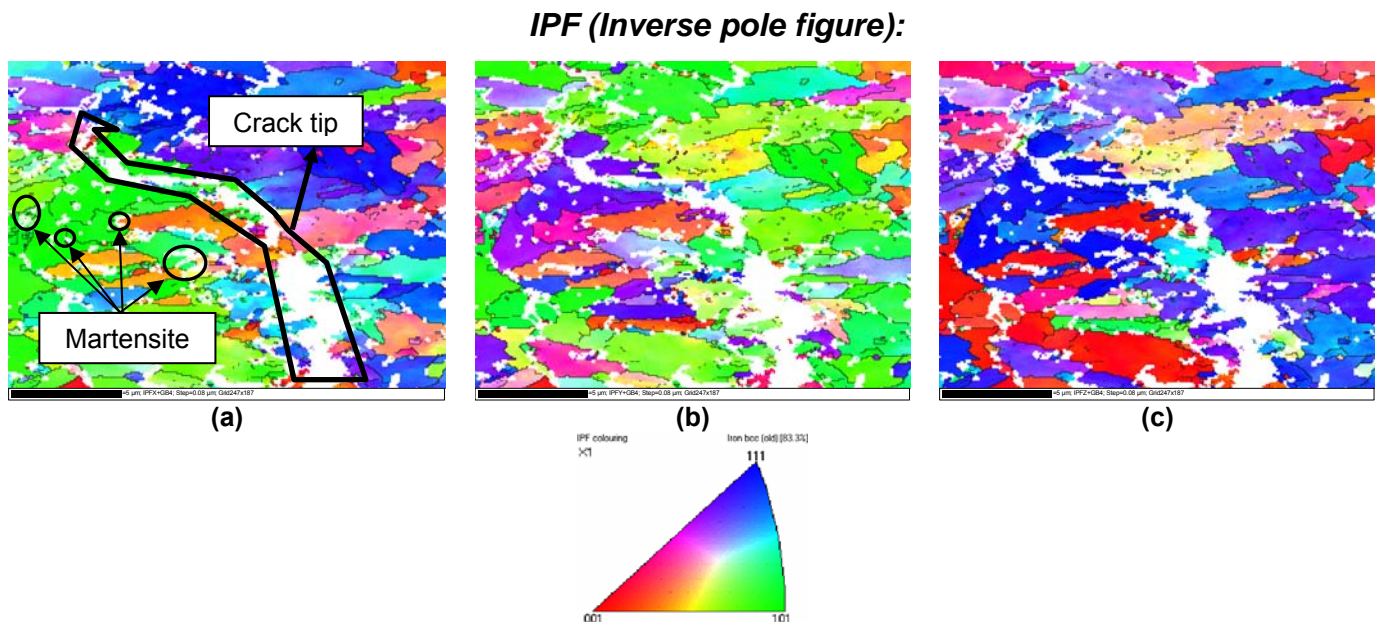


Fig 62: Grain orientation of the crack tip of DP980 sample n°3 (a) respect X (Rolling direction) axis; (b) respect Y (Transversal direction) axis; (c) respect Z (Normal direction) axis

The Fig 62 shows the grain orientation of the selected zone of the crack tip of the sample n°3 (DP980 pre-charging 15 minutes in “1g Thiourea + 28 ml H_2SO_4 / L H_2O ” and stopped after 2 minutes testing with in-situ H-charging). The three axis analysis is needed to know the exactly orientation of each grain. When one same grain shows different colors means deformation is present on it.

Despite of the crystallographic orientation, this type of analysis IPF should give information about the crack propagation type. For this case, is not clear to identify if the crack is being propagating via intergranular or among the grain boundaries, probably is a mixture of both types but can't be confirmed.

The white points on the Fig 62 are the zones that the software couldn't identify the phase. The crack appear in white color for that reason and the rest of white points are related to the martensite structure.

Band Contrast:

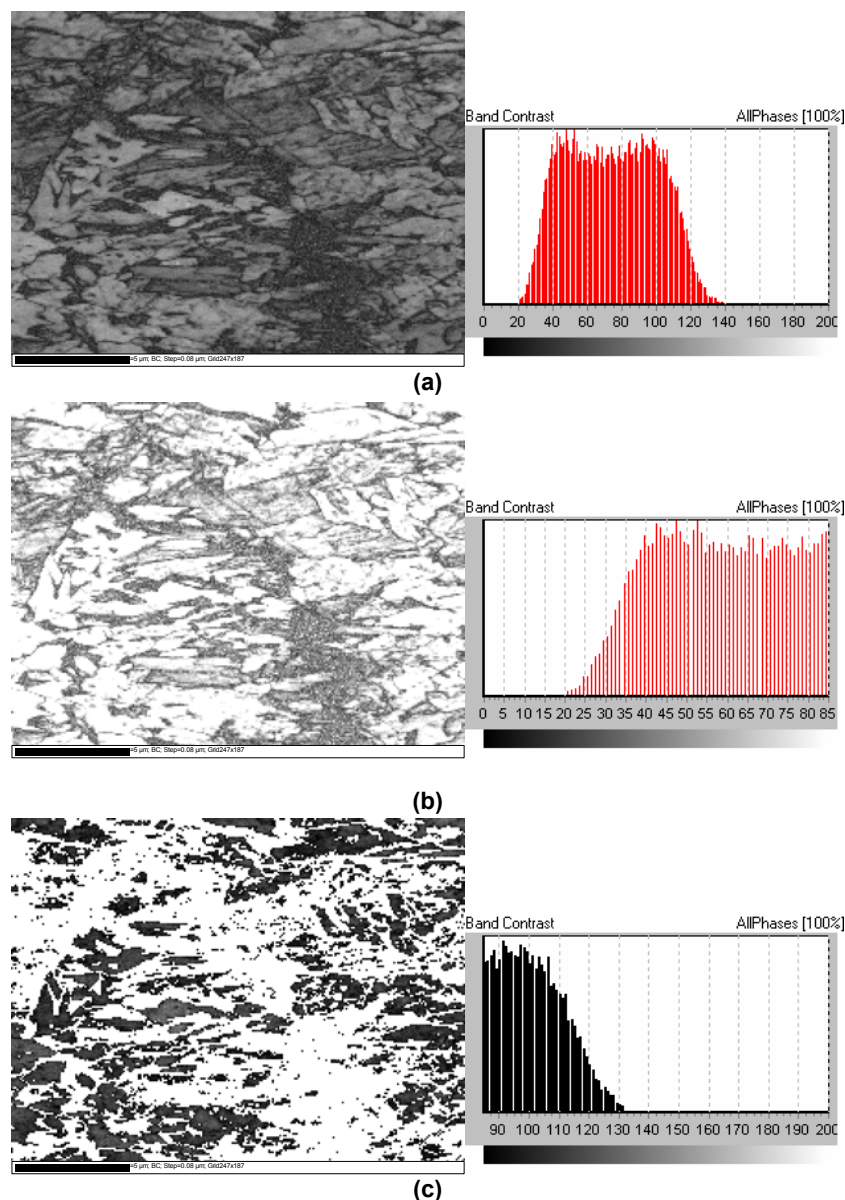


Fig 63: Band contrast on the tip crack of DP980 sample n°3 (a) All phases (b) crack and martensite (c) ferrite

The band contrast can be understood as the quality of the image scanned. The band contrast values are from 0 to 200 being 200 the highest quality. When an image zone is not identified as a crystallographic phase (e.g. a region

without material, dirt on the surface, cracks...), the lowest band contrast values are obtained, i.e. a bad image quality.

Fig 63 shows the same region as Fig 62 of the crack tip. On the Fig 63(a) all the phases present on the crack tip zone are represented on the image; on the band contrast graph two peaks can be distinguished and were separated in two different graphs as shows (b) and (c).

(b) Represents the first peak, the one with lowest band contrast values related to a unidentified phases, i.e the crack, the grain boundaries and martensite phase.

(c) Represents the ferrite phase with good image quality.

Local Misorientation:

Two samples were studied: DP980 sample n°3 and S700MC sample n°8. For each one, undeformed (A) and deformed (B) zones were analyzed (Fig. 64):

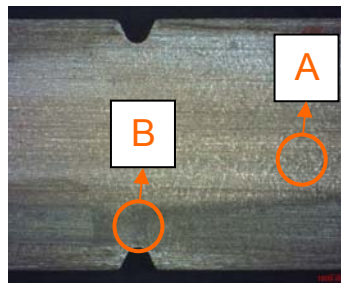


Fig 64: notch zone of the sample with marked points for study

The local misorientation gives information about the deformation in a specific zone of the material studied. It generates an image composed by different colors as the following color scale:

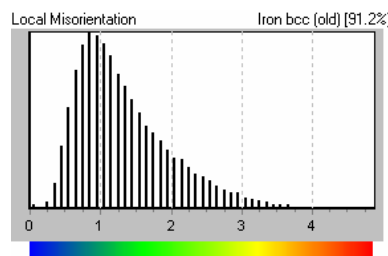


Fig 65: Intensity Vs Degrees

The color scale is followed by a scale of degrees from 0 to 5 °; the blue color has to be interpreted as totally undeformed area and the red color as maximum deformed area.

The software takes pixel by pixel of a SEM image and check if the pixels around the one selected have the same or different orientation. If some of them

are different; the color changes automatically depending on the difference between the degrees. The maximum misorientation is 5 ° (red color) between two pixels. In case of higher of 5° means that exist a grain boundary.

Sample 8.- S700MC pre-charging 15 minutes in “1g Thiourea + 28 ml H_2SO_4 / L H_2O ” and stopped after 14 minutes 20 seconds testing with in-situ H-charging:

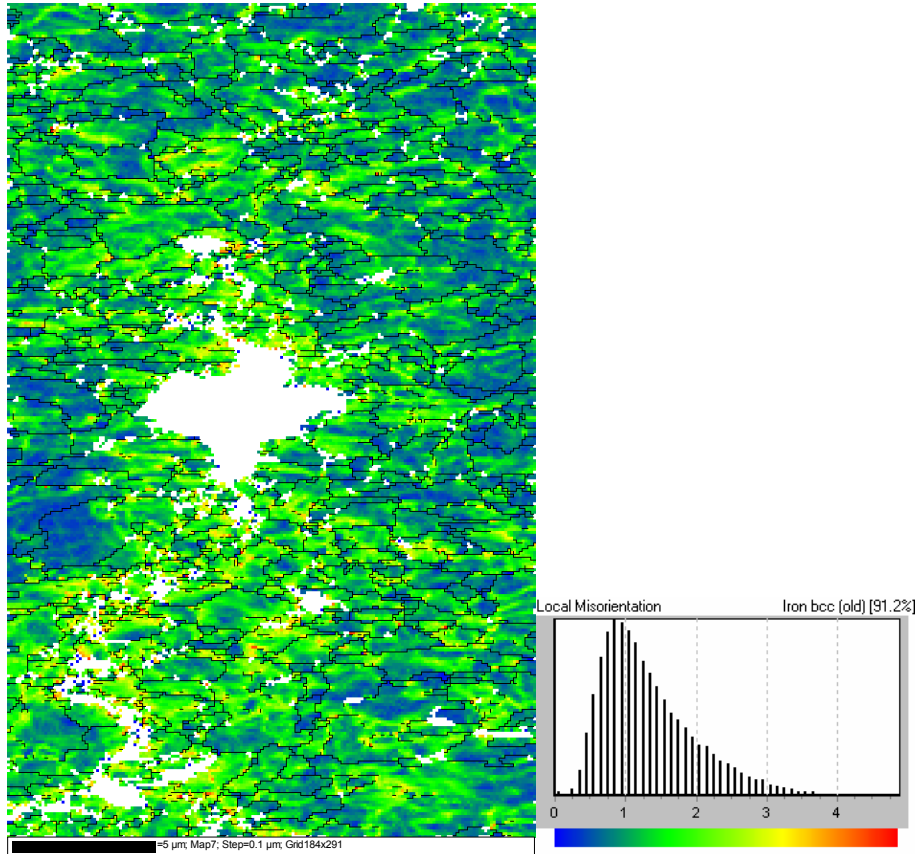


Fig 66: Zone B of S700MC.

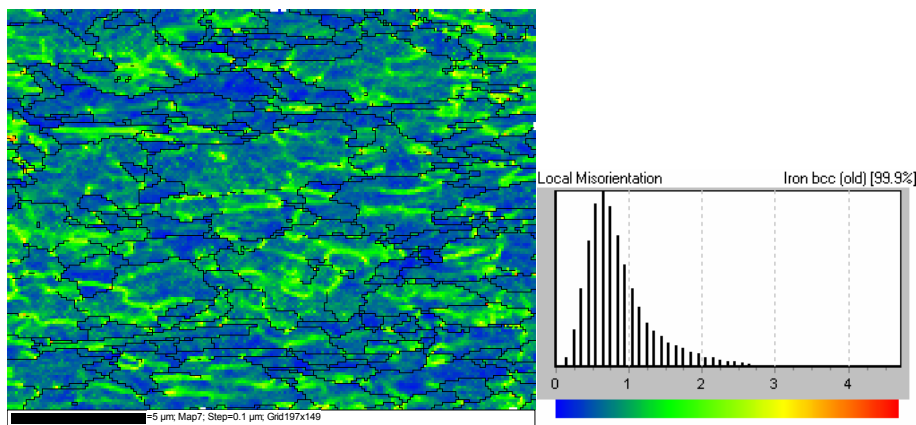


Fig 67: Zone A of S700MC

Sample 3.- DP980 pre-charging 15 minutes in “1g Thiourea + 28 ml H₂SO₄ / L H₂O” and stopped after 2 minutes testing with in-situ H-charging.

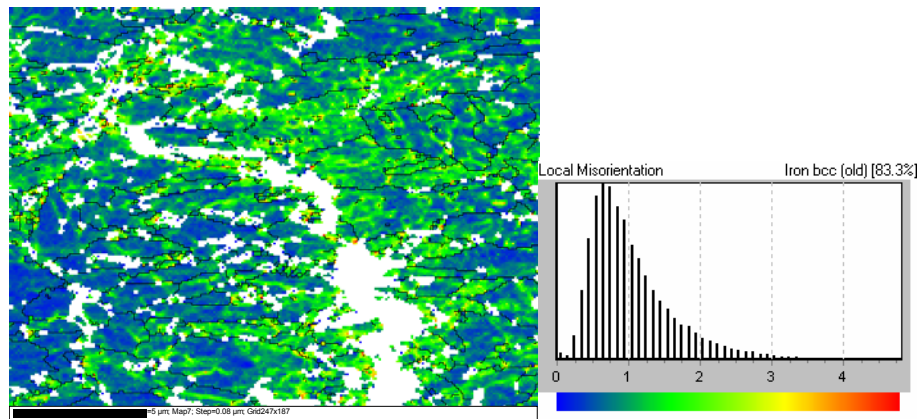


Fig 68: Zone B of DP980

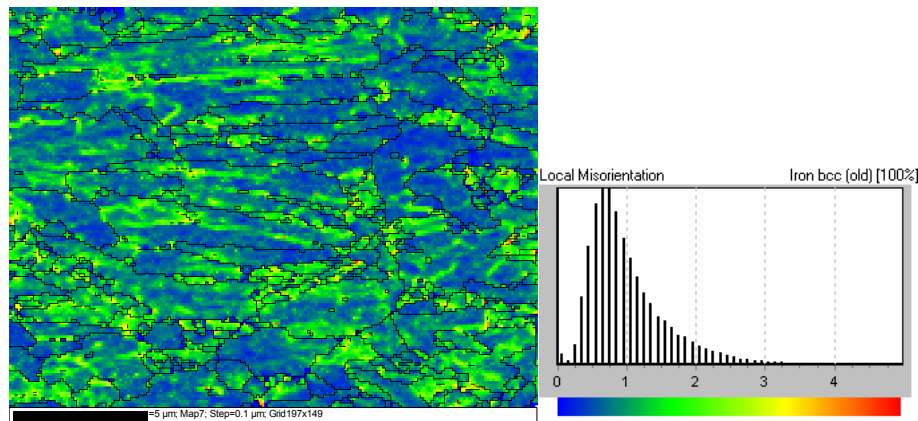


Fig 69: Zone A of DP980

Fig 66 shows the deformed area (on the crack tip) of the sample n°8; the Fig 67, the undeformed area (far from the crack).

The differences between both are significant. On the Fig 66, all the area around the crack is between green-yellow and some red points, confirming that exists plastic deformation around the crack. Out from the boundary of the crack, more blue areas can be appreciated.

On the Fig 67, to have the major part of the image blue was expected, but; as can be seen on the image, there are several green regions, letting know either in a point far from the notch, exists deformation on the material.

The results for the DP980 in Fig 68 & 69 give the same information than the ones of S700MC. The most remarkable difference between both materials on

the crack area is that for DP980, the level of deformation is lower than for S700MC. On the far crack area, both are very similar.

7.5 Discussion

- The SEM images reveal the DP980 is more sensitive to hydrogen when stress is applied than S700MC. A higher amount of cracks are present on DP steel than on the Ferritic-bainitic.
- The EBSD confirms the DP cracks needs less strength to propagate than S700MC which needs a strongest strength to propagate becoming more deformed the area around the crack.
- The EBSD results don't gives a clear answer about the type of crack propagation, a mixture between intragranular and propagation along the grain boundary propagation can be seen.

8 CONCLUSIONS AND SUGGESTIONS FOR FUTURE WORKS

An optimized tensile testing methodology was obtained with in-situ H-charging to reveal the hydrogen embrittlement in various high strength C-steels, basically Dual Phase steels with a ferritic-martensitic (DP600 / DP980 / DP1200) microstructure and ferritic-bainitic steels (FB450 / S700MC).

Other steel grades should be tested on future works.

The mechanical characterization of the Hydrogen effect on those steels was done, and to understand better the initiation and propagation of cracks during tensile testing with in-situ H-charging and the correlation with crystallographic orientation, some materials have been analyzed in the SEM in combination with the EBSD technique.

More deeply EBSD tests should be done in the future works to interpret the different steel grades behaviors.

The main conclusions are:

- The experimental results on the charging methods reveal that the potentiostatic method is rather complex for the in-situ H-charging during tensile testing; the galvanostatic method gives an open range of H-charging applications in comparison with potentiostatic method.
Other solutions should be tested in future works with the aim to avoid the corrosion on the samples that could have influence on the results.
- The electrolytes containing Thiourea + H_2SO_4 permit to select the introduction of specific amounts hydrogen into the materials from 6 to 20 ppm of hydrogen when varying the current density on the galvanostatic power source.
- The introduction of a notch on the tensile samples permits to reach a significantly improved reproducibility of the results, forcing the rupture on this area.

On future studies should be studied the sample's thickness effect on the in-situ H-charging tensile testing results.

Also the pre-charging time effect should be deeply studied with different H-charging times.

- To study the effect of hydrogen embrittlement during tensile testing with in-situ H-charging, the constant load tests were the one which gave better results, although incremental step loading seems a powerful test for future studies, but needing to be improved (avoiding the extensive sample preparation, the shape of the round bars to flat ones, etc)

For the future should be reached the manner to apply the potentiostatic charging method in tensile testing with in-situ H-charging due to in most part of standards about this topic is the method used.

- The constant load testing reveal that Dual Phase (ferritic-martensitic) steels are more sensitive to hydrogen induced cracking than FB (ferritic-bainitic) ones. This higher sensitivity to hydrogen was found back in the reduced failure times, increased creep rates and enhanced crack initiation (SEM) for Dual Phase steels in comparison with FB steels.

On future works should be useful to study the precipitations effect e.g. on S700MC the Ti and Nb precipitates.

- EBSD technique confirms the different sensitivity of DP steels by the local misorientation maps obtained where less plastic deformation around the cracks are found in comparison with FB steels.

The IPF technique (EBSD) doesn't reveal clearly which type of crack propagation is present on both types of steels.

On the future, deep analysis on crack phenomenon should be done by using EBSD technique, focusing basically on the local misorientation mappings in High Resolution. Also study with other materials states, i.e. samples stopped after different testing times and in other solutions, different sample thickness, different H-charging methods.

9 BIBLIOGRAPHIC REFERENCES

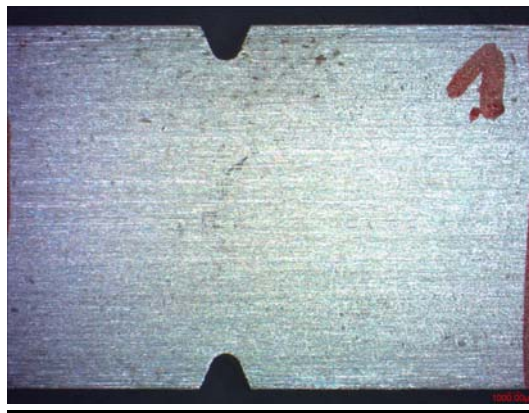
- HySafe, *BRHS Chapter 3 – Material Considerations when working with Hydrogen*
1 http://www.hysafe.org/download/1002/BRHS%20Chap3%20-%20material%20consideration-version%201_0_1.pdf January 2007
- 2 J.P. Mercier, G. Zambelli, W. Kurz: *Introduction to Materials Science*, Elsevier, Paris, 2002
- 3 Dull, D.L. and Raymond, Louis, “Electrochemical Techniques” *Hydrogen Embrittlement Testing*, ASTM ST P 543, American Society for Testing and Materials, 1974, pp. 20-33
- 4 Dr. Marc Verhaege, *Electrochemical study of the hydrogen evolution reaction at metallic substrates*, Dept. Materials Science and Engineering, Ghent, 2007
- 5 Han J. N.; Pyun S.I.; Yang T.H. *Roles of thiourea as an inhibitor in hydrogen absorption into palladium electrode*, J. Electrochem. Soc., 1997
- 6 Wu T.I.; Wu J. K.; *Effects of thiourea and its derivatives on the electrolytic hydrogenation behavior of Ti-6Al-4V alloy*, Materials Letters, 2002
- 7 T. Zakroczymski; *Entry of Hydrogen into Iron Alloys from the Liquid Phase*, Institute of Physical Chemistry ; Polish Academy of Sciences, Warsaw
- 8 ASTM F 1624-06 standard test method, *Measurement of Hydrogen Embrittlement Threshold in Steel by incremental Step Loading Technique*, 2006
- 9 P.S. Tyler, M. Levy., L. Raymond, *Investigation of the conditions for Crack Propagation and Arrest Under Cathodic Polarization by Rising Step Load Bend Testing*, National Association of Corrosion Engineers, 1991
- 9 P.S. Tyler, M. Levy., L. Raymond, *Investigation of the conditions for Crack Propagation and Arrest Under Cathodic Polarization by Rising Step Load Bend Testing*, National Association of Corrosion Engineers, 1991
- 10 ASTM E 8/E 8M - 08 standard test method, *Tension Testing of Metallic Materials*, 2008
- 11 ASTM G129 standard test method, *Standard Practice for Slow Strain Rate Testing to Evaluate the Susceptibility of Metallic Materials to Environmentally Assisted Cracking*, 2006
- 12 <http://www.ebsd.com/ebsd-explained>

APPENDICE

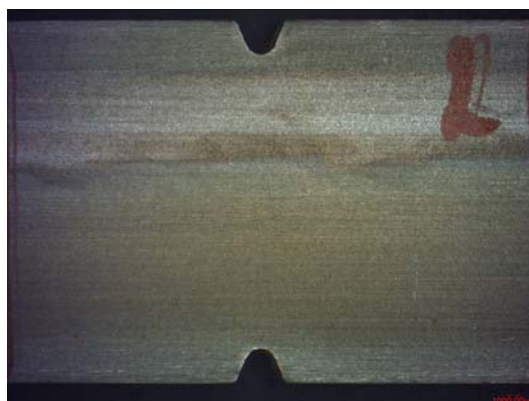
APPENDIX 1: OPTICAL MICROSCOPE IMAGES

DP980

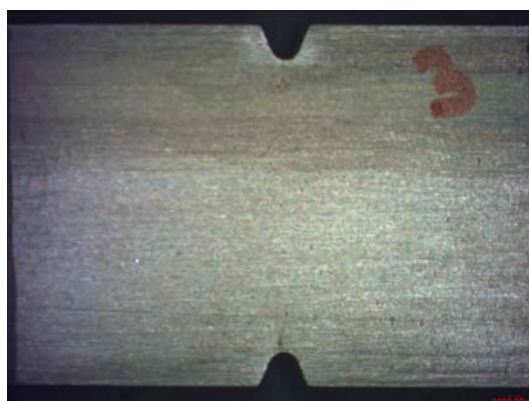
1. Tested in air and stopped after 2 minutes testing



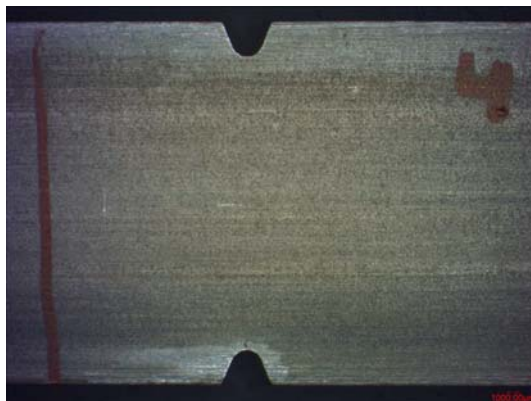
2. pre-charging 15 minutes in “1g Thiourea + 28 ml H_2SO_4 / L H_2O ” and stopped after 1 minute testing with H-charging insitu



3. pre-charging 15 minutes in “1g Thiourea + 28 ml H_2SO_4 / L H_2O ” and stopped after 2 minutes testing with H-charging insitu



4. pre-charging 15 minutes in “1g Thiourea + 28 ml H_2SO_4 / L H_2O ”
and stopped after 3 minutes testing with H-charging insitu

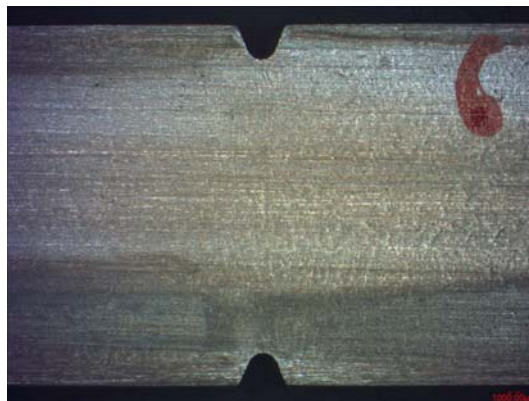


S700MC

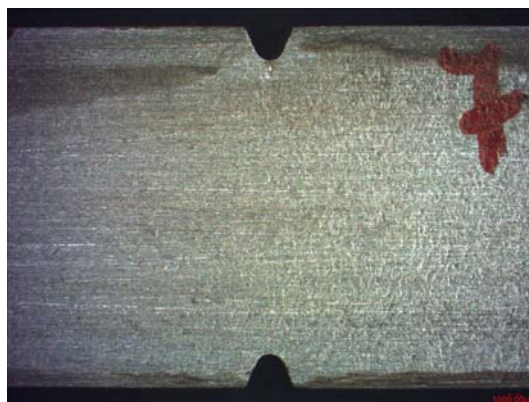
5. in air and stopped after 10 minutes testing.



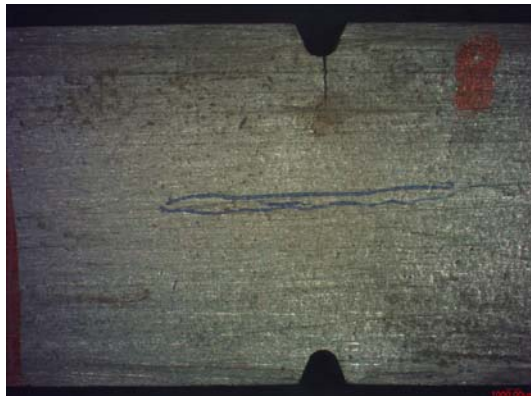
6. pre-charging 15 minutes in “1g Thiourea + 28 ml H_2SO_4 / L H_2O ” and stopped after 5 minutes testing with H-charging insitu.



7. pre-charging 15 minutes in “1g Thiourea + 28 ml H_2SO_4 / L H_2O ” and stopped after 10 minutes testing with H-charging insitu.



8. pre-charging 15 minutes in “*1g Thiourea + 28 ml H₂SO₄ / L H₂O*” and stopped after 14 minutes and 20 seconds testing with H-charging insitu.

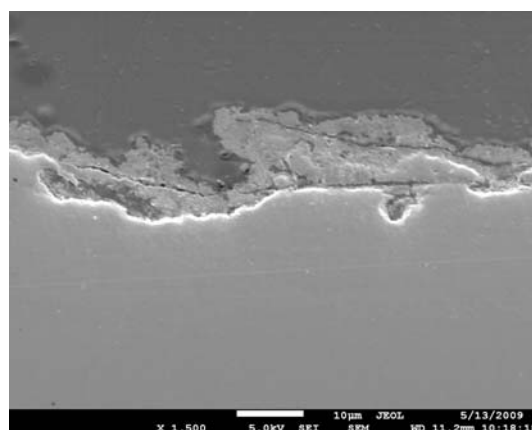
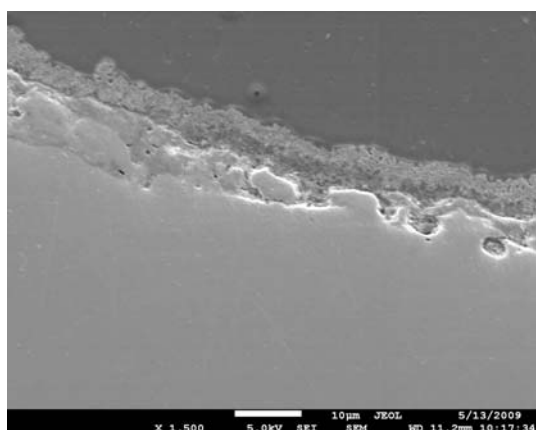
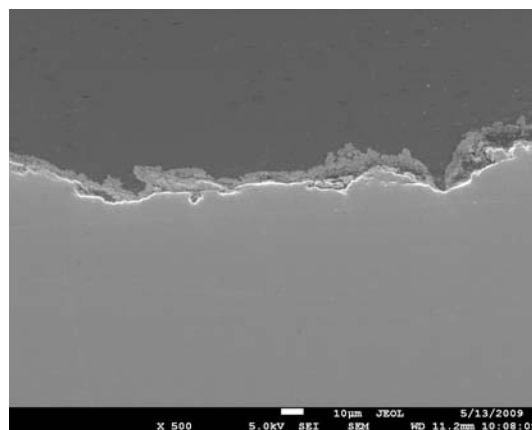
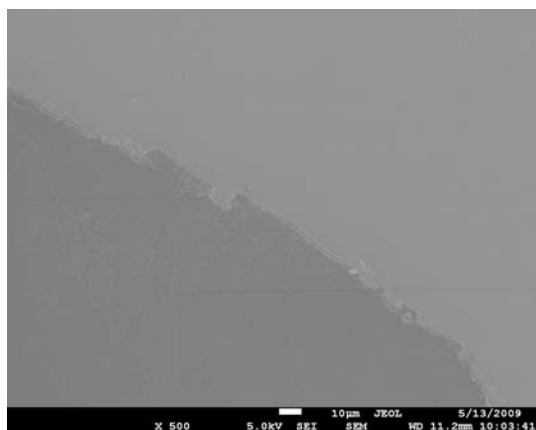


APPENDIX 2: SEM IMAGES

DP980

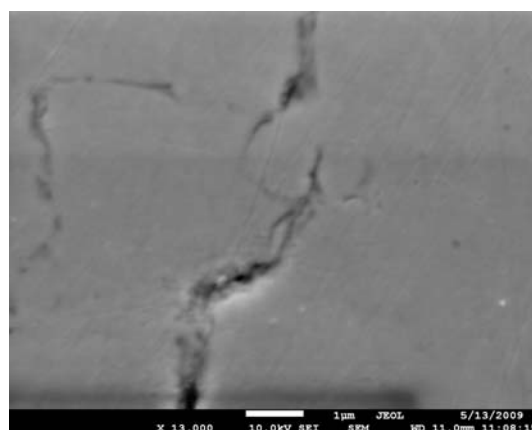
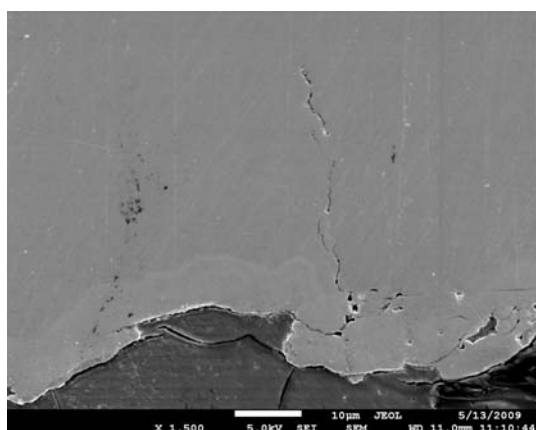
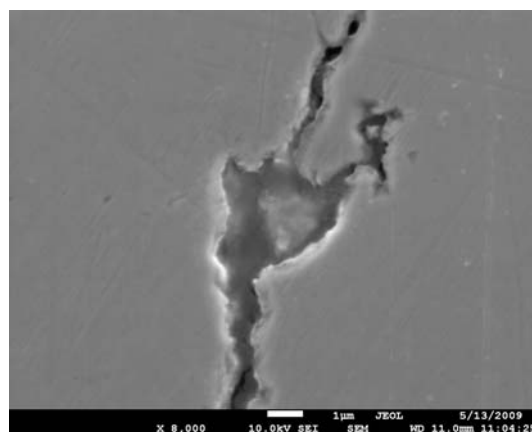
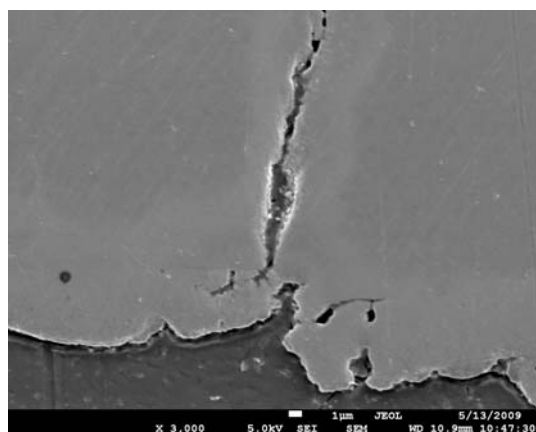
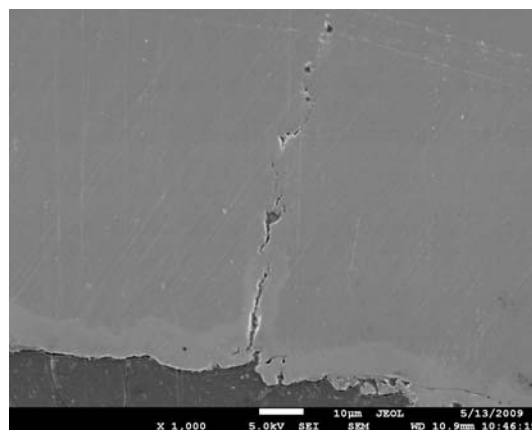
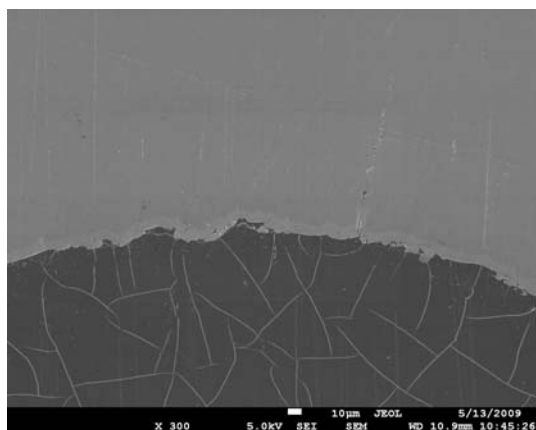
1. Tested in air and stopped after 2 minutes testing

UNETCHED:



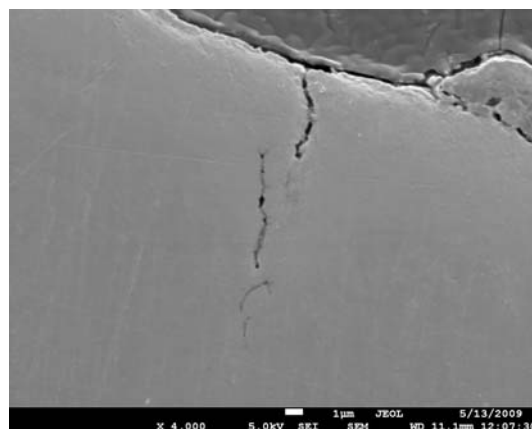
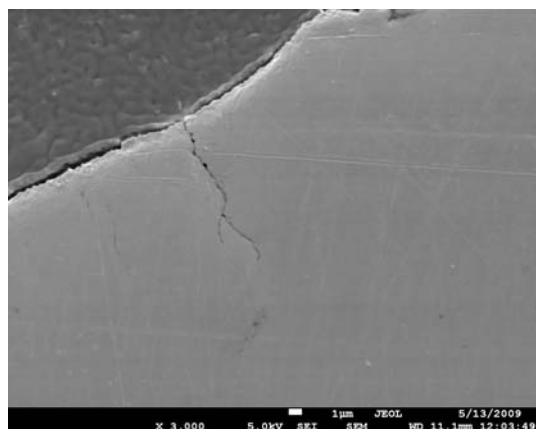
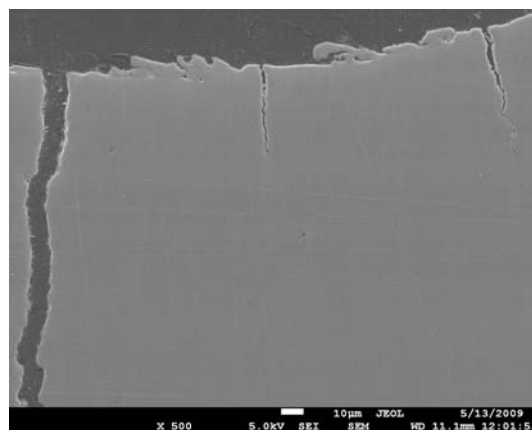
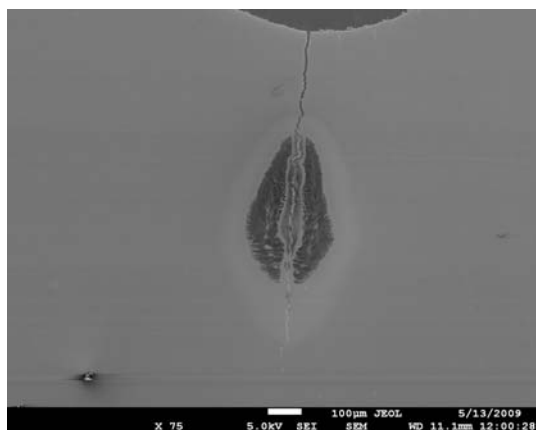
2. pre-charging 15 minutes in “1g Thiourea + 28 ml H_2SO_4 / L H_2O ”
and stopped after 1 minute testing with H-charging insitu

UNETCHED:

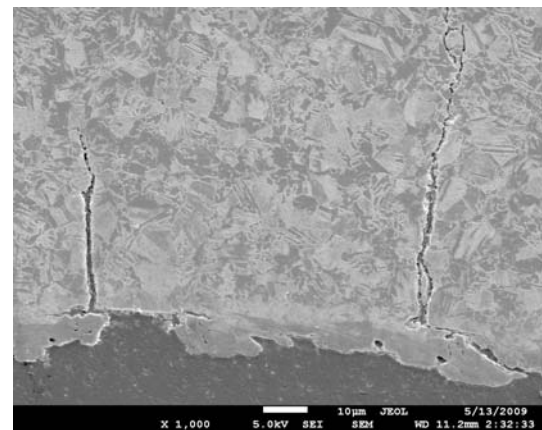
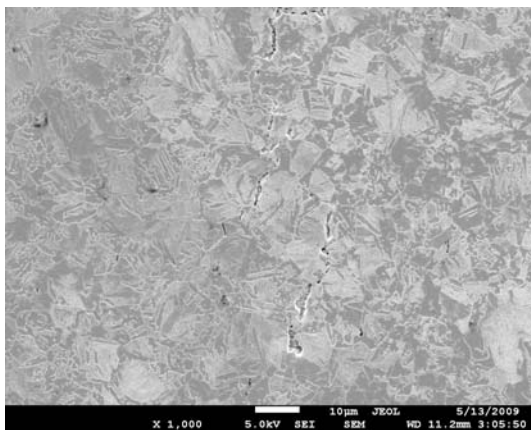
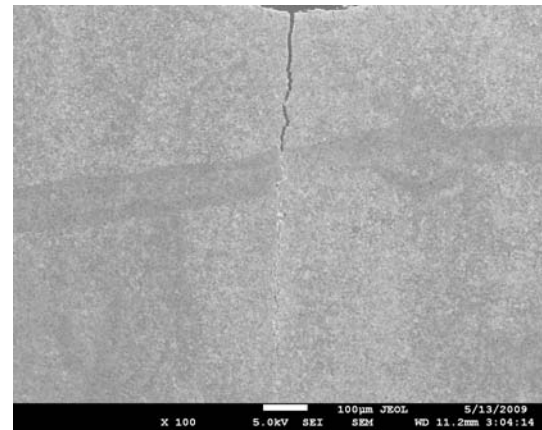
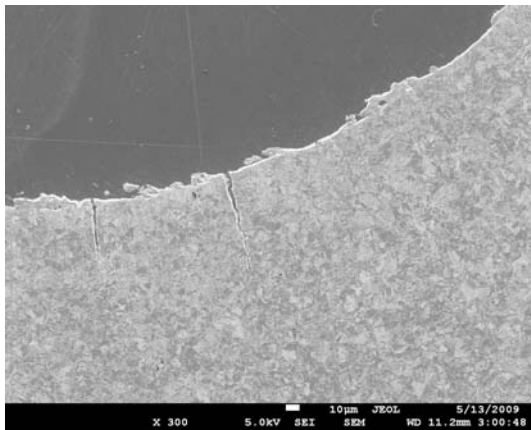


3. pre-charging 15 minutes in “1g Thiourea + 28 ml H_2SO_4 / L H_2O ”
and stopped after 2 minutes testing with H-charging insitu

UNETCHED:



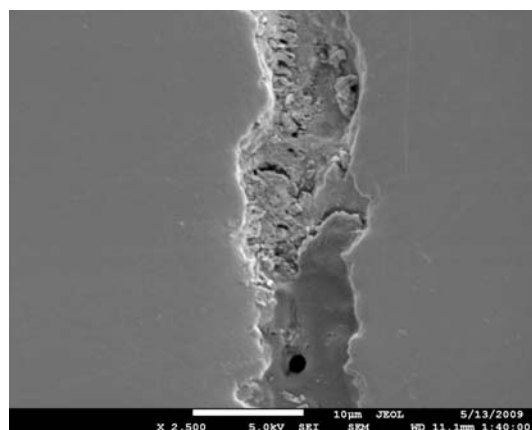
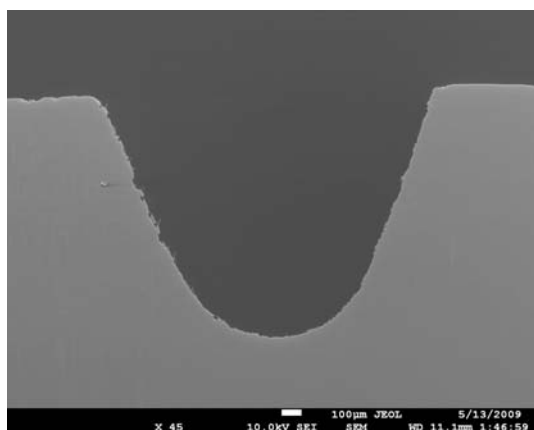
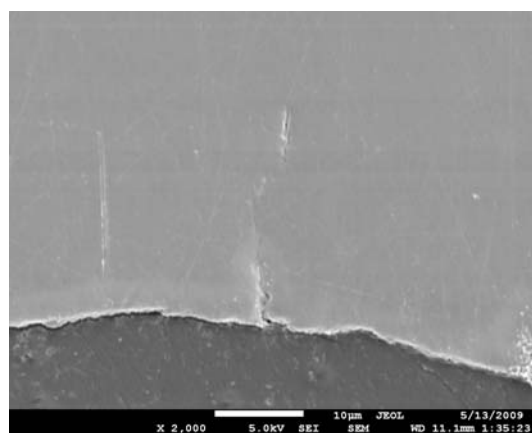
ETCHED:



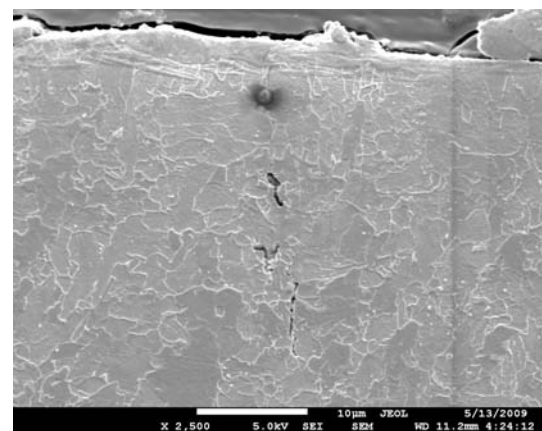
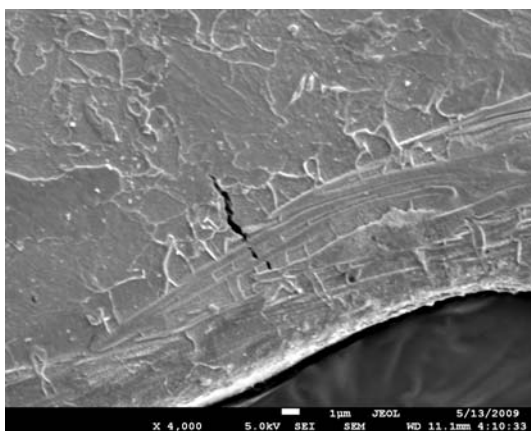
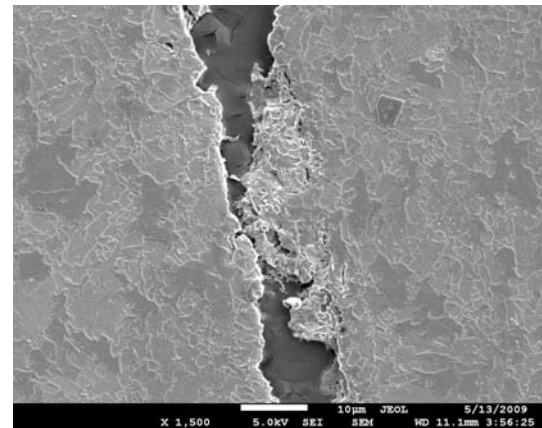
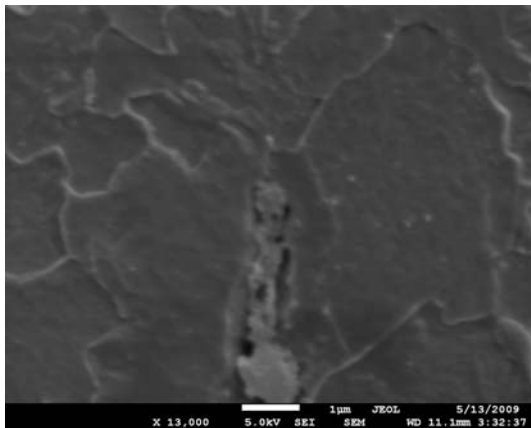
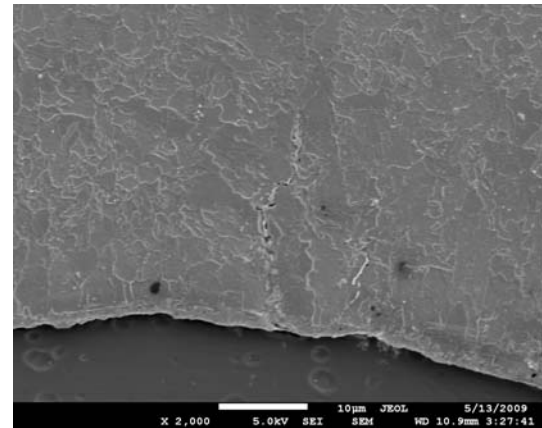
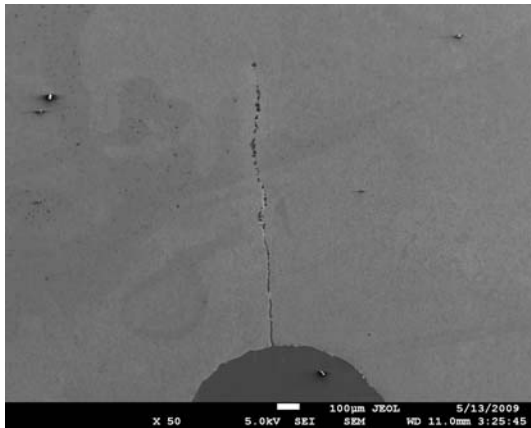
S700MC

7. pre-charging 15 minutes in “1g Thiourea + 28 ml H_2SO_4 / L H_2O ” and stopped after 14 minutes and 20 seconds testing with H-charging insitu

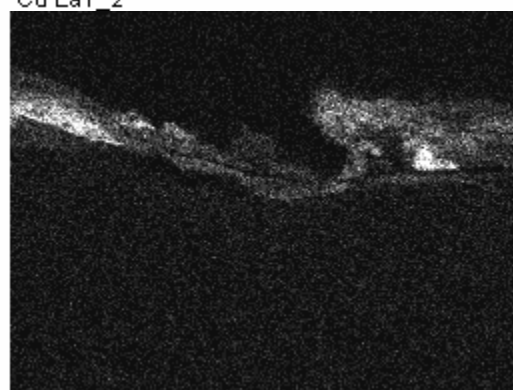
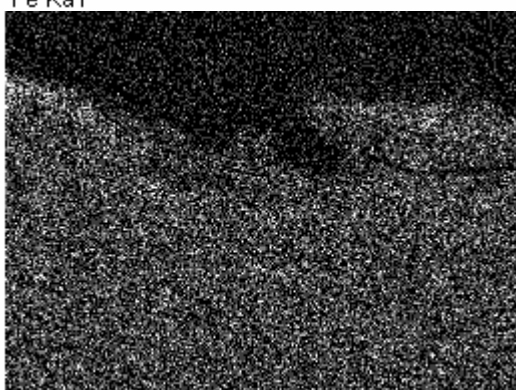
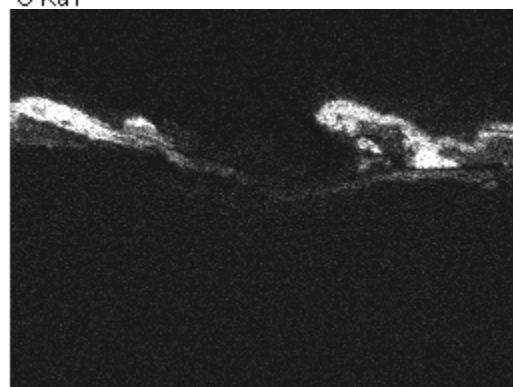
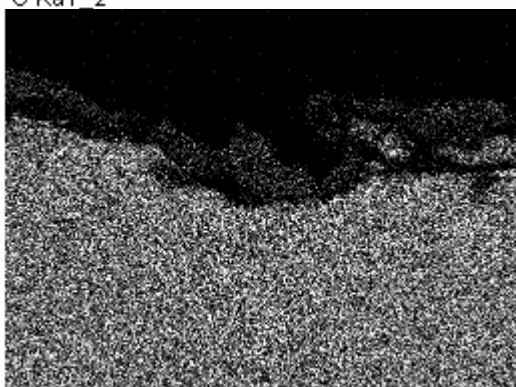
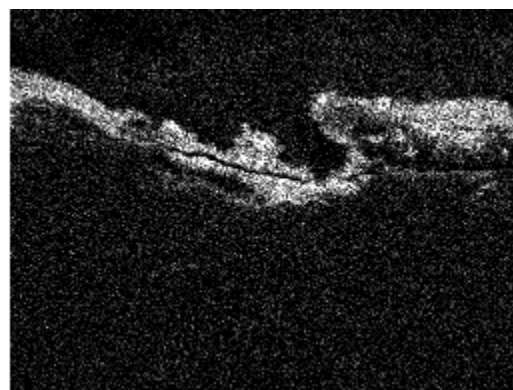
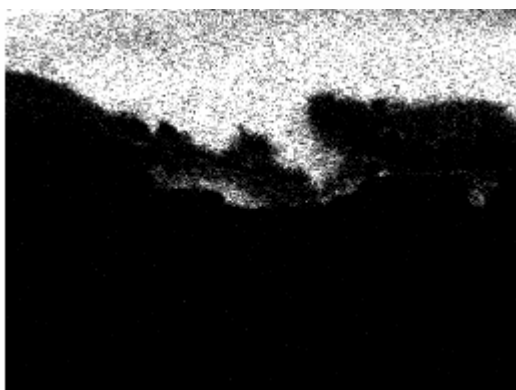
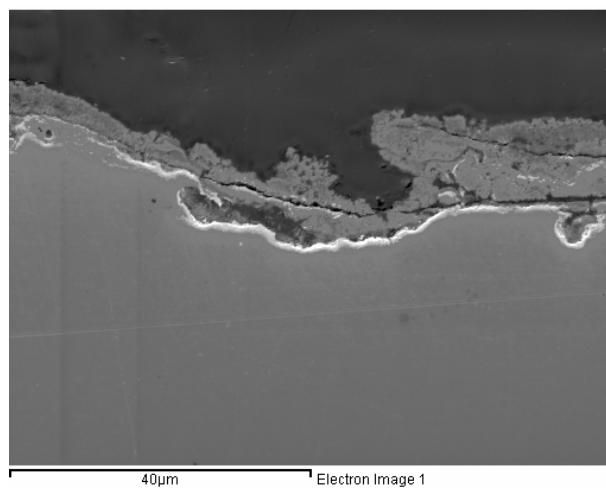
UNETCHED



ETCHED

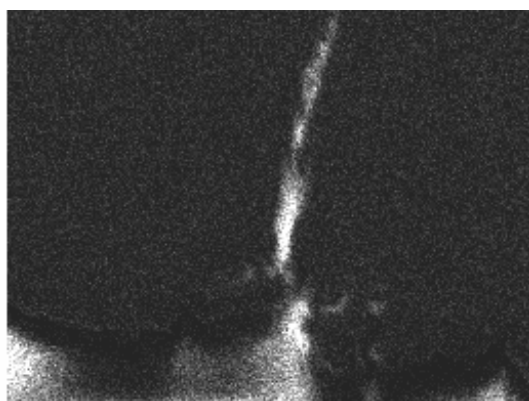
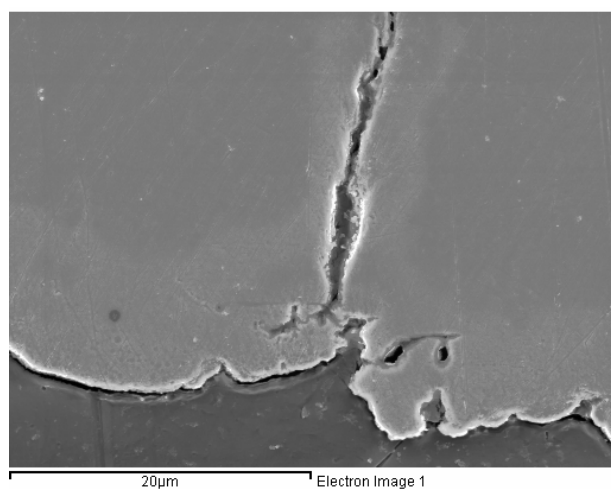


APPENDIX 3: EDX MAPPING

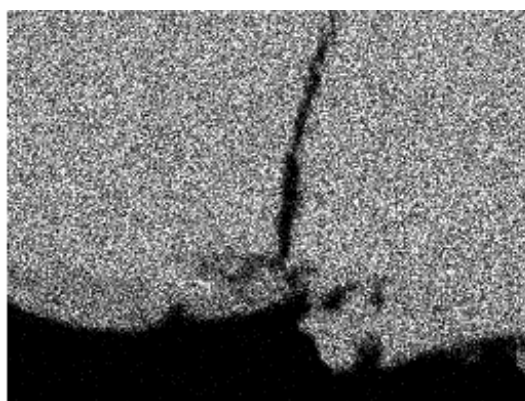


Mapping 1 monster 2 DP980

13/05/2009 11:04:17



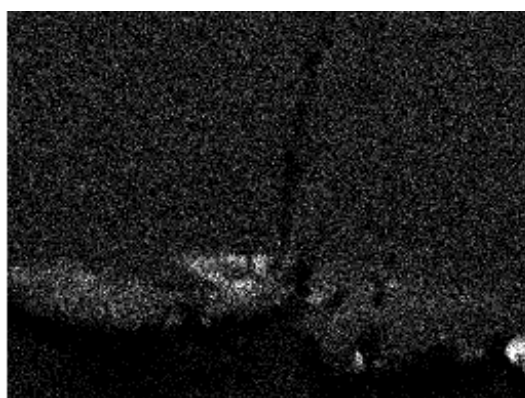
C Ka1_2



Fe Ka1



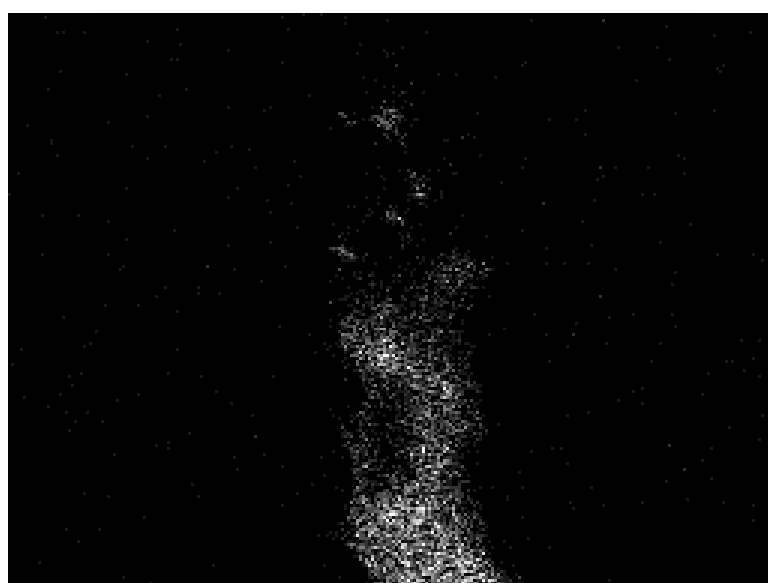
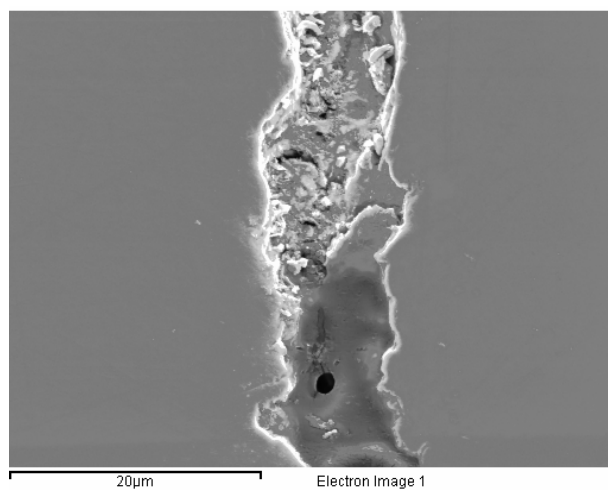
Cu La1_2



Zn La1_2

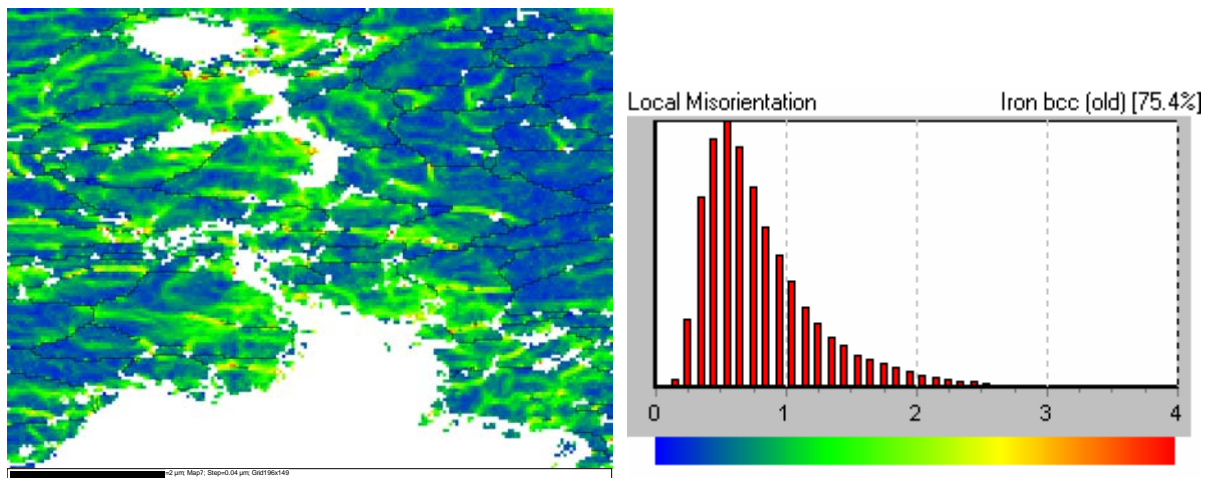
Mapping 1 monster 7 S700MC

13/05/2009 13:45:09

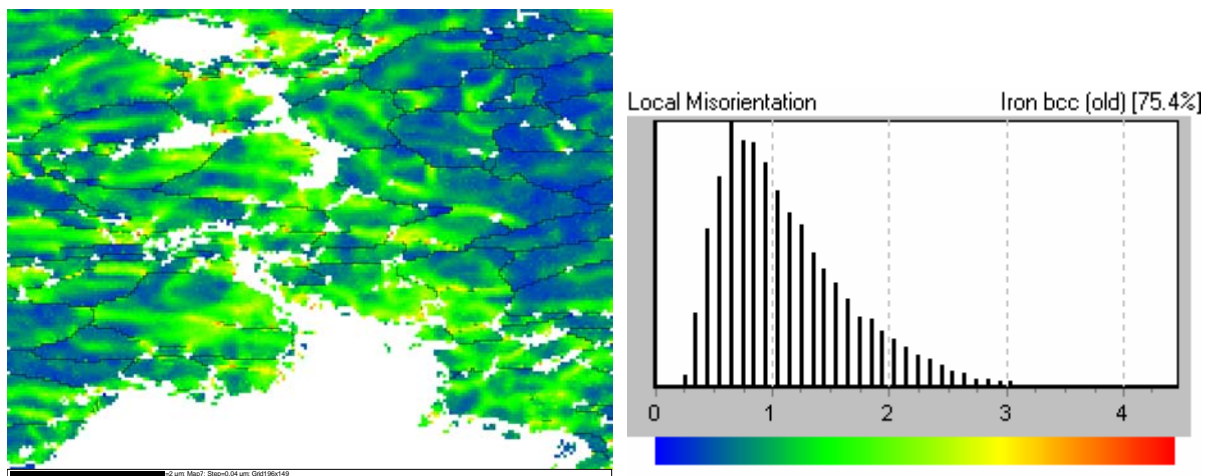


APPENDIX 4: EBSD IMAGES

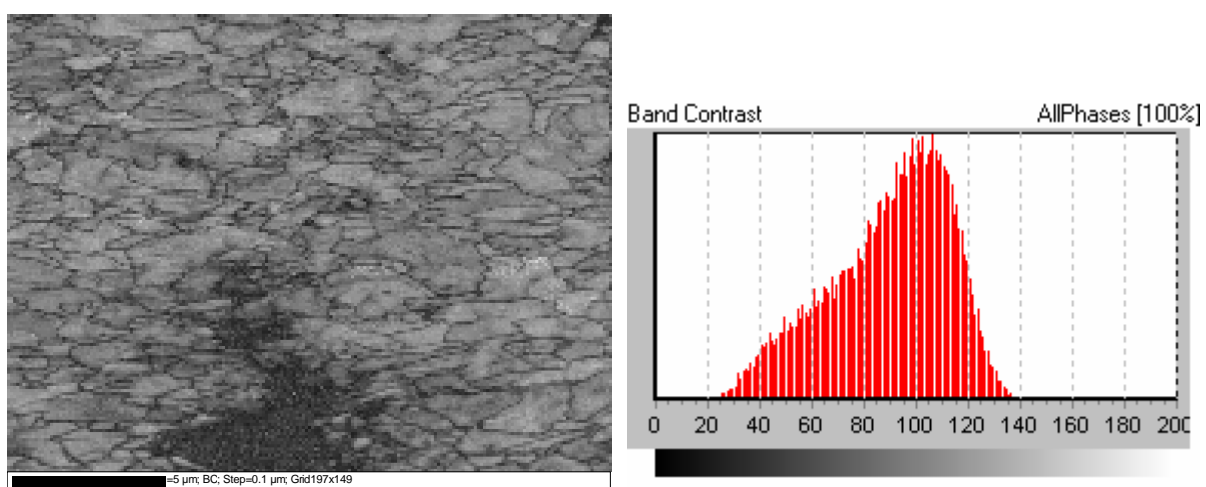
SAMPLE 8 - CRACK 3x3 pixels



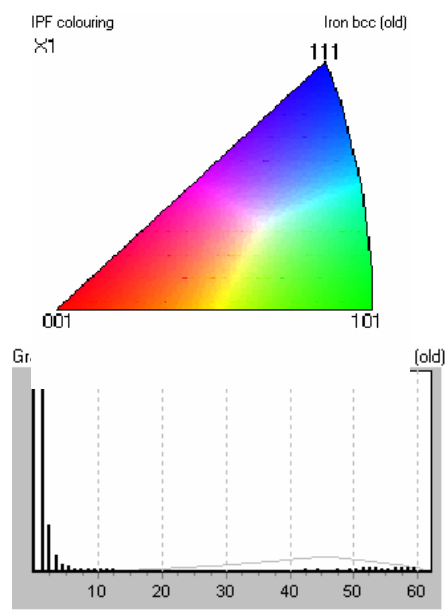
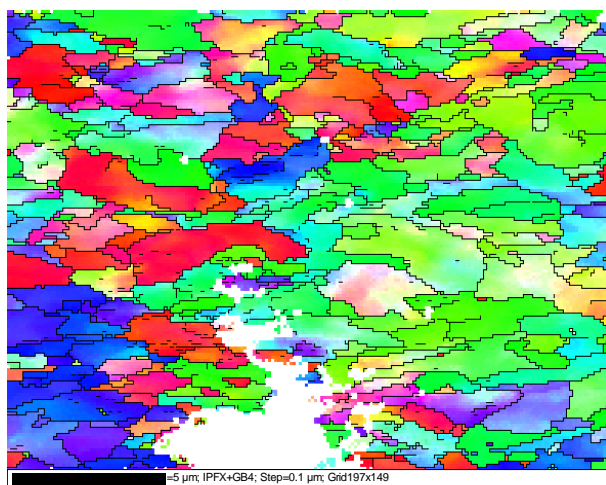
SAMPLE 8 - CRACK 5x5 pixels



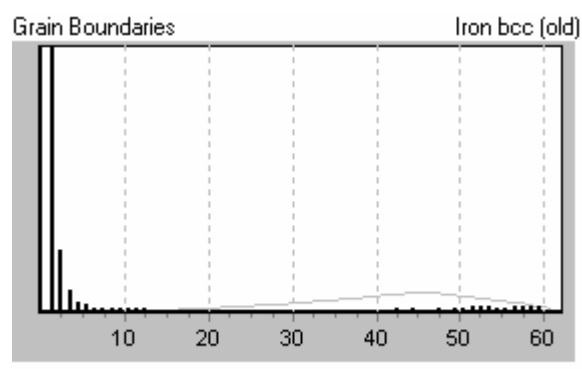
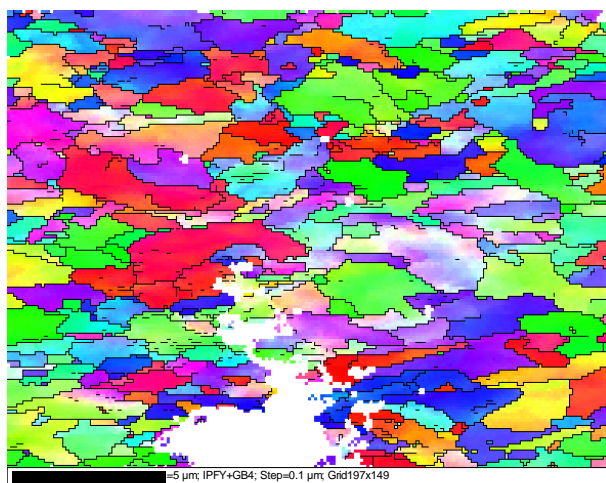
SAMPLE 8 - CRACK TIP detailed Band contrast



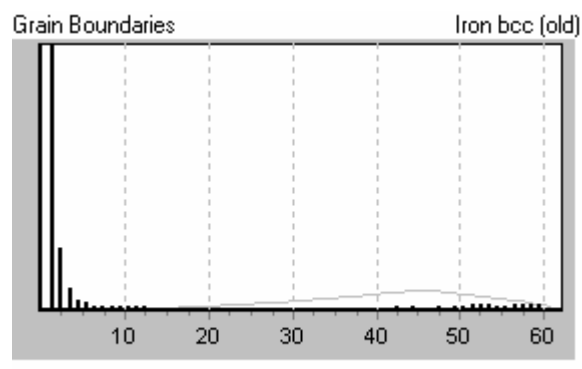
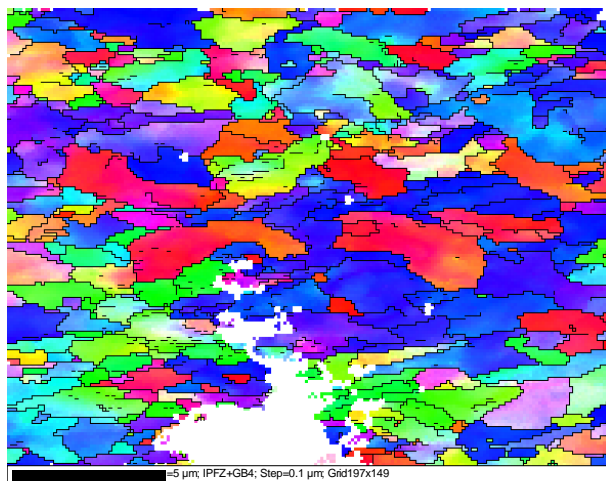
SAMPLE 8 - CRACK TIP IPFX



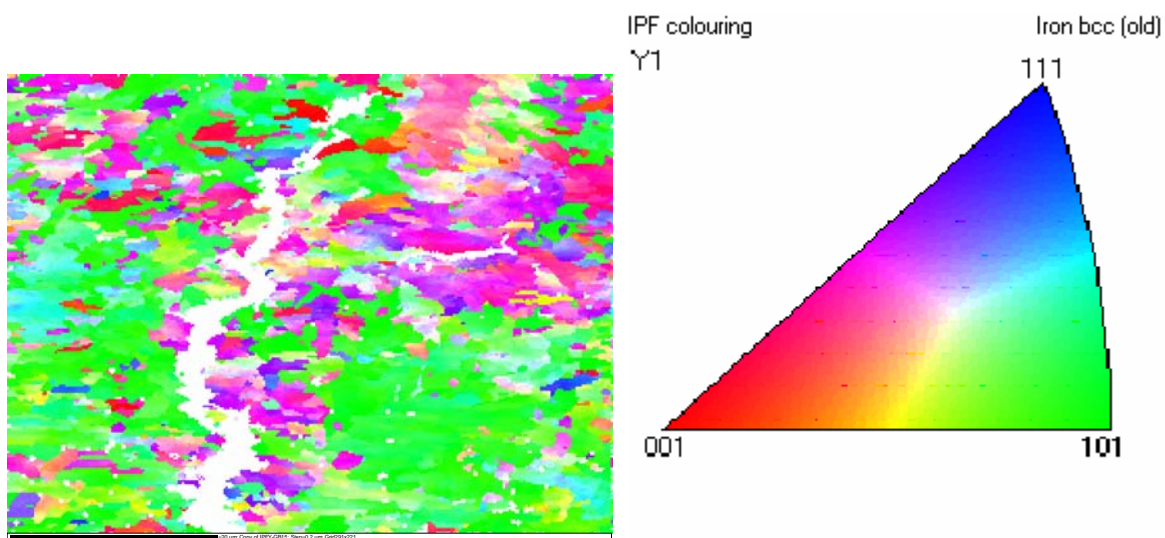
SAMPLE 8 - CRACK TIP IPFY



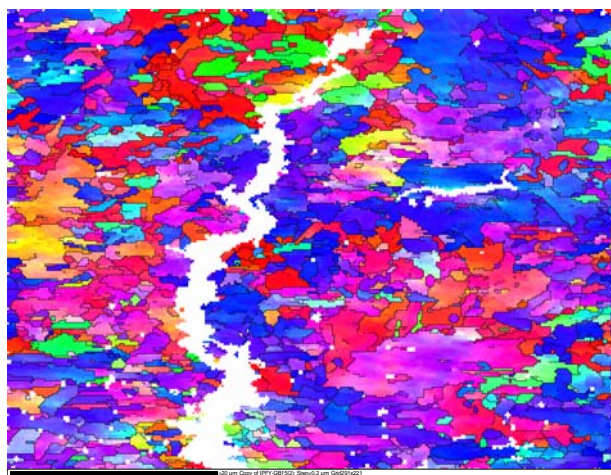
SAMPLE 8 - CRACK TIP IPFZ



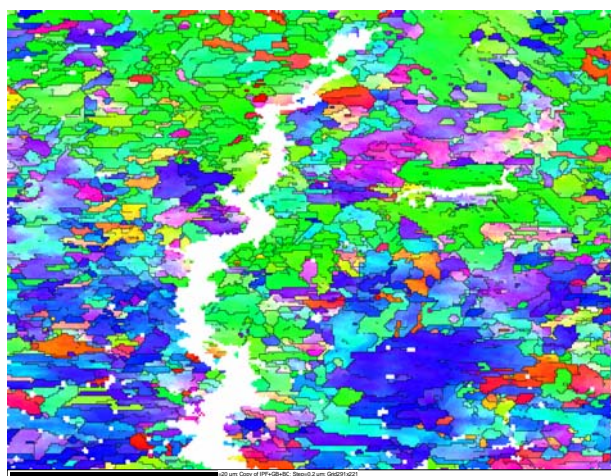
SAMPLE 7 - CRACK IPFX



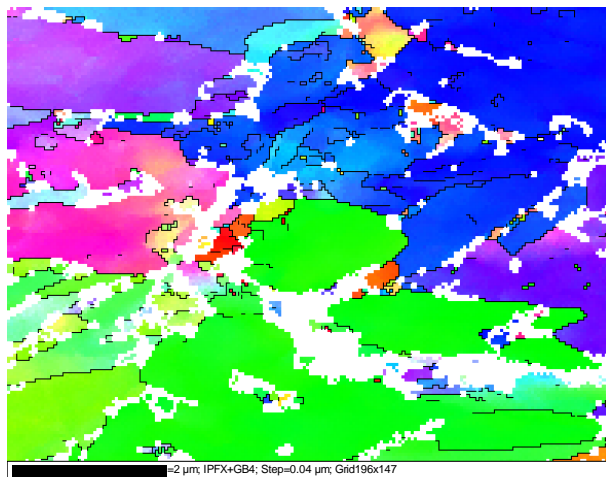
SAMPLE 7 - CRACK IPFY



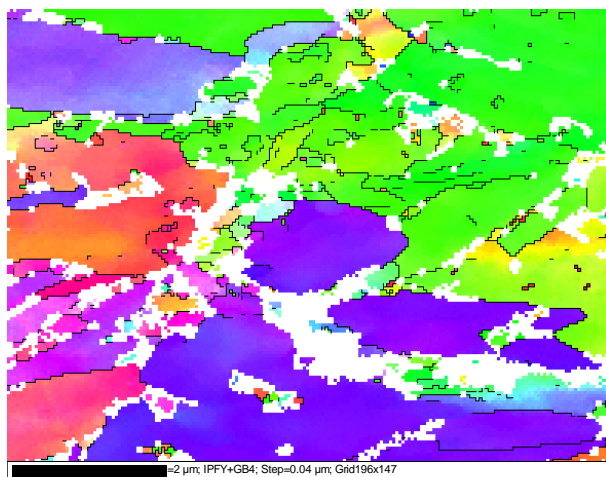
SAMPLE 7 - CRACK IPFZ



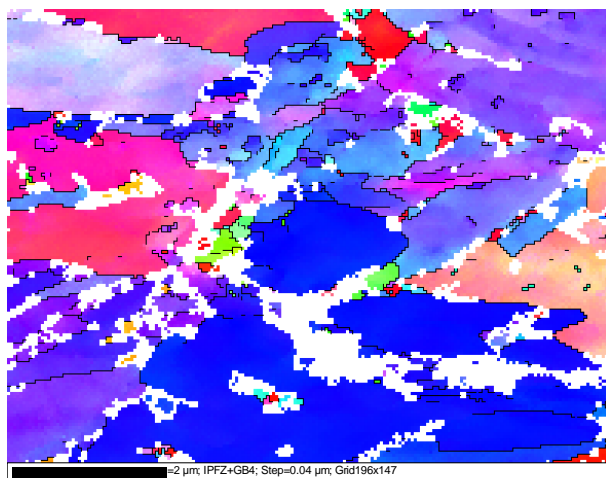
SAMPLE 3 – IPFX crack tip area



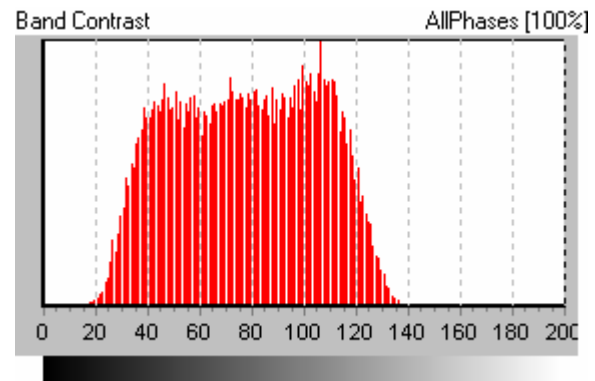
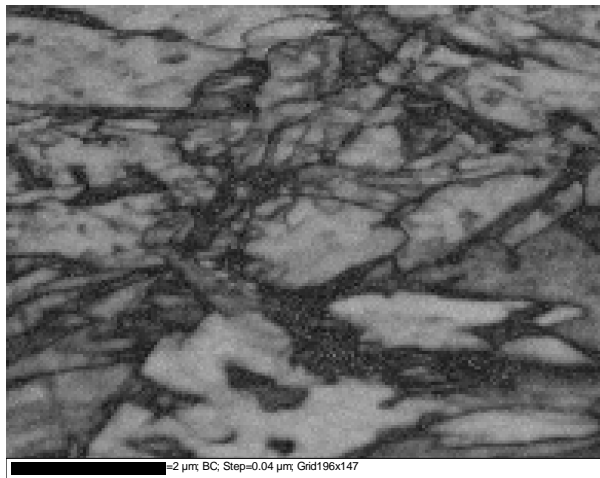
SAMPLE 3 – IPFY crack tip area



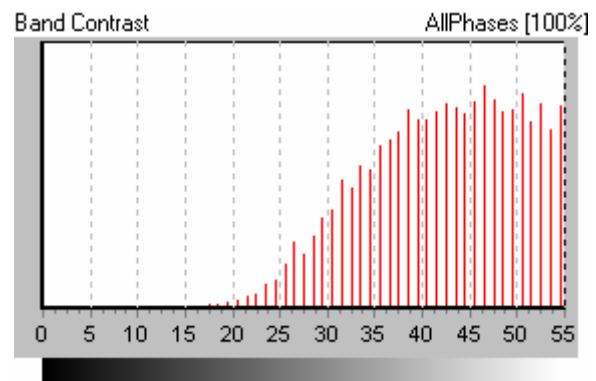
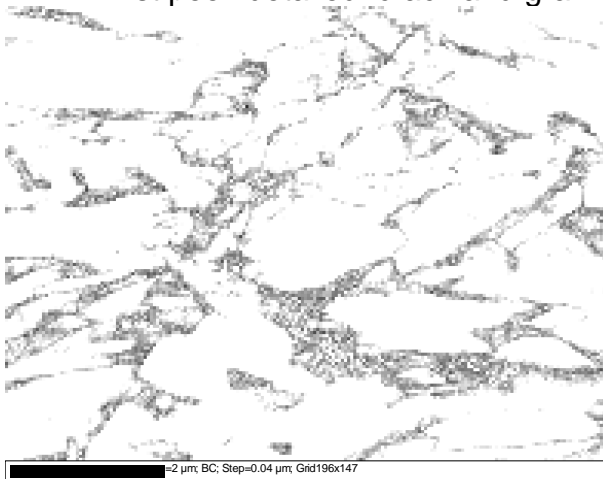
SAMPLE 3 – IPFZ crack tip area



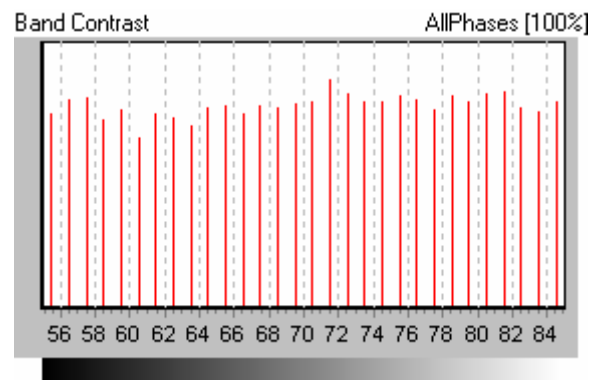
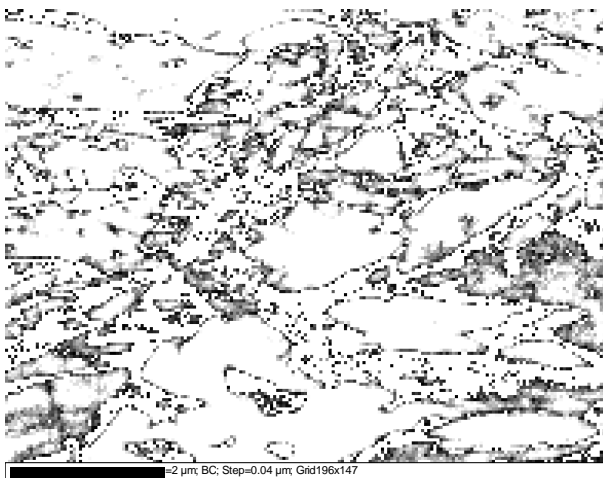
SAMPLE 3 crack tip area BAND CONTRAST



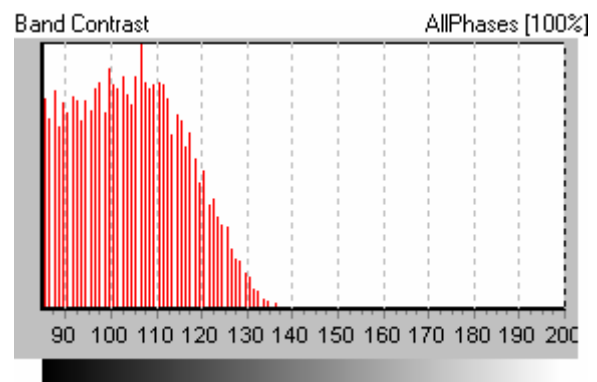
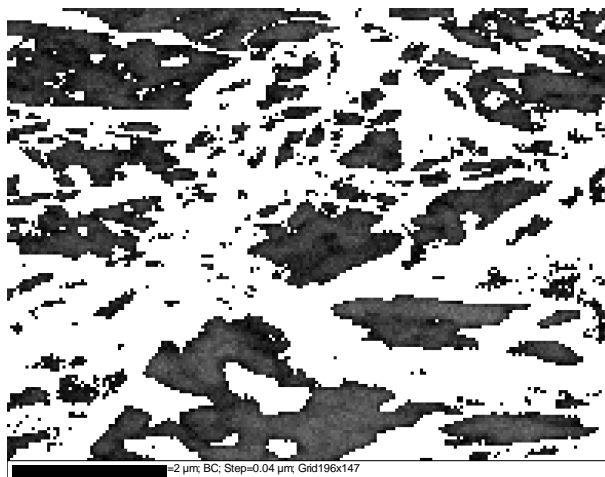
- First peek detailed: crack and grain boundaries



- Second peek detailed: martensite + crack + grain boundaries

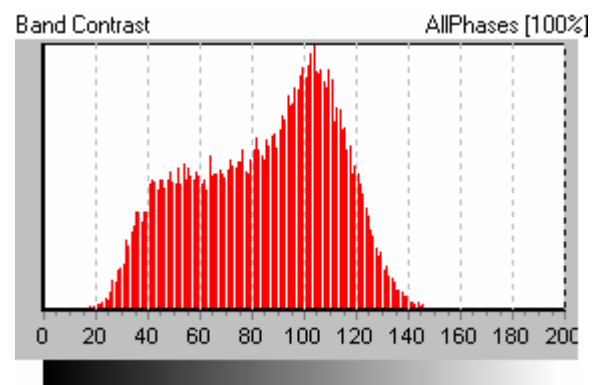
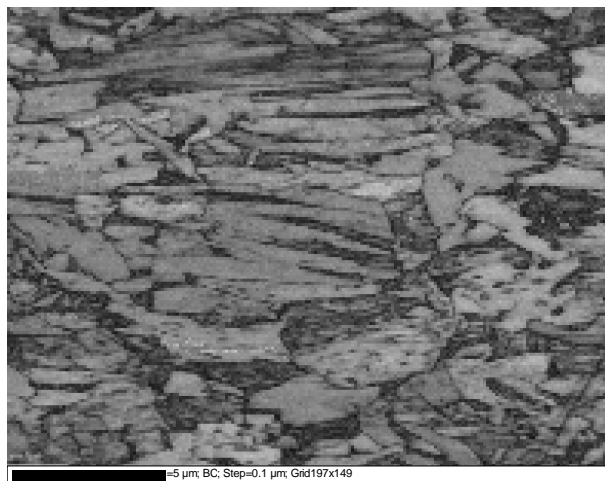


- third peek detailed: ferrite

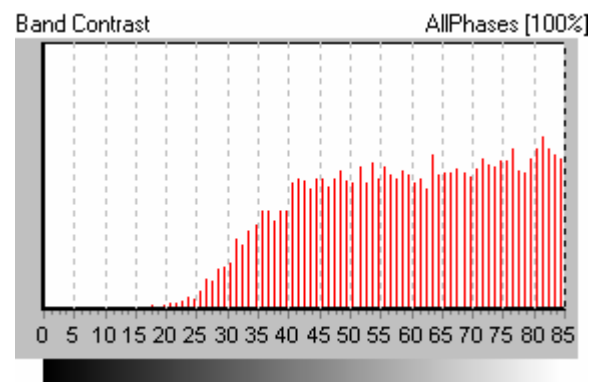
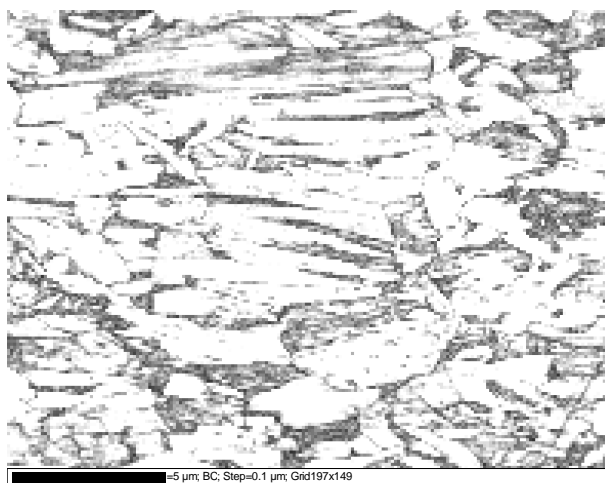


SAMPLE 3 undeformed area

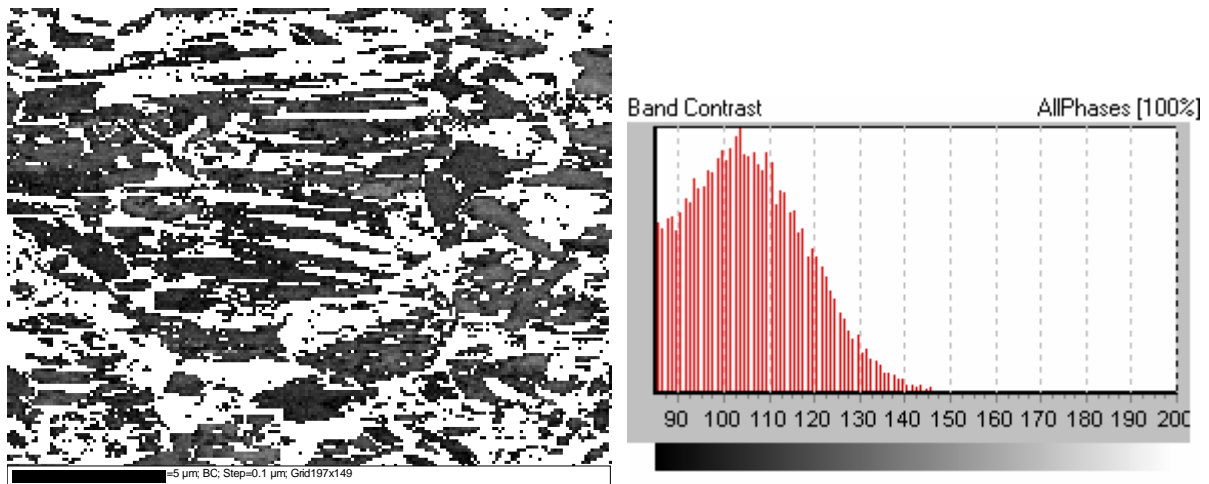
BAND CONTRAST



- SAMPLE 3 undeformed area first Peek: martensite and graing boundaries

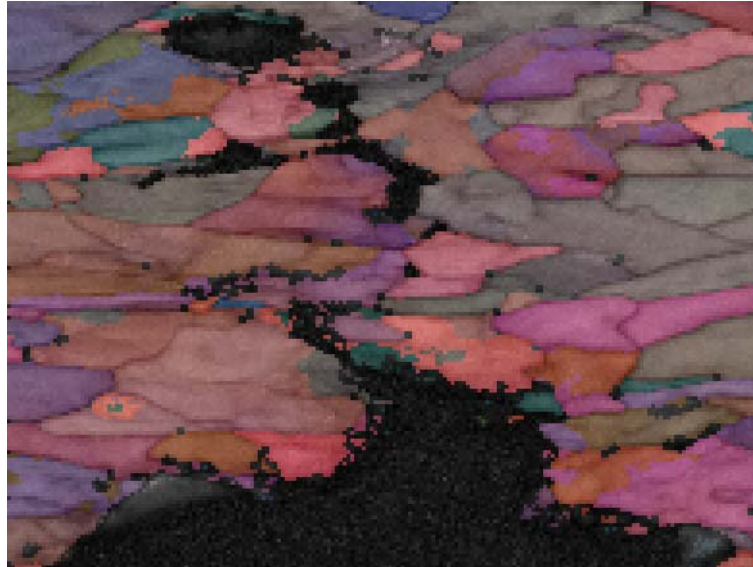


- SAMPLE 3 undeformed area secondt Peek: ferrite



PAU CUADROS FERNANDEZ

JUNE, 2009



Development of an optimized methodology for tensile testing of Carbon steels in Hydrogen environment

The study was performed at OCAS, the Steel Research Centre of ArcelorMittal for the Industry market. The major aim of this research was to obtain an optimized tensile testing methodology with in-situ H-charging to reveal the hydrogen embrittlement in various high strength steels. The second aim of this study has been the mechanical characterization of the hydrogen effect on high strength carbon steels with varying microstructure, *i.e.* ferrite-martensite and ferrite-bainite grades. The optimal parameters for H-charging - which influence the tensile test results (sample geometry, type of electrolyte, charging methods effect of steel type, etc.) - were defined and applied to Slow Strain Rate testing, Incremental Step Loading and Constant Load Testing. To better understand the

initiation and propagation of cracks during tensile testing with in-situ H-charging, and to make the correlation with crystallographic orientation, some materials have been analyzed in the SEM in combination with the EBSD technique.

The introduction of a notch on the tensile samples permits to reach a significantly improved reproducibility of the results. Comparing the various steel grades reveals that Dual Phase (ferrite-martensite) steels are more sensitive to hydrogen induced cracking than the FB (ferritic-bainitic) ones. This higher sensitivity to hydrogen was found back in the reduced failure times, increased creep rates and enhanced crack initiation (SEM) for the Dual Phase steels in comparison with the FB steels.